

FIELD VALIDATION OF PROXIMAL SENSORS ON A TYPICAL PRAIRIE FIELD

By

Olayinka Adamolekun

A Thesis

Submitted to the Faculty of Graduate Studies of

The University of Manitoba

in partial fulfilment of the requirements of the degree of

MASTER OF SCIENCE

Department of Soil Science

University of Manitoba

Winnipeg, Manitoba

Copyright © 2019 by Olayinka Adamolekun

ABSTRACT

Olayinka Adamolekun, M.Sc., The University of Manitoba, April 2019. Field Validation of Proximal Sensors on a Typical Prairie Field.
Advisor: Dr. Wole Akinremi

Spatial variability of soil properties across fields affect crop yield potential, available water, and other site-specific management zones. The concept of Precision Agriculture can only be achieved when operationally feasible methods of depicting spatial variability in soil properties have been devised. Hence, the use of proximal sensors to estimate soil properties at the field scale. The objectives of this study were to investigate the spatial distribution of bulk density with depth, compare the spatial pattern of soil moisture in two seasons (Spring 2014 and Fall 2017), determine the potential of using proximal sensors to estimate soil organic carbon, total carbon, total nitrogen, and soil moisture. Bulk density and soil moisture content showed strong spatial correlation from the soil surface to 75 cm depth. The spatial pattern of soil moisture content was temporally invariant as similar spatial coherent regions were found in both seasons (Spring of 2014 and Fall of 2017). Measurements made using the Veris OpticalMapper had a good correlation with soil organic carbon, total carbon, and total nitrogen that were measured in the lab. Measurements made with the ground penetrating radar was also well correlated with soil moisture content determined by the thermogravimetric method. Soil organic carbon had a root mean square error of 0.28, an R^2 of 0.70, and ratio of prediction to deviation of 2.40, total carbon had a root mean square error of 0.57, R^2 of 0.67, and ratio of prediction to deviation of 2.01, and total nitrogen had a root mean square error of 0.58, R^2 of 0.68, and ratio of prediction to deviation of 1.80. Ground penetrating radar measurements of soil moisture content had a R^2 of 0.83 and root mean square error of 0.014.

Our results showed that variation of bulk density and soil moisture content exists within the field and at various depths that the stability in the spatial pattern of soil moisture content with time was due to soil texture. Both sensors have the potential to estimate soil properties with an acceptable degree of accuracy, the Veris OpticalMapper for soil organic carbon, total carbon, total nitrogen, and ground penetrating radar for soil moisture content on a Canadian Prairies field.

ACKNOWLEDGEMENTS

My sincere appreciation goes to my Advisor, Dr. Wole Akinremi for his encouragement, advice, and Fatherly care towards the successful completion of my master's program. My gratitude also goes to all members of my advisory committee, Dr. Alan Moulin, Dr. Jason Morrison, and Dr. Wole Akinremi for their support and guidance in the completion of my research. My deepest gratitude towards Dr. Alan for his statistical guidance.

I also appreciate the support and help of my research team, John Fitzmaurice, Rob Butler, Nick Lyon, Chubey Mike, Jacqueline Freeman, Erle Einarsson for your selfless support in my field work. My sincere thank also goes to Rob Ellis, Bo Pan, and Justin Soucie for their support in field sampling and laboratory analysis.

I also want to appreciate the support of Arnie Waddell for his help and guidance during spatial variability analysis. My sincere thanks go to my team, Theresa Adesanya, Ahmed Lasisi, Mayowa Adelekun and Chamara, for their advice and support. Special thanks to all faculty, staff and student in the department of soil science for making my stay wonderful.

I am also grateful to the Manitoba Graduate Scholarship for the financial support during the entire period of my studies.

Lastly, I would like to thank my husband for his support and love, my parents for their advice and prayers, and my siblings for their encouragement in making this project a success.

FOREWORD

Guidelines of the Department of Soil Science, University of Manitoba were taken into consideration in the preparation of this thesis in manuscript format. Chapter 1 consists of an extensive literature review of spatial variability in soil properties and the use of proximal sensors along with the objectives of this research. Chapter 2 describes the spatial variability of bulk density with depth and the spatial pattern of soil moisture in two seasons (Spring of 2014 and Fall of 2017) on a loamy sand over the Assiniboine Delta Aquifer. Chapter 3 explores the potential of the Veris OpticalMapper to make real time measurements of soil organic matter, total carbon and total nitrogen and produce maps of the spatial variability within field. Chapter 4 will focus on the use of Ground Penetrating Radar to estimate soil moisture content. Chapter 5 summarizes the findings of the research, implications, and recommendation for further research. Chapter 2, 3, and 4 will be a manuscript each, and will be submitted for publication.

TABLE OF CONTENTS

ABSTRACT.....	ii
ACKNOWLEDGEMENTS.....	iv
FOREWARD.....	v
LIST OF TABLES.....	viii
LIST OF FIGURES.....	ix
INTRODUCTION.....	1
References.....	10
2. SPATIAL VARIABILITY OF BULK DENSITY AND SOIL MOISTURE ON A LOAMY SAND OVER THE ASSINIBOINE DELTA AQUIFER.....	18
2.1. Abstract.....	18
2.2. Introduction.....	19
2.3. Materials and Methods.....	25
2.4. Results.....	30
2.5. Discussion.....	46
2.6. Conclusions.....	50
2.7. References.....	51
3. FEASIBILITY OF MEASURING SOIL CHEMICAL PROPERTIES USING THE VERIS SENSOR.....	61
3.1. Abstract.....	61
3.2. Introduction.....	62
3.3. Materials and Methods.....	67
3.4. Results.....	71

3.5. Discussion.....	81
3.6. Conclusions.....	84
3.7. References.....	85
4. SOIL MOISTURE CONTENT ESTIMATION USING GROUND PENETRATION RADAR.....	94
4.1. Abstract.....	94
4.2. Introduction.....	95
4.3. Materials and Methods.....	100
4.4. Results and Discussion.....	109
4.5. Conclusions.....	114
4.6. References.....	115
5. GENERAL SYNTHESIS.....	123
References.....	127

LIST OF TABLES

Table	page
2.1. Descriptive summary statistics for bulk density sampled in the Fall of 2017	30
2.2. Parameter for Semivariogram models for bulk density along the soil depth (Fall 2017)	32
2.3. Descriptive summary statistics for soil moisture content sampled in the Fall of 2017.....	37
2.4. Parameter for Semivariogram models for soil water content (Fall, 2017) along the soil depth.....	38
2.5. Parameter for variogram models for soil water content (Spring, 2014) along the soil depth.....	40
3.1. Descriptive statistics of soil organic carbon % (SOC), total carbon % (TC), and total nitrogen % (TN) at the surface (0-15 cm)	71
3.2. Summary of the PLSR results for the soil properties dataset.....	72
3.3. Parameter for Semivariogram models for lab-analyzed SOC, TC, and TN and Veris estimated SOC, TC, and TN.....	75
3.4. Pearson correlation coefficient for Veris SOC with other variables.....	76
4.1. Descriptive summary statistics for measured soil moisture content, GPR estimated soil moisture content and dielectric permittivity (0-90 cm)	109

LIST OF FIGURES

Figure	page
2.1. Geospatial soil sampling design for the study area in the Spring of 2014, and the selected 50 sampling points for Fall 2017.....	27
2.2. Kriged map of bulk density at 0-15 cm depth across the field.....	33
2.3. Kriged map of bulk density at 15-20 cm depth across the field.....	34
2.4. Kriged map of bulk density at 30-45 cm depth across the field.....	35
2.5. Kriged map of bulk density at 45-60 cm depth across the field.....	35
2.6. Kriged map of bulk density at the 60-75 cm depth across the field.....	36
2.7. Kriged map of bulk density at the 75-90 cm depth across the field.....	36
2.8. Fitted theoretical Semivariograms for soil water content at depth 75-90 cm.....	39
2.9. Kriged map of soil water content (Johnson SI transform) at 0-15 cm across the field for (a) Spring 2014 (b) Fall 2017.....	42
2.10. Kriged map of soil water content (Johnson SI transform) at 30-45 cm depth across the field for (a) Spring 2014 (b) Fall 2017.....	43
2.11. Kriged map of soil water content (Johnson SI transform) at 60-75 cm depth across the field for (a) Spring 2014 (b) Fall 2017.....	44
2.12. Kriged map of soil water content (Johnson SI transform) at 75-90 cm depth across the field for (a) Spring 2014 (b) Fall 2017.....	45
3.1. Correlation between conventionally measured and Veris estimated soil (a) organic carbon, (b) total nitrogen, and (c) total carbon.....	73-74
3.2. Kriged maps of soil organic carbon content as measured (a) conventionally and (b) as estimated using the Veris OpticalMapper.....	78

3.3. Kriged maps of soil total carbon content as measured (a) conventionally and (b) as estimated using the Veris OpticalMapper.....	79
3.4. Kriged maps of soil total nitrogen content as measured (a) conventionally and (b) as estimated using the Veris OpticalMapper.....	80
4.1. Raw GPR data (radargram) showing hyperbolic reflections.....	103
4.2. Typical GPR radar trace (thick black line) and corresponding envelope (broken line) from a sampling point in the field.....	104
4.3. Shape of the SEC gain function.....	105
4.4. Semblance plot of the wide-angle reflection and refraction measurement to illustrate how electromagnetic wave velocity Vs time are obtained. The red colour indicate high semblance.....	106
4.5. Relationship between dielectric permittivity estimated from the GPR and soil moisture content from volumetric method.....	111
4.6. Validation graph of conventionally measured and GPR estimated soil moisture content derived from Topp's equation.....	112

INTRODUCTION

1.1. Precision Agriculture

Our ability to measure spatial and temporal variation of soil properties within fields, and the development of Global Positioning Systems have resulted in the advent of Precision Agriculture (Stenberg et al., 2010). Site specific management / Precision Agriculture (PA) is a term used to encompass a range of devices that are used to collect agriculture information and the geospatial tools that enable resources to be applied and take advantage of the inherent field variability. The advent of site-specific management requires the utilization of a large data set and detailed soil information to enhance crop productivity and environmental quality at a finer spatial resolution (Harmon et al., 2005). The intent of site-specific management is to maximally utilize soil, water resources, and chemical inputs based on the variability in soil properties and this can only be achieved when accurate information about soil properties are obtained (Cho, 2016; Perron et al., 2018).

1.2. Spatial variability in soil properties

Numerous studies have shown the variability of soil within a landscape, and within the soil profile, as well as its importance in agriculture (Miller, 2012; Joao et al., 2014). Sudduth et al., (2015) reported spatial and temporal variability of electrical conductivity. Jonard (2013) also reported the characterization of tillage effects on spatial variation of soil properties. Delbari et al., (2011) investigated the spatial structure of soil texture within landscape, at the field scale and in both landscape and field levels and found that samples taken in close proximity are efficient in mapping spatial variation with low uncertainty of prediction than samples taken further apart. Most farmers consider the soil to be uniform for its management, but soil properties are variable in space and time.

Soils commonly exhibit inherent variability of properties such as texture, depth of soil, and organic carbon content, which influences many physical and chemical properties that can affect available plant nutrients leading to variability in yield (Shahandeh et al., 2011). Castrignanò et al., (2015) reported that agricultural management practices applied to fields such as tillage, irrigation, and the use of heavy machinery can affect edaphic properties leading to variation in soil. Soil variability within field brings about variation in yield potential, and because this yield varies, there is the need to improve the utilization of inputs by varying the rate of application based on the pattern of soil variation. The concept of Precision Agriculture can only be achieved when operationally feasible methods of depicting spatial variability in soil properties are devised.

1.3. Proximal soil sensing

Proximal soil sensing is the use of field-based sensors to measure signals directly from the soil while in close proximity (<2 m) (Viscarra Rossel et al., 2011). Adamchuk et al. (2004a) categorized different sensors based on their design concept. They include the Reflectance based soil sensors (Visible–near infrared and Mobile (on-line) field vis–NIR), conductivity, resistivity, and permittivity based soil sensors (time domain reflectance (TDR), frequency domain reflectance (FDR), ground penetrating radar (GPR), and electromagnetic induction (EMI) (Mahmood, 2013), passive radiometric based soil sensors (Gamma-ray spectrometers), strength based soil sensors (draught sensors), electrochemical based soil sensors (Ion-sensitive field-effect transistors). Allred et al., (2008) reported that conventional methods of soil sampling are labour intensive and are not cost effective. The labour and cost requirement associated with conventional sampling sets in limitation to sampling at a density that precisely maps the variability existing in the field.

Therefore, the use of soil sensors has provided spatially dense data that are cost effective (Dhillon et al., 2010). In addition, soil sensors have the potential to obtain large sample data compared to other sampling techniques, as well as increase the entire spatial accuracy when that of individual measurement is low (Daran, 2014). This makes it an attractive tool for site-specific decisions in many environments, particularly with regards to soil characterization.

1.4. Non-invasive Geophysical methods applied to Agriculture.

Bulk density is a vital property of the soil that varies with the soil structural conditions. The knowledge of bulk density is important in precision agriculture as it affects plant nutrient availability, movement of air and water through the soil, the rooting depth, ease of seedling emergence, permeability of soil to water, and can be used to assess soil compaction as well as in the planning of modern farm techniques (Ping et al., 2016). Bulk density increases with depth due to overburden pressure, low organic matter content and reduced pore space that occurs subsurface, resulting in soil variability at depth. Due to the vast nature of agricultural soil systems, the use of sensing techniques that can provide information about the soil from a single sensor has been said to be inadequate and invalid. Therefore, to obtain more accurate information, sensors based on different measurement principles should be used to separate various soil properties (Castrignanò et al., 2015), hence the use of a Ground Penetrating Radar.

1.4.1. Ground Penetrating Radar (GPR)

Doolittle et al., (2012) reported that over the last three decades, the use of geophysical methods has remarkably grown in soil investigation. Geophysical methods most commonly used in these pursuits include electromagnetic induction (EMI), ground penetrating radar, transient EMI, galvanic resistivity, and magnetics (Allred, 2011).

These methods are used to infer and better understand the spatial variability of soils and its properties, and to guide observations and sampling. GPR is a time-dependent geophysical

technique and nondestructive method which uses electromagnetic radiation with central frequencies ranging from 50 -1200 MHz (Lunt et al., 2005) to map shallow subsurface properties at field scale with high temporal and spatial resolutions (Jonard et al., 2011). Jeffery et al., (2008) reported that GPR can provide precise information about buried objects as well as a three-dimensional pseudo image of the subsurface with an accurate depth estimate. Three GPR techniques are used to map soil moisture variability in an agricultural field. The direct ground wave (Mahmoudzadeh, et al., (2012), surface reflection coefficient (on-ground GPR), and surface reflection inversion (off-ground GPR) (Reza, 2013). Furthermore, off-ground and on-ground penetrating radar was used in a study carried out by (Jonard et al., 2013) in characterizing spatial variation in soil moisture.

1.4.2. Basic principle of the GPR.

Ground Penetrating Radar works on the principle of electromagnetic energy in the form of an electromagnetic wave (Jeffery et al., 2008). Electromagnetic pulse is transmitted through a medium, and the receiving antenna(s) collects the reflected energy (Francesco and Fabio, 2013). Ground Penetrating Radar systems transmit short pulses of very high and ultrahigh frequency (30 MHz to 1.2 GHz) electromagnetic energy into the ground from the antenna. Each pulse consists of a spectrum of frequency (Butnor et al., 2001). The transmitted pulse of energy is propagated downward into the soil. The receiving unit intensifies and samples the reflected energy converting it to a similarly shaped waveform in a lower frequency range. The period it takes for the electromagnetic energy to move from the antenna to a subsurface and back is measured by the GPR.

Rial et al., (2005) reported that for GPR data to be more useful, it must be integrated with a GPS (Global Positioning System), which helps in obtaining visually georeferenced data. This is also useful during post analysis whereby the position of the radar can be adjusted per the

time stamp of the two closet positions recorded with the GPS. The integration of geophysical methods with GPS, data processing software, and GIS (Geographical Information Systems) have fostered the expanded use of geophysical techniques in soil investigations (Castrignano et al., 2018).

1.4.3. Applications and limitations of GPR

Ground Penetrating Radar is principally used as a superior control device to estimate spatial and temporal variations in soil properties. Ground Penetrating Radar has been applied widely in many fields in civil engineering and geosciences (Salucci et al., 2014), archeological research (Conyers, 2013) investigation of water table depth (Mahmoudzadeh et al., 2012) animal burrow detection (Chlaib et al., 2014) and to assess the inorganic pollutant contamination in ground water (Wijewardana et al., 2015). Ground Penetrating Radar has been used extensively in estimating soil water content and in measuring water content profile, estimating the spatial variability of soil water content, and under irrigation conditions (Liu et al., 2016). Huisman et al. (2002) reported that in mapping an extensive area (> 5 m) for soil water content, GPR is a better method than a Time Domain Reflectometry (TDR).

The main constraint of GPR is the relationships between the antenna frequency, penetration depth and resolution. Buynevich et al., (2009) reported that higher frequency antennas provide higher resolution but have less penetration depth than lower frequency antennas. Depth penetration is controlled by soil electrical conductivity.

Ground Penetrating Radar is highly sensitive to soil texture and soils with high electrical conductivity and thus reduces penetration thereby reducing the range of soil where GPR can be successfully applied (Huisman et al., (2003). Lebron et al., (2004) also reported that the high adsorptive capacity of clays for water and exchangeable cations is inversely related to the depth

of penetration of the GPR. Soils with substantial amounts of CaCO_3 at similar moisture and clay content also reduces the penetration depths of GPR.

1.5. Non-invasive Geoelectrical methods applied to Agriculture.

Soil organic matter plays a vital role in ecosystems functioning and soil productivity. Soil organic carbon has a significant effect on soil structure and this can affect the physical, chemical and biological processes taking place in the soil, specifically affecting the capacity to supply nutrient and to store water for plant uptake (Knadel, 2015). Preserving soil organic carbon improves the productivity and quality of the soil as well as sustains the production of food while alleviating the emission of greenhouse gases (Viscarra-Rossel, 2016). The knowledge of soil carbon distribution is important in managing the fertility of the soil as well as improving the soil structure and soil health through the promotion of the factors leading to aggregation. The sequestration of soil carbon is an important mitigation factor in greenhouse gas accounting. This has prompted increased attention to delineating and observing changes in soil carbon (Miklos, 2010).

Recent research shows that electromagnetic sensors can be used to obtain indirect measures of organic matter, soil moisture content, clay content, cation exchange capacity, if the contributions of other soil characteristics influencing EC_a are known or can be determined.

1.5.1. Basic principle of the Veris OpticalMapper.

Veris technology has developed innovative spectroscopic products and real-time sensors to tackle the challenges of precision agriculture. Veris uses the optical mapper, a two-wavelength optical module, to measure the reflectance of soil in both visible and Near-infrared ranges. A two-wavelength optical mapper is used to measure reflectance in both visible and near-infrared ranges. It operates under the surface residue and soil with a depth gauging side wheel to control the depth and produce a constant soil position. Optical sensing uses near-infrared spectroscopy.

Veris technology (2009) reported that the energy of near-infrared light depending on the wavelength corresponds to overtones and combination bands of fundamental molecular vibrations of C-H, O-H, and N-H (Wetterlind, 2009) making this area perfect for expressing various forms of carbon, nitrogen and water respectively. Molecules absorb light only at energy that coincides with the energy difference between the quantized energy levels of different vibrational states of the molecule. Light energy is inversely proportional to its wavelength; therefore, only certain wavelengths of light can be absorbed by a molecule.

1.5.2. Applications and limitations of Veris OpticalMapper

The Veris OpticalMapper has been evaluated in the scientific literature for determination of soil properties such as electrical conductivity, soil water content, organic matter, soil nitrogen, soil total carbon (Giyong et al., 2013) and cation exchange capacity (Adamchuk et al., 2004). Sudduth et al., (2003) reported that one of the operational disadvantages of the Veris EC mapper is that it is very heavy and requires the aid of a tractor to pull it while in operation, and this limits its use to unplanted fields. For soils that are dry with low conductivity, Veris data is limited due to poor electrical contact of the coulter with the ground. Joao et al., (2014) explained that the Veris OpticalMapper must be in good contact with the soil during sampling. Giyong and Chase (2013) reported that a gap between the sensor and sapphire window reduces the potential to estimate soil organic matter. They also explained the complexity in processing the data as well as the calibration procedure, and this has restricted its extensive use by farmers. Variations in soil moisture interferes with spectral reflectance by darkening the soil and smoothing the spectra (Nocita et al., 2013).

1.6. Spatial variation of Soil moisture content

Variation in soil moisture content occurs due to the interaction of various soil properties such as depth of soil, texture, structure, soil organic matter content, temperature, and density. To

spatially characterize nutrient up-take by plants for quality crop yield and development, soil water must be determined across the field as transpiration is correlated with plant growth and crop yield. Knowledge of soil moisture content is also useful for efficient irrigation processes as stated by (Grote et al., 2010). The evolution of soil moisture sensing techniques in various applications such as agriculture, climate, and hydrology are as a result of the importance of obtaining accurate and precise soil moisture characterization at various time and space (Minet et al., 2012).

1.6.1. Soil Moisture Sensors

Mahmoudzadeh, et al., (2012) showed that laboratory-based techniques such as soil sampling for characterizing soil water content, are limited and invasive. On the other hand, remote sensors on platforms such as satellites (Kerr et al., 2010; Franz et al., 2013) are limited to large-scale analyses at the field scale. The electrical property of the soil is used to deduce the soil water content by dielectric soil moisture sensors. Saito et al., (2016) reported that dielectric soil moisture sensors have the potential to determine real-time soil water content and are non-destructive.

A 100 MHz frequency is generally used because it reduces the influence of ionic conductivity. As a result, a change in the transmission line impedance depends only on the soil's dielectric constant (Kargas and Kerkide, 2008).

The direct relationship between the voltage and contrast in amplitude of the standing wave at two points forms a precise measure of soil moisture content. (Kargas and Kerkide, 2009). Haung et al., (2004) reported that the Theta Probe was more accurate than watermark, Aqua-Tel, and Aquaterr when compared in the laboratory. The Hydra Probe (POGO) which is a frequency domain reflectometry sensor functions at a frequency of 50 MHz. The reflected voltage corresponds to the real dielectric constant of the soil (Rowlandson et al., 2013).

1.7. Research Objective

A review of the literature showed that several studies have been carried out on the use of Veris OpticalMapper for measuring soil chemical properties such as organic carbon and electrical conductivity, total carbon and total nitrogen and the use of Ground Penetrating Radar for measuring soil moisture content. The increase in the demand for soil moisture data has led to the development of various techniques to quantify soil moisture. But, we are not aware of studies that mapped the spatial variability of bulk density on a Canadian Prairies with depth. Therefore, the objectives of this study were to investigate the spatial distribution of bulk density with depth, compare the spatial pattern of soil moisture in two seasons (Spring 2014 and Fall 2017), determine the potential of using proximal sensors to estimate soil organic carbon, total carbon, total nitrogen, and soil moisture.

Hypothesis:

Proximal sensors can provide estimates of soil organic carbon, total carbon, total nitrogen, and soil moisture content, and quantify the spatial variability of soil bulk density and moisture content, both horizontally and with depth.

References

- Adamchuk, V. I., Hummel, J. W., Morgan, M. T., and Upadhyaya, S. K. 2004a.** On-the-go soil sensors for precision agriculture. *Computer Electron. Agric.* 44: 71–91.
- Allred, B. 2011.** The Second Global Workshop on Proximal Soil Sensing – Montreal 2011 24 Keynote Presentation Agricultural Geophysics: Past/Present Accomplishments and Future Advancements.
- Allred, B.J., Ehsani, M.R. and Daniels, J.J., 2008.** General considerations for geophysical methods applied to agriculture, p. 3-16. *In* Allred, B.J., Ehsani, M.R., Daniels, J.J (eds.) handbook of agricultural geophysics. CRC press, Taylor & Francis, Boca Raton, FL.
- Audun, K., 2008.** Dependence of soil apparent electric conductivity upon soil texture and ignition loss at various depths in two morainic loam soils in southwest Norway. *Handbook of agricultural geophysics.*
- Barry, J. A., Jeffrey, J., Daniels, M. and Reza, E. 2008.** Handbook of Agricultural Geophysics.
- Bo Stenberg, Raphael A. Viscarra Rossel, Abdul Mounem Mouazen, and Johanna Wetterlind. 2010** Visible and Near Infrared Spectroscopy in Soil Science. In Donald L. Sparks, editor: *Advances in Agronomy*. Burlington: Academic Press. 107: 163-215.
- Butnor, R., Doolittle, J.A., Kress, L., Cohen, S. and Johnsen, K.H. 2001.** Use of ground-penetrating radar to study tree roots in the southeastern United States. *Tree physiology*. 21: 1269-1278.

- Buynevich, I.V., Jol, H.M. and itzGerald, D.M., 2009.** Coastal environments. In: Jol, H.M., Ground penetrating radar: theory and application. Elsevier, Amsterdam, the Netherlands. 299-322.
- Castrignanò, A., Landrum, C. and De Benedetto, D. 2015.** Delineation of Management Zones in Precision Agriculture by Integration of Proximal Sensing with Multivariate Geostatistics. Examples of Sensor Data Fusion. Agric. Conspectus Science. 80: 39-45.
- Castrignanò, A., Buttafuoco, G., Quarto, R., Parisi, D., Viscarra Rossel, R.A., Terribile, F., Langella, G., Venezia, A. 2018.** A geostatistical sensor data fusion approach for delineating homogenous management zones in Precision Agriculture. Catena. 167: 293-304.
- Chlaib, H.K., Mahdi, H., Al-Shukri, H., Su, M.M., Catakli, A. and Abd, N., 2014.** Using ground penetrating radar in levee assessment to detect small scale animal burrows. Journal of applied geophysics. 103: 121-131.
- Cho, Y., Sudduth, K.A. and Chung, S. 2016.** Soil physical property estimation from soil strength and apparent electrical conductivity sensor data. Journal of Biosystems engineering. 152: 68 -78
- Conyers, L.B., 2013.** Ground penetrating radar for archeology. Rowman and Littlefield publishers, Alta Mira press, Latham, MD, USA.
- Daran, R. R. and Suat, I. 2014.** American Society of Agricultural and Biological Engineers 57: 1359-1373.

- Delbari, M., Afrasiab, P., and Loiskandl, W. 2011.** Geostatistical analysis of soil texture fractions on the field scale. *Soil Water Res.* 6: 173-189.
- Dhillon, S.R., Adamchuk, V.I., Holland, K.H. and Hempleman, C.R. 2010.** Development of an integrated on-the-go sensing system for soil properties. ASABE paper No.1009817. ASABE, St. Joseph, Mich.
- Doolittle, J., Zhu, Q., Zhang, J., Guo, L. and Lin, H. 2012.** Geophysical Investigations of Soil–Landscape Architecture and Its Impacts on Subsurface Flow. *Journal of Hydrogeology* 413–447.
- Francesco, B. and Fabio, T., 2013.** GPR spectral analysis for clay content evaluation by the frequency shift method. *Journal of applied geophysics* 97: 89-96.
- Franz, T.E., Zreda, M., Rosolem, R, and Ferre, T.P.A. 2013.** A universal calibration function for determination of soil moisture with cosmic-ray neutrons. *Journal of Hydrology Earth System Science.* 17:453–460.
- Giyoung, k. and Chase, M., 2013.** Soil organic matter sensing with an on-the-go optical sensor. *Journal of Biosystems engineering.* 115: 66-81.
- Giyoung, k., Chase, M. and Eric, L. 2013.** Soil organic matter and cation-exchange capacity sensing with an on-the-go electrical conductivity and optical sensor. *Journal of Biosystems engineering.* 199: 80-89.
- Grote, K., Anger, C., Kelly, B., Hubbard, S., and Rubin, Y. 2010.** Characterization of Soil Water Content Variability and Soil Texture using GPR Groundwave Techniques. *Journal of Environmental and Engineering Geophysics.* 15: 93–110.

- Hamon, T., Kvien, C., Mulla, D., Hoggenboom, G., Judy, J. and Hook, J. 2005.** Precision agriculture scenario P. Arzberger (Ed.), NSF workshop on sensors for environmental observatories, World Tech. Evaluation Center, Baltimore, MD, USA.
- Huisman, J., Snepvangers, J., Bouten, W. and Heuvelink, G., 2002.** Mapping spatial variation in surface soil water content: comparison of ground penetrating radar and time domain reflectometry. *Journal of hydrology*. 269: 194-207.
- Huang, Q., Akinremi, O.O., Sri Rajan, R. and Bullock, P. 2004.** Laboratory and field evaluation of five soil water sensors. *Canadian journal of soil science* 84: 431-438.
- Huisman, J.A., Hubbard, S.S., Redman, J.D. and Annan, A.P., 2003.** Measuring soil water content with ground penetrating radar: A review. *Vadose Zone J.* 2: 476-491.
- Jeffrey, D., Reza, M.E., Barry and J.A., 2008.** Ground penetrating methods (GPR). *Handbook of agricultural geophysics*.
- Joao S., Shakib, S. and Jose, M. 2014.** Spatial and temporal patterns of apparent electrical conductivity: DUALEM vs Veris sensors for monitoring soil properties. www.mdip.com/journal/sensors. ISSN 1424-8220.
- Jonard, F., Mohammad, M., Christian, R., Lutz, W., Frederic, A., Julien, M., Harry, V. and Sebastien, L., 2013.** Characterization of tillage effects on the spatial variation of soil properties using ground penetrating radar and electromagnetic induction. *Geoderma* 207: 310-322.
- Jonard, F., Weihermuller, L., Jadoon, K.Z., Schwank, M., Vereecken, H. and lambot, S. 2011.** Mapping field-scale soil moisture with L band radiometer and ground penetrating radar over bare soil. *IEEE transactions on geoscience and remote sensing* 49: 2863-2875.

- Kargas, G. and Kerkides, P. 2008.** Water content determination in mineral and organic porous media by ML2 theta probe. *Irrigation and drainage*. 57: 435-449.
- Kargas, G. and Kerkides, P. 2009.** Performance of the theta probe ML2 in the presence of nonuniform soil water. *Soil and Tillage research*. 103: 425-432.
- Kerr, Y.H., Waldteufel, P., Wigneron, J.P., Delwart, S., Cabot, F. and Boutin, J. 2010.** The SMOS Mission: New tool for monitoring developments of the global water cycle. *Journal of Hydrology*. 98: 666–687.
- Knadel, M., Thomsen, A., Schelde, K. and Greve, M.H. 2015.** Soil organic carbon and particle sizes mapping using vis–NIR, EC and temperature mobile sensor platform. *Journal of Computers and Electronics in Agriculture*. 114: 134–144.
- Lebron, I., Robinson, D.A., Goldberg, S. and Lesch, S.M., 2004.** The dielectric permittivity of calcite and arid zone soils with carbonate minerals. *Soil science society of America journal*. 68: 1549-1559.
- Liu, X., Dong, X. and Daniel, I.L., 2016.** Ground penetrating radar for underground sensing in agriculture: a review. *Journal of international agrophysics*. 30: 533-543.
- Lunt, I.A., Hubbard, S.S. and Rubin, Y., 2005.** Soil moisture content estimation using ground penetrating radar reflection data. *Journal of hydrology* 307: 254-269.
- Mahmood, H.S. 2013.** Proximal soil sensors and data fusion for precision agriculture. Master's thesis
- Mahmoudzdeh, M., Frances, A., Lubczynski, M. and Lambot, S., 2012.** Using ground penetrating radar to investigate the water table depth in weathered granites-Sardon case study. *Spain journal of applied geophysics*. 79: 17-26.

- Miller, B.A., 2012.** The need to continue improving soil survey maps. *Soil horizons* 53: 11-15.
- Minet, J., Bogaert, P., Vanclooster, M. and Lambot, S. 2012.** Validation of ground penetrating radar full-waveform inversion for field scale soil moisture mapping. *Journal of Hydrology*. 424: 112–123.
- Nocita, M., Stevens, A., Noon, C. and Van Wesemael, B., 2013.** Prediction of soil organic carbon for different levels of soil moisture using VIS-NIR spectroscopy. *Geoderma* 199: 37-42.
- Perron, I., Cambouris, A. N., Chokmani, K., Vargas Gutierrez, M. F., Zebarth, B. J., Moreau, G., Biswas, A. and Adamchuk, V. 2018.** Delineating soil management zones using a proximal soil sensing system in two commercial potato fields in New Brunswick, Canada. *Canadian Journal of Soil Science* 98(4):724-737.
- Ping, W., Zhenqi, H., Yanling, Z. and Xinju, L. 2016.** Experimental study of soil compaction effects on GPR signals. *Journal of Applied Geophysics*. 126: 128–137.
- Rial F.I., Pereira, M., Lorenzo, H., Arias, P., 2005.** Acquisition and synchronism of GPR and GPS data. Application on road evaluation. *In* L. Bruzzone (ed.) *Image and signal processing for remote sensing XI*. Article no. 598219, September 2006, Bruges, Belgium. *Proceedings of SPIE*. 5982: 20-22 The international society of optical engineering, Bellingham, WA.
- Rowlandson, T.L., Berg, A.A., Bullock, P.R., Ojo, E.R., McNairn, H., Wiseman, G. and Cosh, M.H. 2013.** Evaluation of several calibration procedures for a portable soil moisture sensor. *Journal of hydrology*. 498: 335-344.

- Saito, T., Yasuda, H., Sakurai, M., Acharya, K., Sueki, S., Inosako, K., Yoda, K., Fujimaki, H., Mohamed, A.M., Elbasit, A., Eldoma, A.M. and Nawata, H. 2016.** Monitoring of stem water content of native and invasive trees in Arid environments using GS3 soil moisture sensors. *Vadose zone journal*. 15.
- Salucci, M., Tenuti, L., Nardin, C., Oliveri, G., Viani, F., Rocca, P. and Massa, A., 2014.** Civil engineering applications of ground penetrating radar recent advances @ the ELEDIA research Centre. EGU general assembly conference abstracts, 1, 1945.
- Shahandeh, H., Wright, A.L. and Hons, F.M. 2011.** Use of soil nitrogen parameters and texture for spatially-variable nitrogen fertilization. *Precision Agriculture* 12: 146-163.
- Sudduth, K.A., Hummel, J.W. and Birrell, S.J., 1997.** Sensors for site-specific management. In: Pierce, F.J., Sadler, E.J. (Eds), *The state of site-specific management for agriculture*. ASA/CSSA/SSSA, Madison, WI 183-210.
- Sudduth, K.A., Kitchen, N.R., Bollera, G.A., Bullock, D.G. and Wiebold, W.J., 2003.** Comparison of electromagnetic induction and direct sensing of soil electrical conductivity. *Agronomy journal*. 95: 427-428.
- Sudduth, K.A., Kitchen, N.R., Wiebold, W.J., Batchelor, W.D., Bollero, G.A., Bullock, D.G., Clay, D.E., Palm, H.L., Pierce, F.J., Schuler, R.T. and Thelen, K.D. 2015.** Relating apparent electrical conductivity to soil properties across the north-central USA. *Journal of Computers and Electronics in Agriculture*. 46: 263-283.
- Veris 3100 (Veris Technologies, Salina, KS).
- Viscarra Rossel, R.A., Brus, D.J., Lobsey, C. and Shi, Z. 2016.** Baseline estimates of soil organic carbon by proximal sensing: Comparing design-based, model-assisted and model-based inference. *Geoderma*. 265. 152–163.

Wetterlind, J. 2009. Improved Farm Soil Mapping Using Near Infrared Reflection Spectroscopy. PhD thesis.

Wijewardana, Y., Galagedara, L., Mowjood, M. and Kawamoto, K., 2015. Assessment of inorganics pollutant contamination in ground water using ground penetrating radar. Tropical agricultural research. 26: 700-706.

www.veristech.com.

2. SPATIAL VARIABILITY OF BULK DENSITY AND SOIL MOISTURE ON A LOAMY SAND OVER THE ASSINIBOINE DELTA AQUIFER

2.1. Abstract

The knowledge of spatial and temporal variation of bulk density and soil water content within a field provides prospects for precision agriculture soil management. The objectives of this study were to investigate the spatial distribution of bulk density with depth and compare the spatial pattern of soil moisture in two seasons (Spring 2014 and Fall 2017). The study was carried out at Carberry, over the Assiniboine Delta Aquifer, on an Orthic Black Chernozem. One hundred and seventy-eight soil cores were sampled in spring of 2014 using a geospatial sampling scheme. Bulk density and soil moisture were determined from fifty (50) of the 179 sampling points in fall 2017. Soil samples were taken from 0-90 cm depth with a Giddings hydraulic punch in a 7.6 cm plastic sleeve. Spatial dependence and variability of bulk density and soil moisture were calculated with kriging and assessed with semi variograms using a Geostatistical software (GS+). Bulk density was strongly spatially correlated from the top soil to the 75 cm depth, and moderately correlated at the 75-90 cm depth. Soil moisture was strongly spatially correlated from the top soil to the 75 cm depth in both seasons. Below the 75 cm depth, soil moisture was weakly to moderately spatially correlated in both seasons. The spatial pattern of soil moisture content was temporally invariant as similar spatially coherent regions were found in both seasons for soil moisture. We concluded that variation of bulk density and soil water content exists within the field and at various depths and that the stability in the spatial pattern of soil water content with time was due to soil texture.

2.2. Introduction

Spatial variability occurs when a property that is measured at distinct spatial locations shows values that vary across the locations. Variation can occur in space and time (spatio-temporal). This variability occurs naturally in soil properties because of the various processes of soil formation (Silva et al., 2016). Aside from natural soil formation, Ozgoz (2009) stated that variation can occur due to tillage effect and field management. The knowledge of spatial variability is crucial in defining relationships between soil properties, identifying factors influencing these properties, and developing management practices to maintain soil productivity (Barik et al., 2014), modelling soil processes at scales applicable to decision makers (Stacey et al., 2018), and precision farming (Cassel et al., 2000).

Spatial variability of soil properties across fields affects crop yield potential, available water, and other site-specific management zones. In quantifying soil spatial variability, it is crucial to divide the site into management zones according to their levels of productivity (Khosla et al., 2002). Mzuku et al., (2005) stated that the knowledge of the roles and interactions of various soil properties can be beneficial in explaining the causes of variation. Productivity of soil is greatly dependent on the varying soil properties within a field (Usowicz and Lipiec, 2017), as it can lead to variability in crop yield (Diacono et al., 2013).

Several studies have investigated the spatial and temporal variation in soil properties. A study by Tagliarolo et al., (2018) investigated the spatial and temporal variability of carbon budgets of shallow South African subtropical estuaries and found that carbon fluxes in sub-tropical estuaries are highly variable in space and time. Gilsonley et al., (2016) reported the influence of landscape curvature on the spatial variability of soil physical and chemical properties.

Spatial variability of soil moisture has been investigated by various researchers (Niether et al., 2017; Fu et al., 2018). Liao et al., (2017) detected spatio-temporal variability of soil moisture content on two contrasting land use hillslopes, where the spatial variability of tea garden hillslope was stronger than the forest hillslope. Neves et al., (2016) investigated the spatial and temporal patterns of soil water content in an agroecological production system, where they reported variation of soil moisture and clay content with depth, and the effect of tillage on the top soil. Spatial variability of physical and chemical soil properties in semi-arid regions was reported by (Diego et al., 2017), and in desert riparian forests (Ding et al., 2017) where they found that spatial variation of bulk density, organic carbon, soil moisture and soil particle distribution are the main factors influencing the spatial variation of these areas. Fu et al., (2017) reported the spatial distribution of soil moisture in different types of sand dunes, where the spatial distribution of soil moisture in the various dunes occurs in relation to the degree of fine particle content.

The bulk density of the soil influences several soil and plant processes such as movement of air and water, compaction, and seedling emergence (Timm et al., 2006). Soil bulk density is an important criterion for evaluating the quality and productivity of soil (Suuster et al., 2011). Bulk density has been observed to have a significant effect on erosion, soil water retention, infiltration (Geng et al., 2014), and organic-carbon stocks (Sequeira et al., 2014). Soil bulk density has been well known to vary significantly within a single field (Ozgoz, 2009). Alletto and Coquet (2009) reported that one of the major sources of variability of bulk density is temporal effect, where the timing of tillage activities corresponding to the time of soil sampling has a strong impact on soil bulk density. Recent studies have shown several factors that can result in spatial variability of bulk density across the field.

Barik et al., (2014) reported that a change in spatial variability of bulk density, aggregate stability, total porosity, and volumetric water content can exist due to field traffic operations. Field traffic operations increase soil bulk density and decrease total porosity. Texture has been reported to be a prime factor affecting the spatial distribution of bulk density even at depth (Yao et al., 2006). Soil bulk density can be estimated using other soil property such as soil moisture content. Zhao et al., (2018) reported that the distribution of bulk density can be estimated using soil moisture content. Spatial variability of bulk density has been studied within field. Silva et al., (2016) investigated the spatial variability of bulk density in Archeological dark earth sites under Cacao cultivation and observed the influence of organic carbon content on soil bulk density.

Soil moisture is an essential variable in water management of the field (Neves et al., 2017). It is also crucial in the distribution of vegetation in arid and semiarid regions (Guo et al., 2017), and acts as a vector between soil plant-atmosphere systems (Arriaga and Rubio, 2017). The knowledge of the spatial and temporal variation of moisture is important in the management of water in the field (Neves et al., 2017), understanding of land surface processes (Lin, 2011), vegetation restoration in terraces (McVicar et al., 2010), and ecosystem sustainability (Yu et al., 2018).

Defining the spatio-temporal variation of soil moisture under field conditions is of importance in Precision Agriculture (Wang et al., 2015). Numerous factors, either singly or in combination, affect the variability of soil moisture under field conditions (Vanderlinden et al., 2012). Yang (2017) reported that aside from vegetation, soil texture and topography were the primary variables having a significant effect on soil moisture variability. A study by Garnaud et al (2017) carried out in Quebec, Canada showed that in drier periods, vegetations, organic matter, and rock fractions affects moisture significantly other than soil texture, but in wet periods,

texture is a crucial factor with respect to the variability of soil moisture. Cho and Choi (2014) reported that meteorological factors also affect the spatio-temporal variability of soil moisture content. An increase in soil depth under shrubland, crop land and fallow land can result in a decrease in variation of soil water content with depth (Zhao et al., 2017; Xu et al., 2017; Yu et al., 2018). Soil texture affects the spatial and temporal variability of moisture content (Miller and Loheide, 2015; Wei et al., 2017; Yongseok and Sanghyun, 2017). Furthermore, Neves et al., (2017) studied the correlation between soil texture (clay) and soil water content and reported that spatial distribution of soil water content is related to soil texture, and the effect of clay content depends on the amount of soil moisture irrespective of the soil profile. Vivakanahan et al. (2018) observed high soil moisture content in regions with high clay content. Spatio-temporal variability in soil moisture content has been used in calibrating soil moisture sensors data (Jacobs et al., 2010; Dorigo et al., 2013;). Temporal variability has been established to be higher in the dry season than in the wet season (Martinez et al., 2013).

Geostatistics, which is based on a probabilistic model, is a widely used method to study and quantify spatial variability in soil science, especially in precision farming, and for the interpretation of semivariograms (Barik et al., 2014). Over the years, this technique has been relevant in investigating soil physical and chemical properties (Diego et al., 2017). Geostatistics has been an important mathematical tool in determining the variation that occurs in soil due to the complex nature of soil (Oliver and Webster, 2014). Zhao et al., (2018) used geostatistical techniques to predict spatial variability of soil bulk density in gravel-mulch fields. Diego et al., (2017) used Geostatistics to determine the spatial variability of soil attributes in the semi-arid regions. Geostatistics has been used on sandy soils to determine the spatial variability of soil physical and chemical properties (Usowicz and Lipiec, 2017).

Geostatistics have been reported to suitably represent the spatial variation of soil properties during mapping. Coefficient of variation (CV) has also been used to investigate spatio-temporal variability of soil properties (Manns et al., 2014; Zhao et al., 2017) although it does not give a corresponding estimate with space like the geostatistical tools (Duffera et al., 2007). Semivariogram has been proven by researchers as an excellent tool for investigating spatial variability. Ceddia et al., (2009) used Semivariogram to investigate the spatial variability that occurs in elevations and soil characteristics. Zhao et al., (2018) investigated the spatial variability of soil bulk density in gravel-mulched fields using Semivariogram with kriging. Spatial dependency has been reported to be strong for various soil properties by several researchers (Liao et al., 2017; Usowicz and Lipiec, 2017; Qiao et al., 2018). Spatial dependence is important in executing a good interpolation when producing maps. Xu et al., (2017) reported a strong spatial dependency for soil moisture content during the whole year and in the rainy season. A strong spatial dependence was observed in clay and sand content, and penetration resistance (Ozgoz 2009).

Kriging, which is used to interpolate and generate maps has been applied in environmental science analysis to help solve precision agriculture problems, especially for unsampled points. According to Oliver and Webster (2014), kriging is more popularly used due to its unbiased linear predictions with minimum errors. A study carried out by Zhao et al., (2018) reported the effectiveness of kriging in estimating the spatial distribution of soil bulk density. Kriging was used in establishing the spatial variability that occurred in a compacted field due to traffic operations (Barik et al., 2014). Silva et al., (2016) analysed the spatial variability of physical properties of cohesive soil under conventional and no-tillage management systems using Semivariogram parameter and ordinary kriging geostatistical interpolation.

The soil overlying the Assiniboine Delta Aquifer (ADA) has been reported to be susceptible to leaching (Nikiema et al., 2013; Vivekanahan, 2018). Vivekanahan et al. (2018) reported the spatial variability of soil texture within the field, and the influence it had on soil moisture content with depth, and the amount of leachate produced. This study was a follow up of Vivekanahan et al. (2018) to see if the pattern of soil moisture that was measured in 2014 persisted to 2017. Vivekanahan et al. (2018) did not measure the spatial variability of bulk density with depth, and we are not aware of studies that mapped the spatial variability of bulk density on a Canadian Prairies with depth. Therefore, the objectives of this study were

- (a) to investigate the spatial distribution of bulk density with depth
- (b) to compare the spatial pattern of soil moisture in two seasons (Spring 2014 and Fall 2017).

Hypothesis: Spatial variability occurs in soil bulk density and moisture content, both horizontally and with depth.

2.3. Materials and methods

2.3.1. Study area description

The study was carried out on a farmer's cooperator field that is located about 10 km, northwest of Carberry in Southwestern Manitoba, Canada (SW-19-11-15W). The region is characterized by an average annual precipitation of 456 mm, with approximately 70 % falling as rain from April-October and 30 % as snow during the winter months and mean annual temperature of 2.1 °C. The site is located over the Assiniboine Delta Aquifer, an unconfined aquifer that is the source of drinking water. The site consists of Orthic Black Chernozem soils, which developed on lacustrine deposits. These are medium textured, well drained soils, where the upper (0 - 90 cm) depth is classified as loamy sand, and the underlying layer (> 90 cm) is sandy loam to loam. Sand content decreases with depth, from about 78% in the upper layer (0-10 cm) (Vivekanahan et al., 2018), while pH increases with depth from 6.37 at the surface layer to 8.33 at the 120 cm depth, and bulk density also gradually increases from 1.31 Mg m⁻³ at the top soil to 1.50 Mg m⁻³ at the 120 cm depth (Enns, 2004).

The experimental field was 65 × 55 m (0.36 ha) in size. The cropping system was a barley-wheat rotation with conventional agronomic management.

2.3.2. Sampling scheme and soil sampling

Vivekanahan et al. (2018) used a method developed by Zar (2010) to determine the number of sampling points (178) for analysis using the variability of sand percentage at 0 - 10 cm and 60 - 90 cm depth of the field. We selected fifty (50) sampling points from the 178 sampling points as the number of samples required to identify significant difference based on variability of bulk density at the site. This was calculated using the bulk density data obtained in 2001 (Enns, 2004) and the preliminary bulk density data for this study acquired in August 2017. Fifty samples were required to detect the variability at 1 % difference with the power of test of 0.8.

The geospatial sampling scheme showed the 178 sampling points used in the Spring of 2014 and the 50 sampling points (shown in circle in Figure 2.1) used in the Fall of 2017. The details of the 2014 soil sampling campaign were described by Vivekanahan et al., (2018). In the Fall of 2017, the site was surveyed, field boundaries were marked and spatial coordinates for each sample points were recorded. In each of the 50 sampling points, Universal Transverse Mercator (UTM) coordinates were measured using a GPS. Undisturbed soil samples were taken from 0 - 90 cm depth in 3" plastic sleeves with a Giddings hydraulic soil punch. After the soil samples were collected, they were stored in totes containing ice during transport to the laboratory and immediately stored in the refrigerator (4 °C) on arrival to prevent moisture loss.

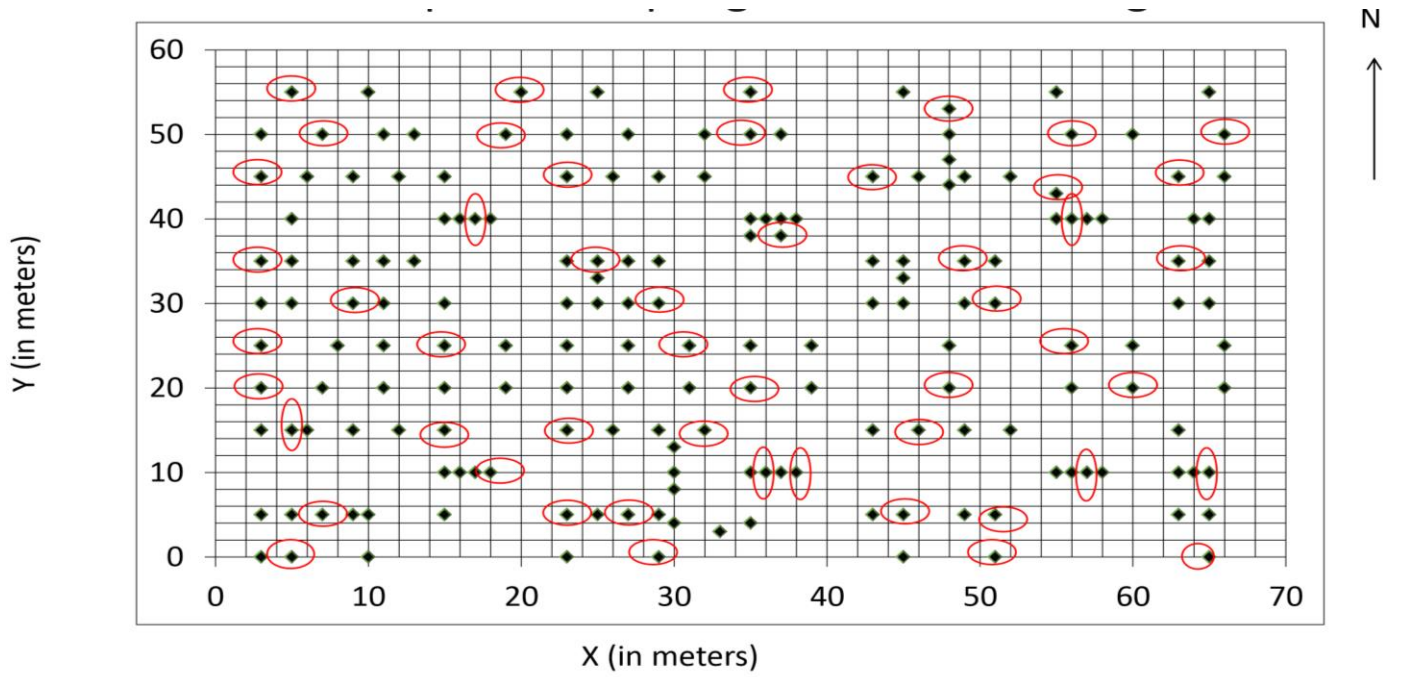


Figure 2.1. Geospatial soil sampling design for the study area in the Spring of 2014 \blacklozenge and the selected 50 sampling points for Fall 2017 \blacklozenge

2.3.3. Laboratory analysis and calculations

The soil in the sleeve was divided into six depths at 15 cm interval (0-15 cm, 15-30 cm, 30-45 cm, 45-60 cm, 60-75 cm, 75-90 cm). The total wet weight of each sample was measured and a subsample (50 g) was taken for moisture content determination by drying in an oven (105 °c) for 48 hours (Gardner, 1986). Gravimetric water content and bulk density were calculated as follows.

$$\theta_g = \frac{M_w}{M_s} \quad (1)$$

where M_s is the mass of dry soil, M_w is the mass of water, and θ_g is the gravimetric water content.

$$\rho_b = \frac{M_s}{V_t} \quad (2)$$

Bulk density (ρ_b) was calculated as the ratio of the total mass of the dry soil (M_s) to the total volume of the soil (V_t). The total volume of soil was calculated using the formula for volume of a cylinder, $\lambda r^2 h$.

2.3.4. Statistical and Geostatistical analysis

Descriptive statistical parameters such as the mean, standard deviation, test for normality were carried out with SAS 9.4 (SAS Institute Inc, 2014) software. Data must be normally distributed before it can be analysed for geostatistical modelling (Moulin et al., 2014). While the bulk density data was normally distributed, soil moisture content was not (Shapiro-Wilk) and was transformed using the Johnson SI in JMP software (Moulin et al., 2011). The spatial and temporal dependence of bulk density and soil moisture content at this site was analyzed using semivariograms (Liao et al., 2017).

All the Geostatistics computations were conducted using the GS + version 10.0 (Gamma Design Software LLC., Plainwell, MI, USA). Four semi-variogram models (exponential, gaussian, linear and spherical) were calculated with the experimental data, and the best-fitted model with the lowest residual sum of squares for predictions and largest coefficient of determination was identified (Oliver and Webster, 2014; Wang et al., 2018). Geostatistical parameters; sill ($C + C_0$), nugget (C_0), and range, were obtained. The sill is the sum of the nugget and the spatial variability. The nugget estimates the spatial variability at distances closer than the minimum sampling space. The range shows the distance at which the sampling points are spatially correlated with each other. The ratio of the spatial variability and the sill is the proportion of total variability which is explained by the spatial autocorrelation (Bong et al., 2018). Kriging, a regression method, provides a means of interpolating values for points not physically sampled. Ordinary kriging was used to interpolate and generate maps of bulk density and soil water content for this study (Diego et al., 2017).

2.4. Results

2.4.1. Bulk density

The descriptive statistics for soil bulk density is summarized in (Table 2.1). The mean bulk density (g cm^{-3}) increased with soil depth. Enns (2004) also reported similar variability for bulk density at this site.

Table 2.1. Descriptive summary statistics of bulk density sampled in the Fall of 2017.

Depth (cm)	Mean (g cm^{-3})	Standard deviation	Coefficient of variation	Skewness	Minimum (g cm^{-3})	Maximum (g cm^{-3})
0-15	1.34	0.10	7.5	0.2	1.11	1.59
15-30	1.44	0.15	10.1	-0.1	1.17	1.68
30-45	1.46	0.09	6.8	-0.3	1.24	1.63
45-60	1.47	0.10	6.8	-0.5	1.23	1.69
60-75	1.47	0.13	8.6	-0.3	1.16	1.70
75-90	1.48	0.13	8.8	-0.4	1.17	1.75

Unlike the mean, there was no consistent pattern of the coefficient of variation (CV) with depth. The CV is an important measure of precision, as it contains all the variation due to experimental error. The lower the CV, the higher the precision of the experiment. The 30-60 cm depth had the lowest CV, while the 15-30 cm depth had the highest CV. Overall, the CV of bulk density was low at this site according to the classification of Warrick and Nielson (1980), who classified CV <12 % as low; between 12 and 60 as medium; and CV > 60 % as high (Table 2.1). The range between the minimum and maximum values increased with depth. For example, the range of bulk density at the surface (0-15 cm) depth was 1.11 g cm^{-3} to 1.59 g cm^{-3} and 1.23 g cm^{-3} to 1.69 g cm^{-3} at the depth of 45 cm, further increasing to 1.17 g cm^{-3} and 1.75 g cm^{-3} at the depth of 90 cm.

The skewness of bulk density varied between -1 and +1. The highest skewness of bulk density data (-0.5) was observed at the 45-60 cm depth. Bulk density was strongly spatially auto-correlated from the top soil to the 75 cm depth, and moderately auto-correlated at the 90 cm depth (Table 2.2). The Nugget value was close to zero, which indicates that the experimental error is null, with the presence of variation at distances closer than the minimum sampling space used. Best-fit semi variograms for bulk density were obtained using Gaussian and Exponential models, and the spatial dependence was strongly and moderately auto-correlated (spatial dependency greater than 75 %, and between 25 -75 % respectively).

The coefficient of determination (R^2), which reflects the significance of the fit of the model to the semi-variogram data, increased from the top soil to the 75 cm depth (Table 2.2.). The R^2 value is not as sensitive as the residual sum of squares for best-fit calculations. The residual sum of squares indicates how well the model fits the data. The lower the residual sum of squares, the better the model fits. GS+ version 10 (Gamma Design Software LLC., Plainwell, MI, USA) uses the residual sum of squares to calculate the model parameter.

Table 2.2. Parameter for semi-variogram models of bulk density along the soil depth (Fall 2017)

Depth (cm)	Variogram (model) *	Nugget variance (Co)	Sill (Co+C)	C/C+Co ** (%)	R ²	RSS ***	Spatial class ****
0-15	Exponential	0.002	0.012	81	0.81	8.74x10 ⁻⁶	S
15-30	Gaussian	0.006	0.041	86	0.98	8.80x10 ⁻⁶	S
30-45	Gaussian	0.002	0.017	86	0.98	2.51x10 ⁻⁶	S
45-60	Gaussian	0.003	0.031	89	0.98	1.68x10 ⁻⁶	S
60-75	Gaussian	0.003	0.027	90	0.99	2.82x10 ⁻⁶	S
75-90	Exponential	0.011	0.032	70	0.89	5.07x10 ⁻⁶	M

* Models are all isotropic

** Nugget to sill ratio (%) = (Nugget semivariance / total semivariance) X 100

*** Residual sum of squares

****S = Strong spatial dependency (C/C+Co % > 75); M = Moderate spatial dependency (C/C+Co % between 75 and 25) Chien et al., (1997).

Maps calculated with point kriging (Figure 2.2) show variability in bulk density within the field at the soil surface. The map can generally be divided into three regions, with the North-East region having a lower bulk density ranging from 1.25-1.30 g cm⁻³ compared to the middle of the field with a moderate bulk density ranging from 1.32-1.34 g cm⁻³, and the South-West region having a high bulk density ranging from 1.36-1.41 g cm⁻³.

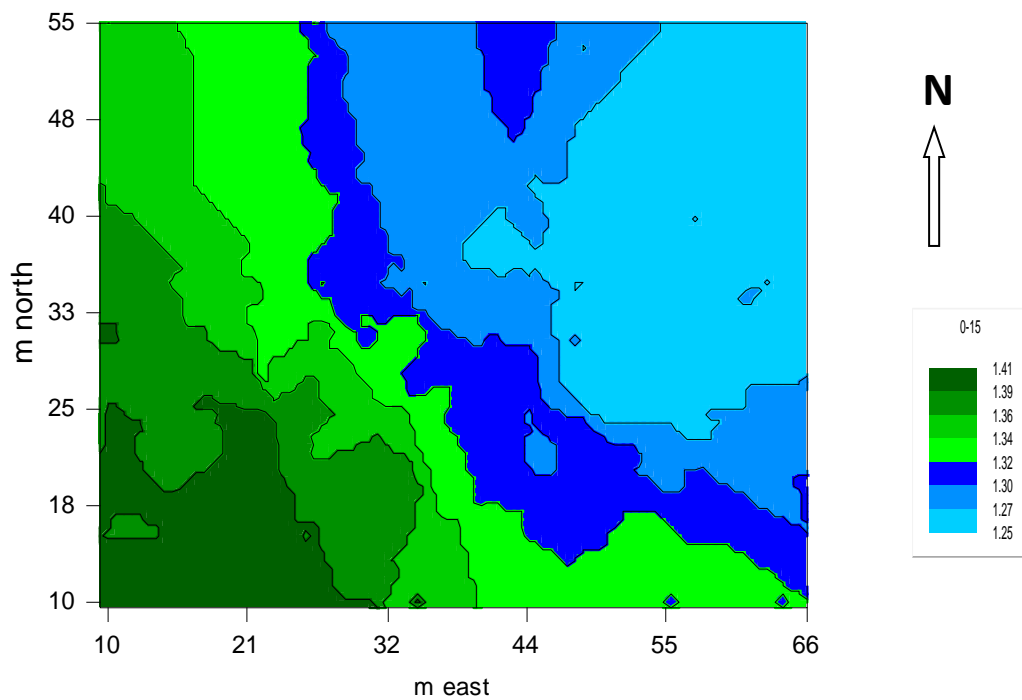


Figure 2.2. Kriged map of bulk density at 0-15 cm depth across the field.

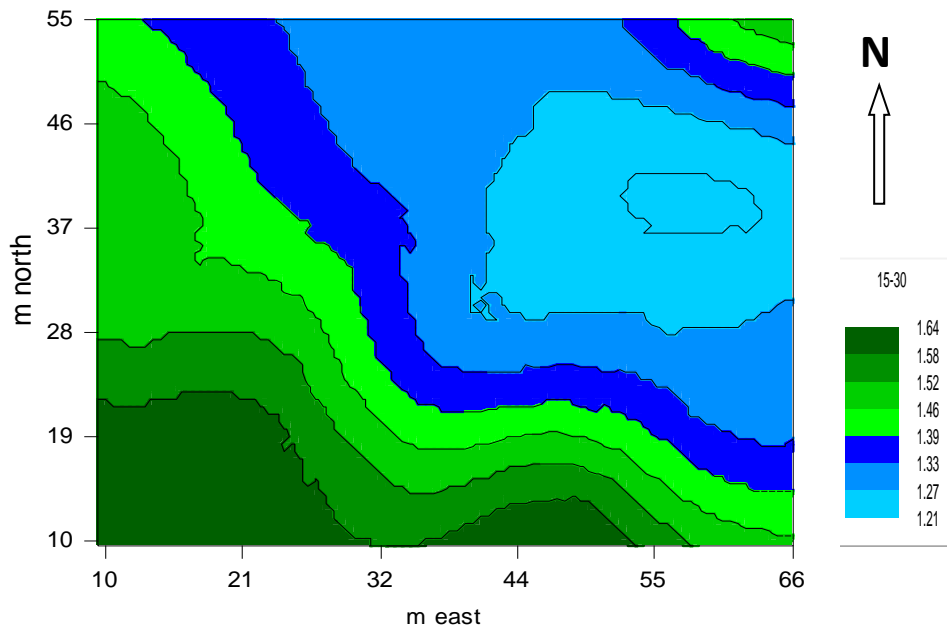


Figure 2.3. Kriged map of bulk density at 15-30 cm depth across the field

A similar trend was observed in the 15-30, 30-45, and 45-60 cm depth intervals with three distinct regions similar to the spatial pattern of the top soil (Figure 2.3, 2.4, and 2.5). Bulk density increased with depth at the 45-60 cm depth (Figure 2.5) relative to the 30-45 cm depth (Figure 2.4). Bulk density also increased with depth from the 60-75 cm depth interval to the 75-90 cm depth. For example, a larger portion of the map in the 75-90 cm depth showed the Southern region with higher bulk density compared to the Southern region of the 60-75 cm depth. The lowest bulk density value for the 75-90 cm depth was higher (1.37 g cm^{-3}) than the lowest bulk density value for the 60-75 cm depth (1.24 g cm^{-3}). The 75-90 cm depth (Figure 2.7) was less spatially coherent than the 60-75 cm depth (Figure 2.6). In general, bulk density was spatially correlated across the field and at various depth intervals, and short scale spatial variability increased with depth.

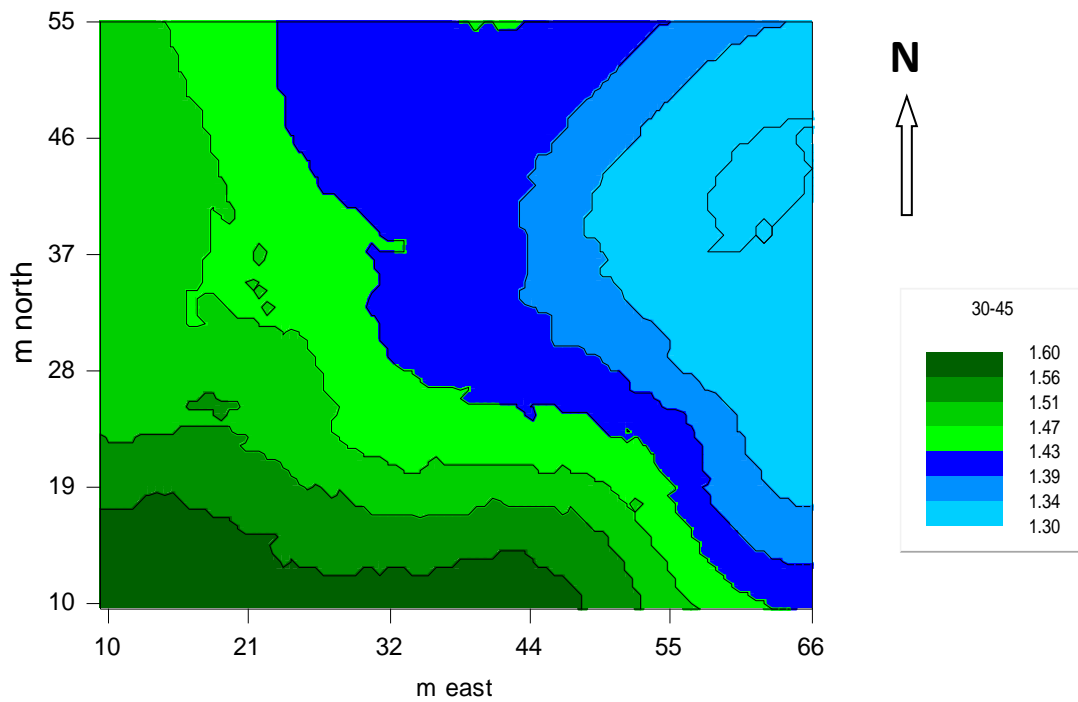


Figure 2.4. Kriged map of bulk density at 30-45 cm depth across the field.

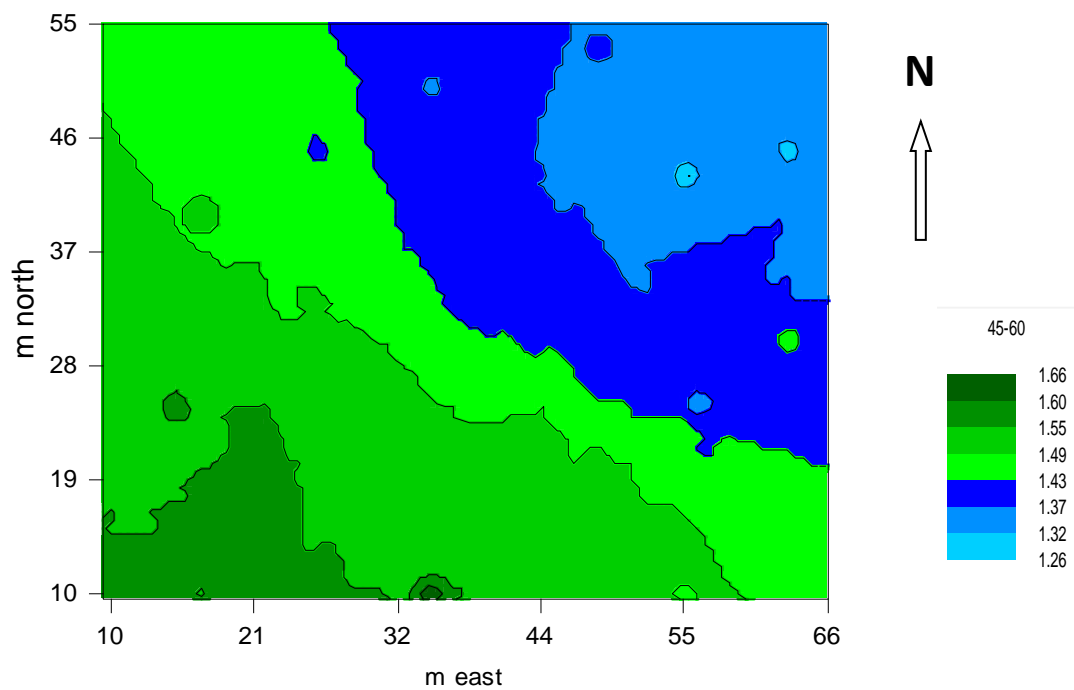


Figure 2.5. Kriged map of bulk density at 45-60 cm depth across the field.

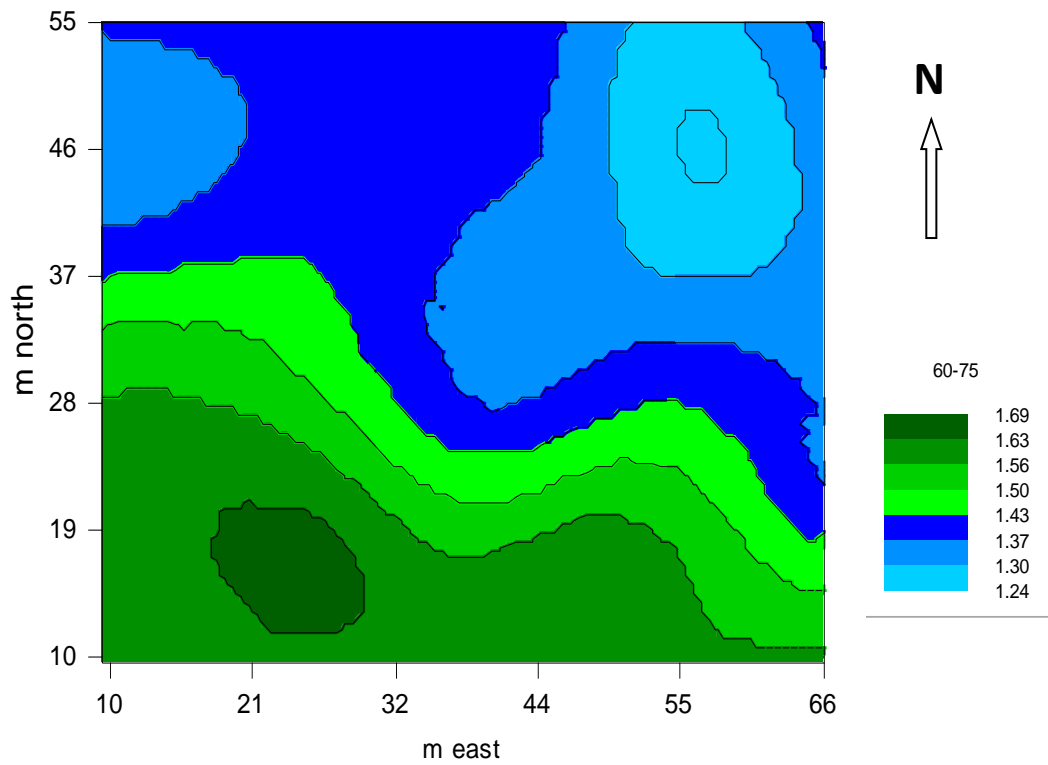


Figure 2.6. Kriged map of bulk density at 60-75 cm depth across the field.

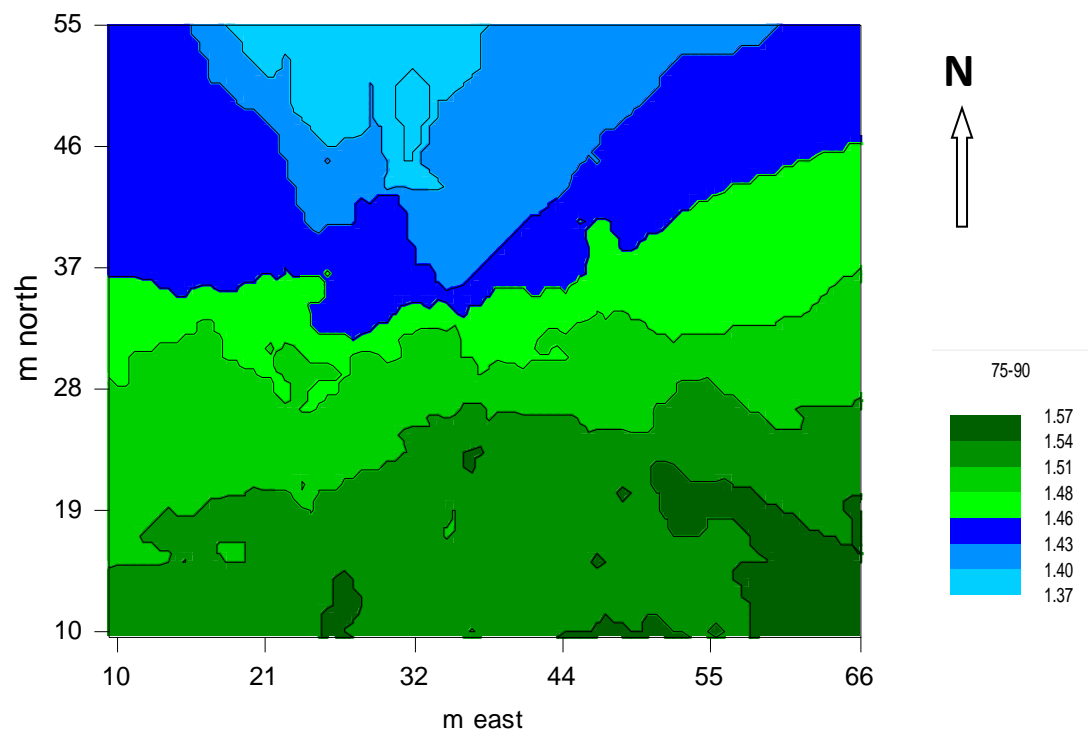


Figure 2.7. Kriged map of bulk density at 75-90 cm depth across the field.

2.4.2. Soil water content

Soil moisture content, measured in two field campaigns in Spring 2014 and Fall 2017, did not change with depth. Soil moisture content was measured just after snow melt in the Spring of 2014 (Vivekanahan, et al., 2018).

Table 2.3. Descriptive summary statistics of soil gravimetric moisture content sampled in the Fall of 2017.

Depth (cm)	Mean (g g⁻¹)	Standard deviation	Coefficient of variation	Skewness	Minimum (g g⁻¹)	Maximum (g g⁻¹)
0-15	0.15	0.04	25.5	0.9	0.09	0.28
15-30	0.14	0.05	36.2	0.6	0.06	0.29
30-45	0.12	0.05	39.7	0.6	0.03	0.25
45-60	0.11	0.05	48.3	1.1	0.04	0.27
60-75	0.12	0.07	59.0	0.7	0.03	0.30
75-90	0.15	0.07	51.1	0.4	0.03	0.32

The soil water content of the six soil depths ranged from 0.11 g g⁻¹ to 0.15 g g⁻¹ in the Fall of 2017 (Table 2.3). The coefficient of variation for soil moisture content in Fall of 2017 increased with increasing soil depth. The coefficient of variation for soil moisture in the Fall of 2017 was moderate with depth, according to the classification of (Warrick and Nielson, 1980). The increase in the coefficient of variation and standard deviation indicated an increase in variability with depth. The minimum soil water content decreased with depth, while the maximum values increased with depth. Skewness varied between 0 and +1. The highest skewness for gravimetric moisture content was at the 45-60 cm depth, similar to that of bulk density.

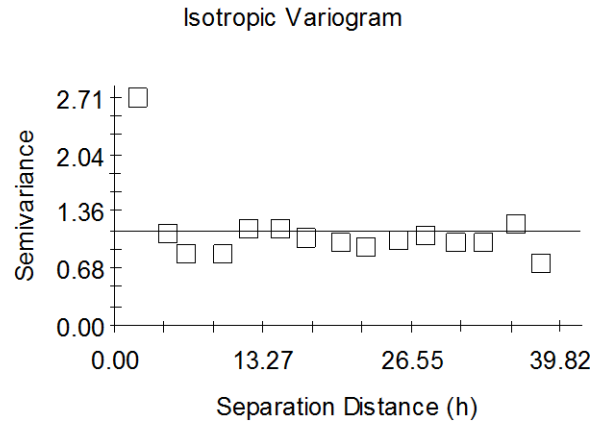
Table 2.4. Parameter for Semivariogram models of soil water content (Fall, 2017) along the soil depth.

Depth (cm)	Variogram (model) *	Nugget variance (Co)	Sill (Co+C)	C/C+Co %	RSS **	Range (m)	Spatial class ***
0-15	Gaussian	0.2	2.52	89	0.38	83.2	S
15-30	Gaussian	0.2	2.50	90	0.25	84.5	S
30-45	Gaussian	0.3	2.79	88	0.34	96.9	S
45-60	Gaussian	0.4	2.89	84	0.56	102.1	S
60-75	Gaussian	0.3	2.71	87	0.91	97.2	S
75-90	Linear	1.1	1.12	00	2.96	38.2	W

* Models are all isotropic ** Residual sum of squares

***S = Strong spatial dependency ($C/C+Co$ % > 75; W = Weak spatial dependency ($C/C+Co$ % < 25. Chien et al., (1997).

(Table 2.4) shows the geostatistical parameter for soil moisture content for Fall 2017. Soil moisture content was strongly spatially correlated from the top soil to the 75 cm depth, as indicated by the Gaussian semivariograms, (as observed for bulk density), and a shift from Gaussian to the Linear model, with the linear model weakly correlated. The proportion of total variance explained by spatial variability ($C/C+Co$) decreased with depth such that at the 75-90 cm, a pure nugget effect was observed (Figure 2.9). The range, which is the separation distance over which the spatial dependence is evident, increased with soil depth with the highest range at the 45-60 cm depth, and the lowest at the 75-90 cm depth.



Linear model ($C_0 = 1.11836$; $C_0 + C = 1.11836$; $A_0 = 38.19$; $r^2 = 0.180$;
 RSS = 2.96)

Figure 2.8. Fitted theoretical semivariograms for soil moisture content at depth 75-90 cm

Table 2.5. Parameter for variogram models of soil water content (Spring, 2014) along the soil depth (Vivekanahan et al., 2018).

Depth (cm)	Variogram (model) *	Nugget variance (Co)	Sill (Co+C)	C/C+Co %	Range (m)	Spatial class **
0-15	Gaussian	0.1	2.2	96	64.1	S
15-30	Gaussian	0.1	2.2	95	65.8	S
30-45	Gaussian	0.2	1.7	89	51.5	S
45-60	Gaussian	0.3	1.8	85	59.2	S
60-75	Gaussian	0.4	1.5	75	55.8	S
75-90	Exponential	0.4	1.2	64	56.9	M

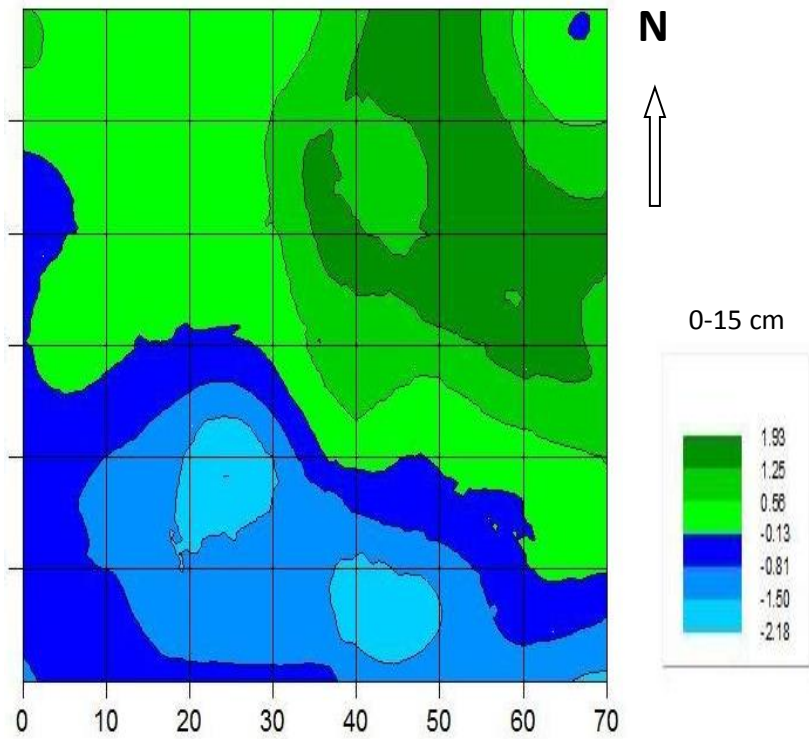
* Models are all isotropic

**S = Strong spatial dependency ($C/C+Co$ % > 75); M = Moderate spatial dependency ($C/C+Co$ % between 75 and 25). Chien et al., (1997).

The nugget effect in both seasons (Spring and Fall), increased with depth (Table 2.4 and 2.5). The sill values in the Spring of 2014 decreased with depth while in Fall 2017 it increased up to the 75 cm depth. The spatial dependencies ('nugget-to-sill') for both seasons decreased with depth. The effective range of the spatial dependency increased with depth for Fall 2017 and decreased with depth for Spring 2014. The ranges for soil moisture content was generally higher in Fall 2017 than in Spring 2014. Soil moisture was strongly spatially correlated from the top soil to the 75 cm depth, and moderately correlated at the 90 cm depth in Spring 2014. A weak correlation at the 90 cm depth was observed in Fall 2017.

The spatial pattern of soil moisture in both seasons was similar as they both had the same regions with high and low soil moisture content (Figure 2.10). The geospatial pattern of soil moisture in both seasons is a mirror image of bulk density as the North-East region with low bulk density have higher moisture content, and the South-West region with high bulk density have lower moisture content (Figure 2.10). At the 90 cm depth, soil water was spatially incoherent (Figure 2.13), unlike what we observed at the other depths.

a. Spring 2014



b. Fall 2017

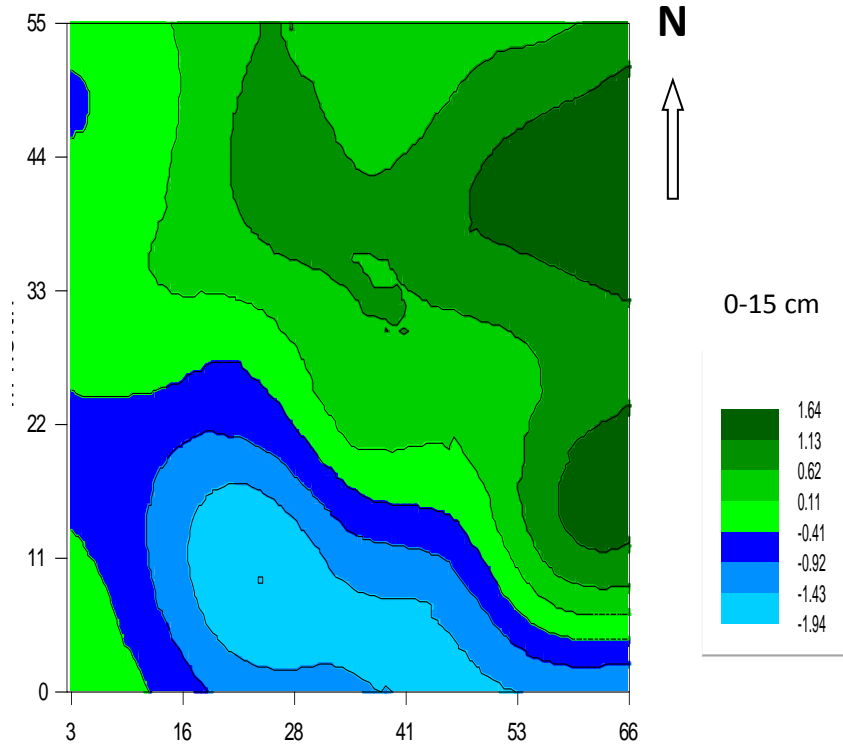
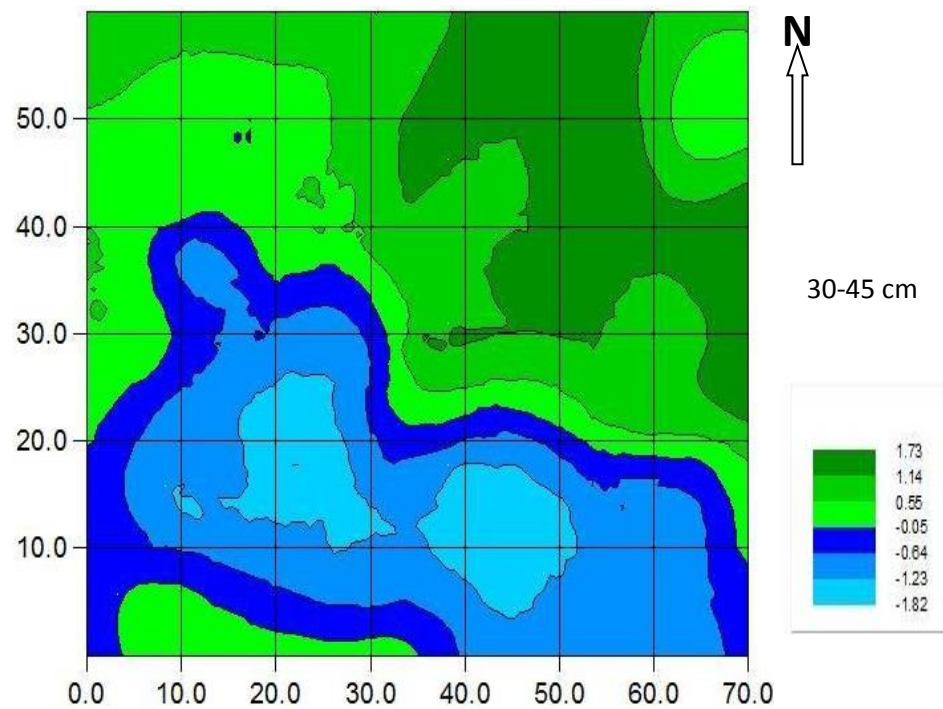


Figure 2.9. Kriged map of soil water content (Johnson SI transform) at 0-15 cm depth across the field for (a) Spring 2014 (b) Fall 2017.

a. Spring 2014



b. Fall 2017

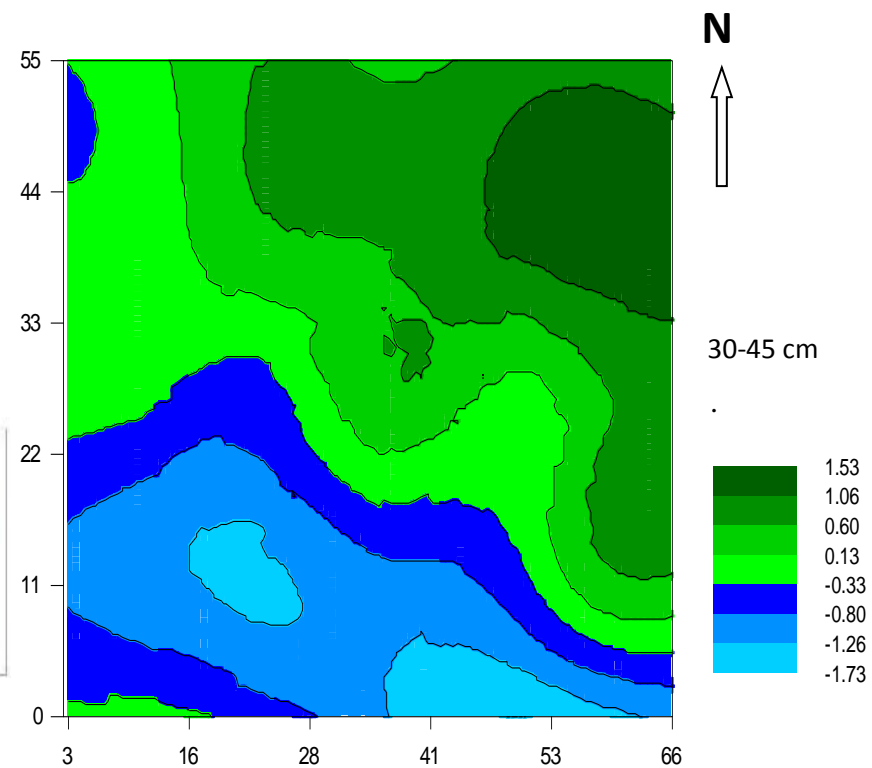
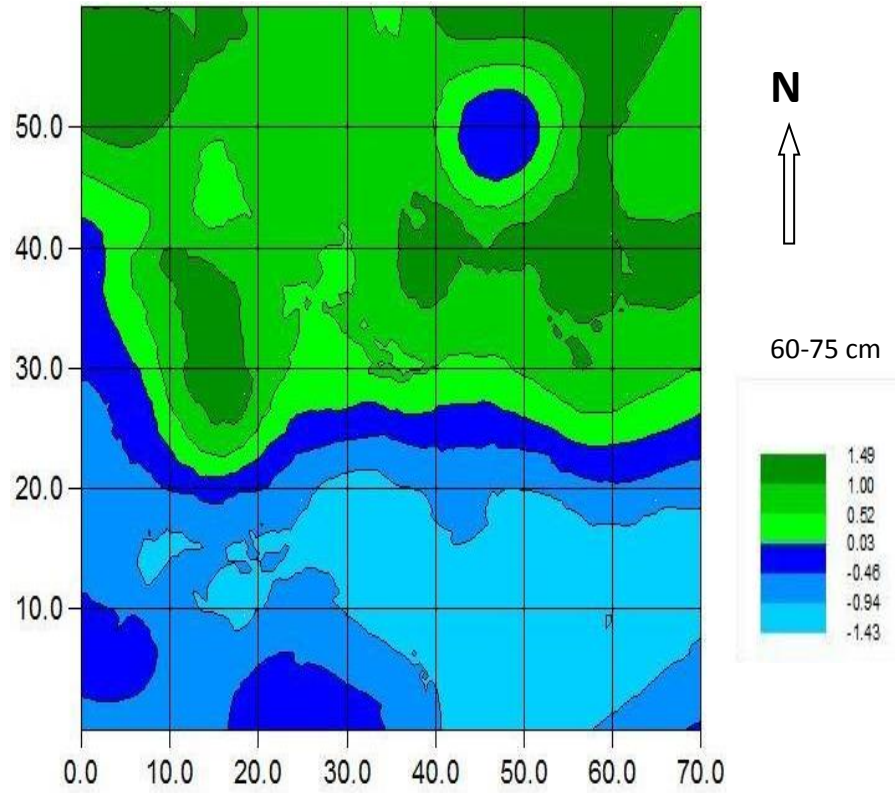


Figure 2.10. Kriged map of soil water content (Johnson SI transform) at 30-45 cm depth across the field for (a) Spring 2014 (b) Fall 2017.

a. Spring 2014



b. Fall 2017

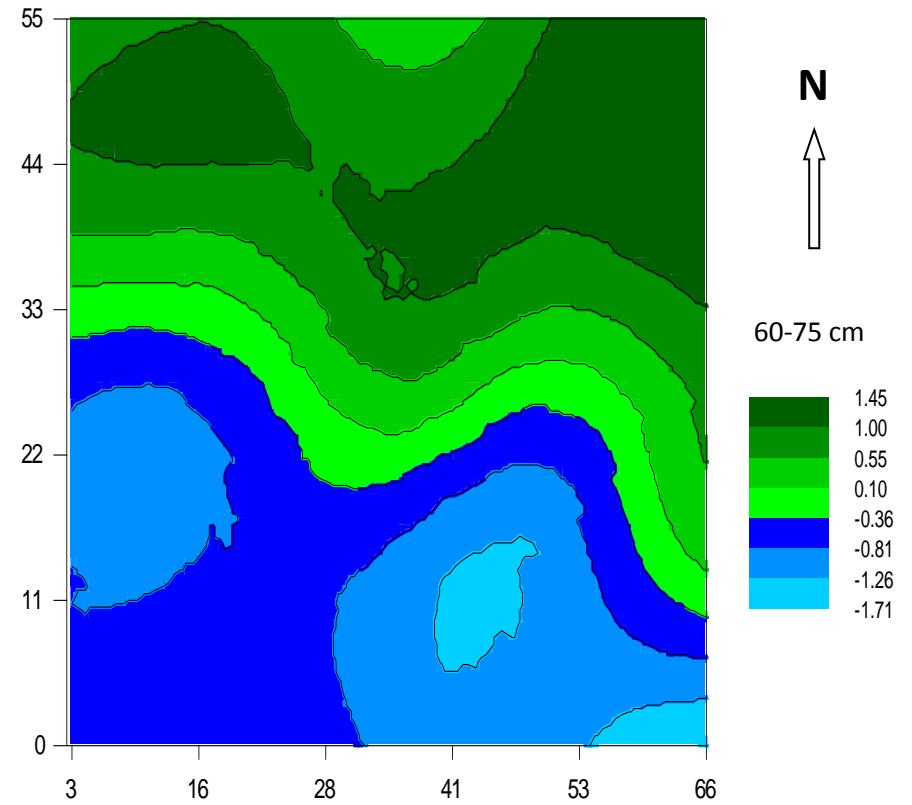


Figure 2.11. Kriged map of soil water content (Johnson SI transform) at 60-75 cm depth across the field for (a) Spring 2014 (b) Fall 2017.

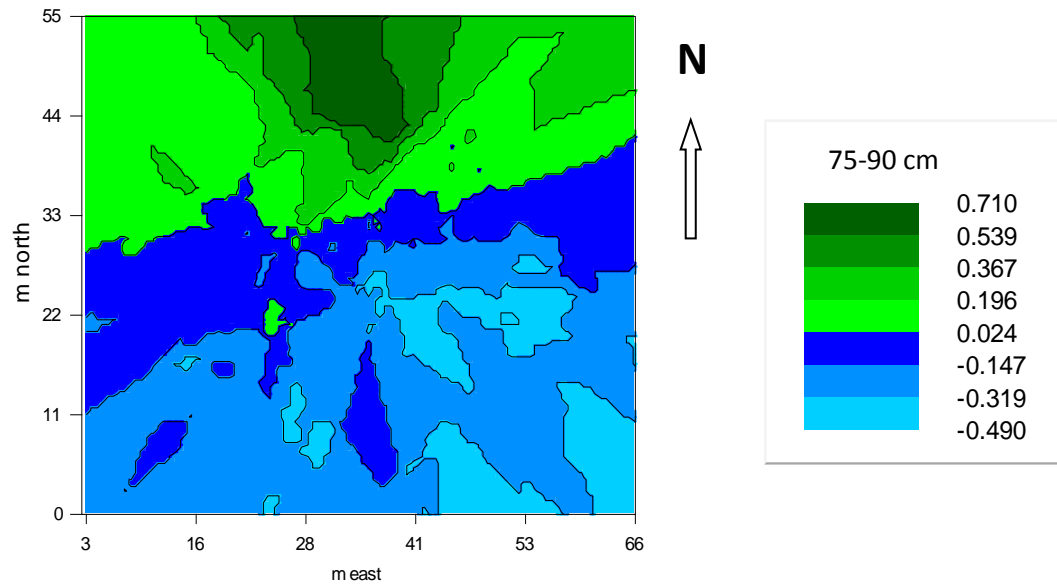


Figure 2.12. Kriged map of soil water content (Johnson SI transform) at 75-90 cm depth across the field for Fall 2017.

2.5. Discussion

2.5.1. spatial structure of soil bulk density

The coefficient of variation of bulk density in this study was low according to the classification of Warrick and Nielson (1980). These results are consistent with those reported by (Ceddia et al., 2009; Silva et al., 2015; Diego et al., 2017; Qiao et al., 2018). The precision of the experiment is determined by the coefficient of variation. Bulk density fitted an exponential model at two depths, with a shift to the Gaussian model at four depths (Table 2.2). Bulk density was strongly spatially autocorrelated from the top soil to the 75 cm depth. A study by Usowicz and Lipiec (2017) on the spatial variability of soil properties and cereal yield in a cultivated field on sandy soil, reported a strong spatial dependence (>75 %) on bulk density. Qiao et al., (2018) investigated the spatial variation and simulation of bulk density in a deep profile (0 - 204 m) on the Loess Plateau and showed that bulk density had a strong spatial dependence (>75 %) with depth. This spatial dependence of bulk density at our site increased from the soil surface to the 75 cm depth (Table 2.2). For examples, only 81 % of total variability was due to spatial variation at the 0-15 cm depth interval and this increased to 86 % at the 15-30 cm depth. There was also a shift of semi variogram from the Exponential to the Gaussian model for the two layers. There was a decrease in the spatial dependency at the 90 cm depth, with a shift of semi variogram from Gaussian to Exponential.

2.5.2. Spatial pattern and distribution of soil bulk density

Variation in bulk density within the field was observed (Figure 2.2). This variability shows the heterogeneous nature of the soil in this area. The South-West region of the field had a higher bulk density compared to the North-East region. Variability of bulk density within the field is consistent with results by Gilsonley et al., (2016), who reported a change in spatial variability in both convex and concave landforms, with an increase in bulk density towards the foot slopes, and a decrease in clay content along the same slope. Variation in bulk density was most likely due to spatial heterogeneities of soil texture in the area, where bulk density was higher in sandy areas. This is so because the total pore space in sands was less than that of silt or clay (Usowicz and Lipiec, 2017), and frequent equipment travel over the top soil. This is consistent with results by Deigo et al., (2017) where they investigated spatial variability of soil attributes in an experimental basin in the semi-arid region of Pernambuco, Brazil. These authors reported an increase in bulk density in the upstream portion of the basin with a higher sand fraction. Ozgoz (2009) observed that bulk density and penetration resistance were higher in sandy areas compared to the rest of the field. Ceddia et al., (2009) reported the influence of sand texture on bulk density values.

Bulk density was less spatially coherent at the soil surface compared to deeper depths probably due to directional tillage over the years (Logsdon and Cambardella, 2000; Ozgoz, 2009). The spatial pattern of soil bulk density in this study was in line with the spatial pattern of sand content obtained by Vivekanahan et al., (2018) for the same study site. Areas with low sand content had low bulk density, and areas with high sand content had high bulk density. Barik et al., (2014) also reported that repeated tillage operations which occurs majorly on the top soil, spatially and significantly influences aggregate stability and bulk density, and a change in bulk density that

occurs at the surface doubles that of other depths approximately. Bulk density increased with depth in this study. This can be due to the compaction because of stress from the top soil (Ozgoz, 2009).

2.5.3. Soil moisture content

The coefficient of variation for soil moisture content in the Fall of 2017 increased with depth. This agrees with the results of Ceddia et al., (2009), who also found an increase in CV with increasing soil moisture. These results contradicted the results of Gwak and Kim (2017) which indicated that soil moisture variability decreases with increasing mean. The coefficient of variation for soil moisture content in the Fall of 2017 was moderate. This CV classification is in line with those of (Xu et al., 2017; Wang and Singh, 2017; Xu et al., 2017; Zhao et al., 2017), who observed a moderate CV values for soil moisture content. There was an increase in standard deviation with depth (Table 2.3) which agrees with previous findings by (Cho and Choi, 2014). Soil moisture content was strongly spatially correlated from the top soil to the 75 cm depth (Usowicz and Lipiec, 2017). The pure nugget effect observed at the 75-90 cm depth indicated that variability was solely due to a random effect at this depth (Table 2.4). At the 75-90 cm depth, there was no spatially dependent variation in soil moisture at the range specified (Figure 2.9).

The geospatial pattern of soil moisture content in the Spring of 2014 and the Fall of 2017 was almost invariant. The mirror image between soil bulk density and soil moisture content may be due to the negative correlation between both variables. Yang et al., (2016) reported a negative correlation between soil bulk density and soil moisture content. The spatial pattern obtained in the Fall of 2017 was similar to that in the Spring of 2014 as the region with high moisture content in the Fall of 2017 had high moisture in the Spring of 2014, and the region with low moisture content in the Fall had low moisture in the Spring.

This was probably due to the spatial pattern of soil texture at this site (Vivekanahan et al., 2018), where the northeastern part of the field had high clay content, hence, high moisture content in both seasons compared to the Southwestern part. This is in agreement with the results obtained by other researchers (Penna et al., 2013; Manns et al., 2014; Chaney et al., 2015; Dong and Ochsner, 2018) where they reported the effect of particle size distribution on the spatial variation of soil water content. Wang and Singh (2017) confirmed texture as the dominant factor controlling soil moisture content variation. Khosla et al., (2005) also reported a significant increase in soil water content in areas with finer soil texture. The 75-90 cm depth was spatially incoherent. This was due to the dominance of random variation and the weak spatial dependency of soil water content at this depth (Table 2.4).

2.6. Conclusion

Spatial variability of bulk density and soil water content on a Canadian Prairies field was evaluated. The results showed that bulk density and water content were both spatially autocorrelated at the field scale. Although soil moisture is known to be temporally variable, our results showed that the spatial pattern of soil moisture is temporally invariant at this site, perhaps due to the dominant influence of soil texture on soil water content. The results from this study show the significance of microspatial variability on a Canadian Prairie field which can be taken advantage of to delineate management zones for precision agriculture.

2.7 References

- Alletto, L., Coquet. 2009.** Temporal and spatial variability of soil bulk density and near-saturated hydraulic conductivity under two contrasted tillage management systems. *Geoderma*. 152: 85-94.
- Arriaga, J. and Rubio, F.R. 2017.** A distributed parameters model for soil water content: spatial temporal variability analysis. *Journal of Agricultural water management*. 183: 101-106.
- Barik, K., Aksakal, E.L., Islam, K.R., Sari, S. and Angin, I. 2014.** Spatial variability in soil compaction properties associated with field traffic operations. *Catena*. 120: 122-133.
- Bong, T. and Armin, W.S. 2018.** Effect of cone penetration conditioning on random field model parameters and impact of spatial variability on liquefaction-induced differential settlements. *Journal of Geotechnical and Geoenvironmental Engineering*. 144: 04018018.
- Cassel, D.K., Wendroth, O. and Nielsen, D.R. 2000.** Assessing spatial variability in an agricultural experiment station field: opportunities arising from spatial dependence. *Journal of Agronomy*. 92: 906-714.
- Ceddia, M.B., Vieira, S.R., Villela, A.L.O., Mota, L.D.S., Anjos, L.H.C. and Carvalho, D.F. 2009.** Topography and spatial variability of soil physical properties. *Brazil journal of soil science*. 66: 338-352.
- Chien, Y.J., Lee, D.Y., Guo, H.Y. and Houng, K.H. 1997.** Geostatistical analysis of soil properties of mid-west Taiwan soils. *Soil science*. 162: 291-298.

- Cho, E. and Choi, M. 2014.** Regional scale spatio-temporal variability of soil moisture and its relationship with meteorological factors over the Korean peninsula. *Journal of hydrology*. 516: 317-329.
- Diacono, M., Rubino, P. and Montemurro, F. 2013.** Precision nitrogen management of wheat. *Rev. Agronomy Sustainable development*. 33: 219-241.
- Diego, C.S.A., Suzana, M.G.L., Abelardo, A, M., Valdemir, P.S., Sylvana, M.S. 2018.** Spatial variability of soil attributes in an experimental basin in the semi-arid of Pernambuco, Brazil. 22: 38-44.
- Ding, J., Zhao, W., Daryanto, S., Wang, L., Fan, H., Feng, Q. and Wang, Y. 2017.** The spatial distribution and temporal variation of desert riparian forests and their influencing factors in the downstream Heihe River basin, China. *Journal of Hydrology and Earth system sciences*. 21: 2405-2419.
- Dong, J. and Ochsner, T.E. 2018.** Soil texture often exerts a stronger influence than precipitation on mesoscale soil moisture patterns. *Water resources research*. 54: 2199-2211.
- Dorigo, W.A., Xaver, A., Vreugdenhil, M., Gruber, A., Hegyiova, A., Sanchis-Dufau, A.D., Zamojski, D., Cordes, C., Wagner, W. and Drusch, M. 2013.** Global automated quality control of in situ soil moisture data from the international soil moisture network. *Vadose Zone Journal*. 12(3).
- Duffera, M., White, J.G. and Weisz, R. 2007.** Spatial variability of Southeastern U.S. Coastal plain soil physical properties: Implications for site-specific management. *Geoderma*. 137: 327-339.

- Enns, J. M. 2004.** The effect of liquid hog manure and commercial fertilizer on nutrient movement in a sandy soil, M. Sc thesis, University of Manitoba.
- Fu, C., Bian, Z., Xi, J. and Zhao, J. 2018.** Spatial distribution characteristics of soil moisture in different sand dune in the Mu Us sandy land, adjacent to north of Chinese Loess Plateau. *Journal of Environmental Earth Science.* 77:151.
- Gardner, W.H. 1986.** Water content. In: Klute, A., ed., *Methods of Soil Analysis: Part I--Physical and mineralogical methods: Soil Science Society of America Book Series No. 5*, Soil Science Society of America, Madison, Wisconsin, p. 493-544.
- Garnaud, C., Belair, S., Carrera, M.L. McNairn, H. and Pacheco, A. 2017.** Field scale spatial variability of soil moisture and L-band brightness temperature from land surface modeling. *Journal of Hydrometeorology.* Vol. 18.
- Geng, R., Zhang, G.H., Li, Z.W., Wang, H. and Luan, L.L. 2014.** Spatial variation of soil bulk density of ephemeral gullies in hilly areas of loess plateau. *Journal of soil water conservation.* 28: 257-262.
- Gilsonley Lopes dos Santos, L.S., Pereira, M.G., Marcos, S.S., Ceddia, B., Mendonca, V.M., Delgado, R.C. 2016. Landform Curvature and Its Effect on The Spatial Variability of Soil Attributes, Pinheiral-Rj/Br. **Cerne.** 22: 431-438.
- Gwak, Y. and Kim, S. 2017.** Factors affecting soil moisture spatial variability for a humid forest hillslope. *Hydrological processes.* 31: 431-445.

- Hermesdorff das Neves, H., Ferreira da Mata, M.G., Guerra, J.G.M. and Fonseca de Carvalho, D. 2017.** Spatial and temporal patterns of soil water content in an agroecological production system. *Scientia Agricola*. 74: 383-392.
- Jacobs, J.M., Hsu, E.C. and Choi, M. 2010.** Time stability and variability of electronically scanned thinned array radiometer soil moisture during Southern great plains hydrology experiments. *Hydrology processing*. 24: 2807-2819.
- Khosla, R., Fleming, K., Delgado, J.A., Shaver, T. and Westfall, D.G. 2002.** Use of site-specific management zones to improve nitrogen management for precision agriculture. *Journal of soil water conversation*. 57: 513-518.
- Liao, K., Lai, X., Zhou, Z. and Zhu, Q. 2017.** Applying fractal analysis to detect spatio-temporal variability of soil moisture content on two contrasting land use hillslopes. *Catena*. 157: 163-172.
- Lin, H. 2011.** Hydropedology: towards new insights into interactive pedologic and hydrologic processes across scales. *Journal of Hydrology*. 406: 141-145.
- Logsdon, S.D. and Cambardella, C.A. 2000.** Temporal changes in small depth incremental soil bulk density. *Soil Science Society of America Journal*. 64: 710-714.
- Lopes dos Santos, G., Pereira, M.G., Santana de Lima, S., Ceddia, M.B., Mendonca, V.M.M. and Delgado, R.C. 2016.** Landform curvature and its effect on the spatial variability of soil attributes, Pinheiral-RJ/BR. *Cerne*. 22: 431-438.

- Manns, H.R., Berg, A.A., Bullock, P.R. and McNairn, H. 2014.** Impact of soil surface characteristics on soil water content variability in agricultural fields. *Journal of Hydrological process.* 28: 4340-4351.
- Martinez, G., Pachepsky, Y.A. and Vereecken, H. 2013a.** Temporal stability of soil water content as affected by climate and soil hydraulic properties: a simulation study. *Hydrological process.* (in press).
- McVicar, T.R., Van Niel, T.G., Li, L.T., Wen, Z.M., Yang, Q.K., Li, R. and Jiao, F. 2010.** Parsimoniously modelling perennial vegetation suitability and identifying priority areas to support China's re-vegetation program in the Loess Plateau: matching model complexity to data availability. *Ecological management.* 259: 1277-1290.
- Miller, J.F. and Loheide, S.P. 2015.** Visualizing large data set: spatial and temporal soil moisture regime dynamics. *Vadose zone Journal.* 14: 0.
- Moulin, A. P., Glenn, A., Tenuta, M., Lobb, D. A., Dunmola, A. S., and Yapa, P. 2014.**
Alternative transformations of nitrous oxide soil flux data to normal distributions.
Canadian Journal of Soil Science. 94: 105-108.
- Moulin, A., Tenuta, M., Lobb, D., Dunmola, A., and Yapa, P. 2011.** Probability distribution functions for short-term daily nitrous oxide fluxes in a prairie pothole agricultural landscape in western Canada. *Canadian Journal of Soil Science.* 91: 303-307.
- Mzuku, M., Khosla, R., Reich, R., Inman, D., Smith, F. and MacDonald, L. 2005.** Spatial variability of measured soil properties across site-specific management zones. *Soil science Society of America Journal.* 69: 1572-1579.

- Nero, B.F. and Anning, A.K. 2018.** Variations in soil characteristics among urban green spaces in Kumasi, Ghana. *Environmental Earth Science*. 77:317.
- Neither, W., Schneidewind, U., Armengot, L., Adamtey, N., Schneider, M. and Gerold, G. 2017.** Spatial-temporal soil moisture dynamics under different cocoa production. *Catena*. 158: 340-349.
- Nikiema, P., Buckley, K. E., Enns, J. M., Qiang, H., and Akinremi, O. O. 2013.** Effects of liquid hog manure on soil available nitrogen status, nitrogen leaching losses and wheat yield on a sandy loam soil of western Canada. *Can. J. Soil Sci.* 93: 573–584.
- Oliver, M.A. and Webster, R. 2014.** A tutorial guide to Geostatistics: computing and modelling variograms and kriging. *Catena*. 113: 56-69.
- Ozgoz, E. 2009.** Long term conventional tillage effect on spatial variability of some soil physical properties. *Journal of sustainable Agriculture*. 33: 142-160.
- Qiao, J., Zhu, Y., Jia, X., Huang, L. and Shao, M. 2018.** Spatial variation and stimulation of the bulk density in a deep profile (0-204 m) on the Loess Plateau, China. *Catena*. 16: 88-95.
- SAS Institute Inc. 2014. SAS® 9.4 Statements: Reference. Cary, NC: SAS Institute Inc.
- Santos, L.A.C., Campos, M.C.C., Bergamin, A.C., Silva, D.M.P. and Mendonca Junior, A.F. 2011.** Physical and chemical characterization of archaeological dark earths and nonanthropogenic soils the Manicore, region, Amazon. *Rev Verde*. 6: 167-74.
- Sequeira, C.H., Wills, S.A., Seybold, C.A. and West, L.T. 2014.** Predicting soil bulk density for incomplete databases. *Geoderma*.213: 64-73.

- Silva, D.M.P., Campos, M.C.C., Franciscan, U., Alho, L.C., Santos, L.A.C., Paula Neto, P., Bergamin, A.C. and Souza, Z.M. 2016.** Spatial variability of soil properties in Archeological Dark Earth Sites under Cacao Cultivation. *Rev Bras Cienc Solo*. 40: e0140816.
- Silva, L.R., Ribeiro de Olivera, I., Dantas, J.S., Viera da Silva, C., Brito da Silva, G. and Ribeiro de Azevedo, J. 2016.** Spatial variability of physical attributes of a cohesive soil under conventional and non-tillage management systems. *Brazilian Agricultural Research*. 51(9).
- Stacey, P., Budiman, M. and Alex, M. 2018.** Spatial variability of Australian soil texture: A multiscale analysis. *GEODERMA* Volume: 309: 60-74.
- Suuster, E., Ritz, C., Roostalu, H., Reintam, E., Kolli, R. and Astover, A. 2011.** Soil bulk density pedotransfer functions of the humus horizon in arable soils. *Geoderma*. 163: 74-82.
- Tagliarolo, M. and Scharler, U.M. 2018.** Spatial and temporal variability of carbon budgets of shallow south African subtropical estuaries. *Science of Total Environment*. 626: 915-926.
- Timm, L.C., Pires, L.F., Roveratti, R., Arthur, R.C.J., Reichardt, K., Martins de Oliveira, J.C. and Bacchi, O.S. 2006.** Field spatial and temporal patterns of soil water content and bulk density changes. *Brazil journal of soil science*. 63: 55-64.

- Tonin, A.M., Hepp, L.U. and Goncalves, J.F. 2018.** Spatial variability of plant litter decomposition in stream networks: from litter bags to watersheds. *Journal of Ecosystems*. 21: 567-581.
- Usowicz, B. and Lipiec, J. 2017.** Spatial variability of soil properties and cereal yield in a cultivated field on sandy soil. *Journal of soil and tillage research*. 174: 241-250.
- Vanderlinden, K., Vereecken, H., Hardelauf, H., Herbst, M., Martinez, G., Cosh, M. and Pachepsky, Y. 2012.** Temporal stability of soil water contents: a review of data and analyses. *Vadose zone journal*. 11: 0.
- Vivekanahan, K, Akinremi, O., Moulin, A.P. and Kumaragamage, D. 2018.** Importance of terrain attributes in relation to the spatial distribution of soil properties at the micro scale: a case study. *Canadian journal of soil science*. 98: 292-305.
- Wang, J., Lu, X., Feng, Y. and Yang, R. 2018.** Integrating multi-fractal theory and Geostatistics methods to characterize spatial variability of particle size distribution of minesoils. *Geoderma*. 317: 39-46.
- Wang, S. and Singh, V.P. 2017.** Spatial-temporal variability of soil water content under different crop covers in irrigation districts of Northwest China. *Entropy*. 19 (410).
- Wang, H., Piazza, S.C., Sharp, L.A., Stagg, C.L., Couvillion, B.R., Steyer, G.D., McGinnis, T.E. 2016.** Determining the spatial variability of wetland soil bulk density, organic matter, and the conversion factor between organic matter and organic carbon across coastal Louisiana, U.S.A. *Journal of coastal research* 33: 507-517.

- Wang, Y.Q., Hu, W., Zhu, Y.J., Shao, M.A., Xiao, S. and Zhang, C.C. 2015a.** Vertical distribution and temporal stability of soil water in 21-m profiles under different land uses on the Loess Plateau in China. *Journal of Hydrology*. 527: 543-554.
- Warrick, A.W. and Nielsen, D.R. 1980.** Spatial variability of soil physical properties in the field. In: Hillel, D, editor. *Applications of soil physics*. New York: Academic press.
- Wei, C., Yu, S., Ji-chun, W. and Jing, L. 2017.** Spatial variability and its main controlling factors of the permafrost soil moisture on the northern slope of Bayan Har mountains in Qinghai-Tibet Plateau. *Journal of Mountain science*. 14: 2406-2419.
- Xu, G., Li, Z., Li, P., Zhang, T., Chang, E., Wang, F., Yang, W. and Cheng Li, R. 2017.** The spatial pattern and temporal stability of the soil water content of sloped forestland on the Loess Plateau, China. *Soil science of America Journal*. 81: 902-914.
- Xu, G., Zhang, T., Li, Z., Li, P., Cheng, Y. and Cheng, S. 2017.** Temporal and spatial characteristics of soil water content in diverse soil layers on land terraces of the Loess Plateau, China. *Catena*. 158: 20-29.
- Yang, J., He, Z., Du, J., Chen, L., Zhu, X., Lin, P. and Li, J. 2017.** Soil water variability as a function of precipitation, temperature, and vegetation: a case study in the semiarid mountain region of China. *Journal of Environmental Earth Science*. 76:206.
- Yang, Q., Luo, W., Jiang, Z., Li, W. and Yuan, D. 2016.** Improve the prediction of soil bulk density by cokriging with predicted soil water content as auxiliary variable. *Journal of soil sediments*. 16: 77-84.

- Yao, R.J., Yang, J.S. and Liu, G.M. 2006.** Spatial variability of soil bulk density in the yellow river delta. *Journal of Irrigation and Drainage Engineering*. 25: 11-15.
- Yongseok, G. and Sanghyun, K. 2017.** Factors affecting soil moisture spatial variability for a humid forest hillslope. *Journal of Hydrological processes*. 31: 431-445.
- Yu, B., Lui, G., Liu, Q., Wang, X., Feng, J. and Huang, C. 2018.** Soil moisture variations at different topographic domains and land use types in the semi-arid Loess Plateau, China. *Catena*. 165: 125-132.
- Zar, J. H. 2010.** Bio statistical analysis, Prentice Hall, Upper Saddle River, NJ. pp 211-213.
- Zhao, C., Jia, X., Zhu, Y. and Shao, M. 2017.** Long term temporal variations of soil water content under different vegetation types in the Loess Plateau, China. *Catena*. 158: 55-62.
- Zhao, W., Cui, Z., Fan, Y. and Cao, Q. 2018.** Predicting spatial variability of soil bulk density in gravel-mulched fields. *Journal of Hydrologic Engineering*. 23: 04018022.
- Zhao, W., Cui, Z., Zhang, J. and Jin, J. 2017.** Temporal stability and variability of soil-water content in a gravel-mulched field in northwestern China. *Journal of hydrology*. 552: 249-257.

3. FEASIBILITY OF MEASURING SOIL CHEMICAL PROPERTIES USING THE VERIS SENSOR

3.1. ABSTRACT

Conventional measurement of soil properties such as organic carbon and nitrogen (OC and ON) is expensive and tedious particularly at the field scale. Yet, such information is required if farmers are to be compensated for adopting agricultural practices that sequester carbon. The Veris OpticalMapper, based on near-infrared (400-2200 nm) soil reflectance spectra, is a practical approach to estimate and map high spatial resolution OC and ON. This study aims to evaluate the potential of the Veris OpticalMapper to measure soil OC and ON across a Canadian Prairies field. The study area was located in Carberry, over the Assiniboine Delta Aquifer, on an Orthic Black Chernozem. The investigated soil properties were soil organic carbon, total carbon, and total nitrogen. To develop the calibration model, 515 soil spectra were collected with the Veris OpticalMapper. Partial least squares regression (PLSR) coupled with leave-one-out cross validation were used to establish the relationship between the near-infrared soil reflectance spectra and the soil properties, whose values were obtained by soil chemical analysis. The accuracy and the goodness of fit were expressed by the coefficient of determination (R^2), root mean square error (RMSE), and residual prediction deviation (RPD). The RMSE was lowest (0.28) and the R^2 value was highest (0.70) for SOC, with RPD 2.40, TC had a RMSE of 0.57, R^2 of 0.67, and RPD 2.01, and TN with RMSE 0.58, R^2 0.68 and RPD 1.80. Ordinary kriging was used to generate maps, with the soil properties showing a strong dependency (> 75) at the soil surface (0-15 cm). Our results showed that the Veris OpticalMapper has the potential to estimate soil OC and ON at the field scale.

3.2. INTRODUCTION

Soil organic carbon and total nitrogen are indicators of soil productivity (Wang et al., 2018). Soil organic carbon affects the soil directly or indirectly through its influence on other soil properties and soil processes (Hbirkou et al., 2012). These include interaction between soil and plants (Ladoni et al., 2010), soil moisture content, aggregate stability, nutrient cycling, and activities of microorganisms (Vasques et al., 2010). Studies have shown that organic matter is spatially variable across the field (Kweon et al., 2013). A knowledge of the spatial variability of soil organic carbon in agricultural fields (Hbirkou et al., 2012) is important for site-specific management in soil carbon monitoring (Gebbers and Adamchuk, 2010). Variation in soil organic carbon has been found to affect the input of fertilizers, herbicide as well as the productivity of crops (Ladoni et al., 2010). Hence, accurate information about its variability within field is crucial to farmers for optimum crop yield.

Conventional mapping of soil organic carbon is time consuming, laborious, destructive, and lacks spatial details (Hill et al., 2010; Hbirkou et al., 2012; Kweon et al., 2013; Perron et al., 2018; Sun et al., 2018) at the field scale (Hill et al., 2010; Vasques et al., 2010). Although, conventional methods have been a standard for calibration for proximal sensors (Vasques et al., 2010). There is therefore the need to use a mapping technique that is non-destructive and can provide detailed information about the concentration of soil organic matter at the field scale.

The Near infrared spectroscopy (NIRS) provides data with high spatial and temporal resolutions, and this technique is very sensitive to organic carbon (Li et al., 2013). This is because the reflectance from NIR conveys vital information (C-H, N-H, and O-H functional groups) relating to the organic and inorganic component of the soil (Stevens et al., 2013; Shi et al., 2015). Over the

years, many efforts have been made to use NIRS to map out soil properties, such as soil organic matter and cation exchange capacity (Bellon-Maurel and McBreatney, 2011; Kweon et al., 2013; Ji et al., 2014), % clay (Bricklemyer and Brown, 2010), electrical conductivity (Sudduth et al., 2003; Sudduth et al., 2005; Serrano et al., 2014), total available water content (Hezarjaribi and Sourell, 2007), available phosphorus, total nitrogen, and moisture content (Kodaira and Shibusawa, 2013). Other investigations that have explored the use of NIRS include land suitability assessment (Fulton et al., 2011), measuring nutrient composition of cattle manure (Malley et al., 2005), measurement of settled and suspended materials in lake, and measurement of mass transport of dissolved chemical through intact soil (Katuwal et al., 2018). These studies have been shown to provide high density data with R^2 as high as 0.93 for organic carbon, and 0.94 for nitrogen (Malley and Williams, 2014).

Studies that used NIRS have been conducted in the field (Fulton et al., 2011; Malley and William, 2014; Aliah Baharom et al., 2015), as well as in the laboratory (Mouazen et al., 2007; Zornoza et al., 2008; Bricklemyer and Brown, 2010; Gomez and Coulouma, 2018). Measurement of soil organic carbon with the NIRS under laboratory condition has been carried out by several researchers and the ability of the sensor to produce satisfactory results have been reported (Christy, 2008; Kweon et al., 2013; Rodionov et al., 2015). Kweon and Maxton (2013) found a strong correlation between the NIR spectral obtained from the OpticalMapper and the lab-analyzed soil organic carbon with an R^2 of 0.87. Soil organic matter, (often approximated as $1.72 \times \text{SOC}$) is the soil property that is widely measured with NIRS. The Veris OpticalMapper combined with the Global Positioning System (GPS) provides real-time data (Fulton et al., 2011). Satisfactory results with the NIRS has been reported for field survey.

Xu et al. (2018) estimated soil organic matter and total nitrogen using the NIR spectroscopy in soil cores of paddy fields with an R^2 of 0.88. Nawar and Mouazen (2018) measured soil organic carbon using the Vis-NIR spectroscopy in the field with an R^2 of 0.74. Vasques et al. (2010) estimated soil organic carbon with depth and reported an R^2 value of 0.86.

The Veris OpticalMapper, a dual wavelength optical sensor works using NIRS to measure soil organic carbon (Veris technology, 2009). Soil organic matter was measured with the OpticalMapper with satisfactory results (Ji et al., 2019), and provided a map of the spatial variability of SOM for potato production in New Brunswick (Ji et al., 2019). Sudduth et al (2003) measured SOC with the optical mapper and reported an R^2 of 0.62. A study by Christy (2008) reported an R^2 of 0.67 with the OpticalMapper in estimated SOC. Kweon and Maxton (2013) measured soil organic matter using the OpticalMapper and reported an R^2 of 0.86. A range of factors affect the effectiveness of the OpticalMapper to measure soil organic matter, the most important of which is varying soil moisture (Christy, 2008; Rienzi et al., 2014). Furthermore, the amount of CaSO_4 and CaCO_3 in arid and semiarid regions, as well as varying parent material and topography, affects reflectance (Ladoni et al., 2010). A study by Vasques et al. (2010) reported a better performance of the laboratory spectrometry than the field spectrometry due to the interference of soil moisture, which alters the refractive index, and diffusion of light.

Partial Least Squares Regression (PLSR) has been the most commonly used model to determine important wavelengths and estimate soil organic carbon from reflectance spectral (Minu and Shetty, 2018). To estimate soil organic carbon, PLSR generates a linear relationship between the predictor variables (spectral reflectance) and the response variables (soil organic carbon) (Peng et al., 2014).

A leave-one-out cross validation is used with PLSR to test how robust the prediction equations are (Jiang et al., 2016; Grinand et al., 2017). Kweon and Maxton (2013) used partial least square regression to determine important wavelengths (660 and 940 nm) and estimated soil organic matter using spectra reflectance with an R^2 of 0.91. Bullock et al., (2004) investigated soil water in small soil volumes using NIR spectroscopy and determined two important wavelengths (1450 and 1940 nm) using partial least squares. Ji et al (2019) used partial least square regression to estimate soil organic matter with the proximal sensor data and reported an R^2 of 0.86.

Once a prediction equation has been generated using PLSR, measures are then taken to determine the accuracy or predictive power of the calibration. The best calibration is the one with the lowest standard error of prediction (SEP) and root mean square error (RMSE), highest coefficient of determination (R^2) between measured and predicted values, and ratio of prediction to deviation / ratio of performance to prediction (RPD) (Mouazen et al., 2007; Zornoza et al., 2008; Aliah Baharom et al., 2015; Clairotte et al., 2016; Xu et al., 2018). The RMSE explains the standard error that occurs during the calibration process (Hbirkou et al., 2012). Performance to prediction (RPD) values < 1.4 indicates no predictive ability, between 1.4 and 2 indicates a moderate predictive ability, and > 2 are said to accurately predict soil parameters (Peng et al., 2014). Analysis using the Near Infrared spectroscopy relies solely on calibration for its effectiveness. Conventional laboratory analysis is being used for calibration (Vasques et al., 2010; Stevens et al., 2013).

A study by Kweon and Maxton (2013) evaluating the performance of a developed sensor in estimating soil organic matter gave an RPD of 2.0. Hbirkou et al. (2012) reported an RPD of 2.08 while studying the spatial heterogeneity of soil organic carbon at field scale. Sun et al., (2018) estimated soil organic carbon in a coal mining area using Vis-NIR spectroscopy and reported an RPD of 2.69.

Precise evaluation of soil organic carbon and other soil properties can help manage long-term sustainability of soils. However, this involves conventional methods, which can be time-consuming and costly. Hence, there is a growing demand for optical sensors that can extensively be used for soil analysis, and on the appropriate management of spatial and temporal variability of soil properties. Therefore, the objectives of this study were

1. to evaluate the potential of the Veris OpticalMapper to measurements of soil SOC, TC, and TN on a Canadian Prairies.
2. to produce soil maps of OC, TC and TN showing its variability within field, as required for Precision Agriculture.

Hypothesis: Veris OpticalMapper can estimate SOC, TC, and TN and that variation in these properties occurs at the soil surface.

3.3. Materials and methods

3.3.1. Study area and soil description

The study was carried out on a farmer's cooperator field that is located about 10 km, Northwest of Carberry in Southwestern Manitoba, Canada (SW-19-11-15W). The region is characterized by an average annual precipitation of 456 mm, with approximately 70 % falling as rain from April-October and 30 % as snow during the winter months and mean annual temperature of 2.1 °C. The site is located over the Assiniboine Delta Aquifer, an unconfined aquifer that is the source of drinking water. The site consists of Orthic Black Chernozem soils, which developed on lacustrine deposits. Further information on the study area was provided in Chapter 2, section 2.3.1.

3.3.2. Sample collection

Soil spatial variability of the 0.36 ha experimental field was characterized by one hundred and twenty-four (124) geo-referenced samples collected with a 3" plastic sleeves with a Giddings hydraulic soil punch, at a depth of 0-15 cm to calibrate the sensor data. Plant residues were removed from the surface during sampling to minimize the impact on the organic carbon analysis. A geospatial sampling scheme was used for sampling, which could detect small scale variability in organic carbon across the field.

3.3.3. Laboratory analysis

Air-dried surface soil samples (0 - 15 cm) (n = 124) were ground with an 8000D mixer/mill high-energy ball mill in preparation for chemical analysis. This sample size provided satisfactory statistical power (0.8) for statistical analysis of SOC, TC, and TN. Soil organic carbon, TC, and

TN were analyzed by dry combustion with a flash 2000 elemental analyzer (Thermo Fisher Scientific). Inorganic carbon was removed with 0.5 mL of 2 mol L⁻¹ HCL before determination of SOC (Vivekanahan et al., 2018).

3.3.4. Spectrum acquisition

The Veris OpticalMapper was used to map a 65 x 55 m (0.36 ha) field using the Veris 3100 (Veris Technologies, Salina, KS) designed for mapping with multiple sensor, and equipped with a Global Positioning System (GPS) antenna to provide positional information. The OpticalMapper consists of six coulter for measuring electrical conductivity and a unit for optical measurement. The optical unit consists of red LED (660 nm) and NIR red (940 nm) collecting red and near-infrared wavelengths through a sapphire window (20 spectra per second with an 8nm resolution), which are both sources of light, and a single photodiode. The sensor was mounted in between two disks which operate at a slight angle, forming a V-shaped slot in the soil. A depth-gauging side wheel for each disk controls sensing depth. The wear plate with window was pressed against the bottom of the slot to provide consistent pressure for self-cleaning function. Veris sensor measurements were continuously measured in a grid transects across the entire site. Data was collected at about 7cm below the soil surface. A total of 583 reflectance data was collected. The GIS software was set to average the reflectance data within 3 m around the sampling points for laboratory analysis. This brought the reflectance data down to 124 points.

3.3.5. Statistical analysis

Prior to analysis, the data was centered and scaled, and the JMP 13.0 SAS institution was used to calculate partial least square regression, with the Nonlinear Iterative Partial Least Squares (NIPALS) method. A prediction model was developed using partial least square regression to calibrate the NIR data (reflectance reading), which were predictor variable, with the reference soil organic carbon, total carbon, and total nitrogen data from the elemental analysis as predicted variables.

A validation step is required to access the accuracy of the calibration model. The validation procedure was done using the leave-one-out cross validation. This procedure leaves one sample out at a time and then uses the equation generated with the other sample to estimate the value of the omitted sample. This procedure was repeated until all samples have been omitted and estimated. The procedure was applied to all possible combinations of independent variables to estimate soil organic carbon, total carbon, and total nitrogen. Root mean square error (RMSE), R^2 , and ratio of prediction to deviation (RPD) were produced for the cross-validation dataset. The RPD was used for assessing the goodness of fit for NIR spectroscopy. The correlation between the predicted Veris OpticalMapper data and the laboratory data was determined. Linear regression between the predicted and measured value was performed using XLSTAT 2017 least squares method (Data Analysis and Statistical Solution for Microsoft Excel. Addinsoft, Paris, France) (Figure 3.1).

3.3.6. Geostatistical data processing

All Geostatistics computations were conducted using the GS + version 10.0 (Gamma Design Software LLC., Plainwell, MI, USA). One Semivariogram model (gaussian) was used to describe the Semivariogram, as it was the best-fitted model with the lowest residual sum of squares for predictions and largest coefficient of determination (Wang et al., 2018). Geostatistical parameters; sill ($C + C_0$), nugget (C_0), and range, were obtained. The sill is the sum of the nugget and the spatial variability. The nugget estimates the spatial variability at distances closer than the minimum sampling space. The range shows the distance at which the sampling points are spatially correlated with each other.

The ratio of the spatial variability and the sill is the proportion of total variability which is explained by the spatial autocorrelation (Bong et al., 2018). Kriging, a regression method, provides a means of interpolating values for points not physically sampled. Ordinary kriging was used to interpolate and generate maps of lab-analyzed and Veris estimated SOC, TC, and TN for this study (Diego et al., 2017).

3.4. Results

3.4.1. Soil organic carbon and related properties

The results obtained from a total of 124 soil samples for the calibration and validation sets are listed in (Table 3.1). The statistical results include the mean, coefficient of variation, standard deviation, minimum, and maximum for each soil parameter. Coefficient of variation for soil organic carbon, total carbon, and total nitrogen were similar (Table 3.1) perhaps as a result of the association of carbon and nitrogen to soil organic matter. Maximum SOC, TC, and TN were about four times greater than their respective minimum values (table 3.1).

Table 3.1. Descriptive statistics of soil organic carbon % (SOC), total carbon % (TC), and total nitrogen % (TN) at the soil surface (0-15 cm).

Soil properties	Number of samples	Mean	Coefficient of variation (%)	Standard deviation	Minimum (%)	Maximum (%)
Organic carbon	124	1.70	29	0.49	0.74	2.80
Total carbon	124	1.74	29	0.51	0.74	2.86
Total nitrogen	124	0.14	28	0.04	0.07	0.22

3.4.2. Performance of the calibration model

The quality of the PLSR model (JMP 13.0 SAS institution) fit was evaluated using performance statistics derived from the regression of values estimated using PLSR versus those that were measured in the laboratory. The PLSR results were obtained as shown in (Table 3.2). Based on the coefficient of determination (R^2), RPD, and RMSE, the accuracy of the model was determined, with SOC having an R^2 of 0.70 and RPD of 2.40, TC with an R^2 of 0.67 and RPD of 2.01, and TN with an R^2 of 0.68 and RPD of 1.80. The predictive ability of this model was considered to be accurate for SOC and TC and moderate for TN according to the RPD.

Table 3.2. Summary of PLSR results of the soil properties dataset

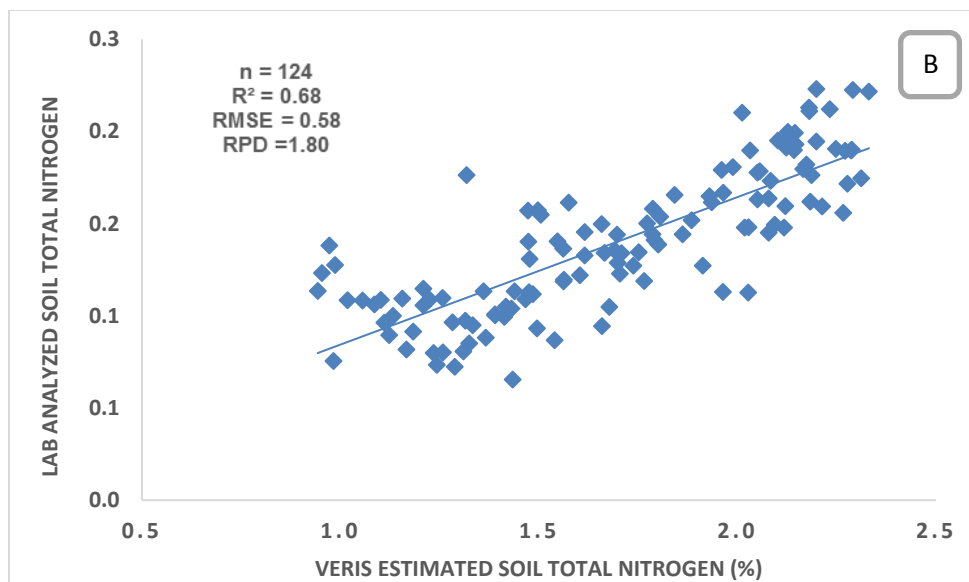
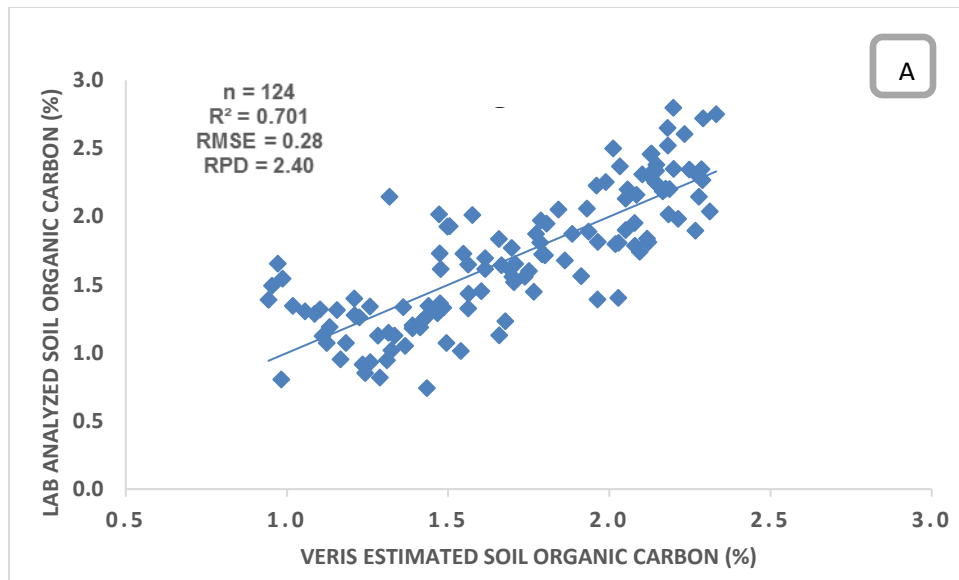
Soil properties	Number of samples	Multivariate method*	RPD**	Predictive ability***	RMSE****
Organic carbon	124	PLSR	2.40	Accurate	0.28
Total carbon	124	PLSR	2.01	Accurate	0.57
Total nitrogen	124	PLSR	1.80	moderate	0.58

*PLSR=Partial least square regression

**RPD = Ratio of prediction to deviation.

***Performance to prediction (RPD): RPD > 2.0 accurate; RPD= 1.4-2.0 moderate; RPD= < 1.4 no predictive ability. (Peng et al., 2014).

****RMSE = Root mean square error.



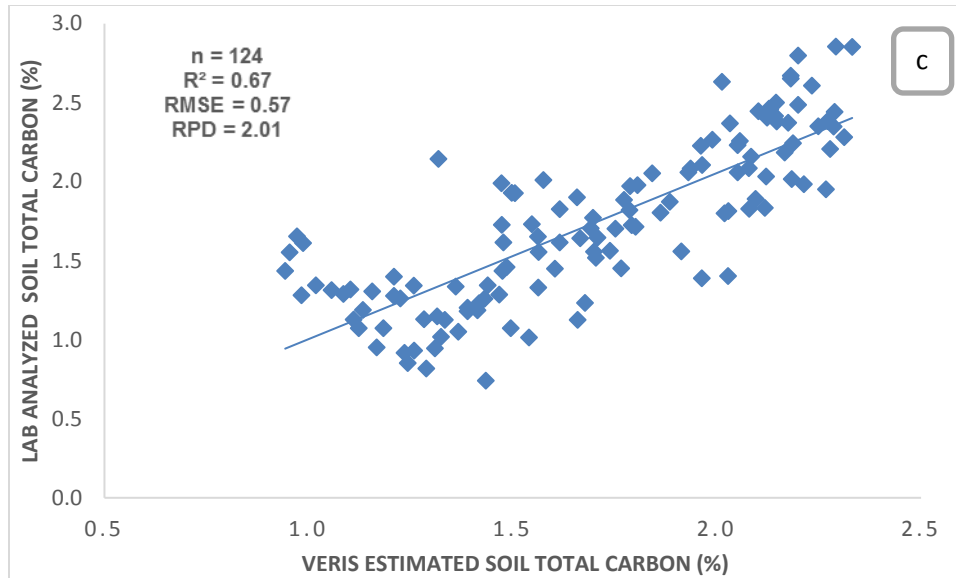


Figure 3.1. Correlation between laboratory measured and Veris estimated soil (a) organic carbon, (b) total nitrogen, and (c) total carbon.

3.4.3. Geostatistics

The investigated soil properties were tested for normality using the SAS 9.4 (SAS institute Inc, 2014) software. The laboratory analyzed organic carbon, total carbon, total nitrogen, and estimated Veris OC, and TC were normally distributed ($p > 0.05$) thus, were not transformed. The Veris estimated TN was not normally distributed and was transformed using the Johnson SI transformation. The best fitted model parameters are presented in Table 3.3. The coefficient of determination (R^2) was 0.98 for laboratory analyzed OC, total carbon, total nitrogen, and Veris estimated OC, and was 0.99 for estimated Veris TC and TN as obtained with the Gaussian model. The residual sum of square was small. The sill ($C_0 + C$) values were higher than the value of the nugget. Ranges of Veris SOC, TC, and TN were large compared to the lab-analyzed values.

The ratio of the sill and nugget reflects spatial autocorrelation and was strong for all soil properties (Table 3.3). For example, only 90 % of total variability of SOC was due to spatial variation in the top soil. Ordinary kriging was used to estimate unsampled location based on the fitted Semivariogram model.

Table 3.3. Parameter for Semivariogram models for Lab analyzed SOC, TC, and TN and Veris estimated SOC, TC, and TN.

Soil property	Variogram Model *	Nugget Variance Co	Sill Co+C	C/Co+C (%) **	R²	Range	Spatial Class ***
Total N	Gaussian	0.000	0.002	89.7	0.98	55.75	S
Total C	Gaussian	0.039	0.477	91.8	0.98	55.32	S
Organic C	Gaussian	0.044	0.451	90.2	0.98	58.66	S
Veris OC	Gaussian	0.024	0.345	93.0	0.98	72.46	S
Veris TC	Gaussian	0.000	0.018	99.0	0.99	88.08	S
Veris TN	Gaussian	0.001	1.985	99.0	0.99	87.72	S

* Models are all isotropic

** Nugget to sill ratio (%) = (Nugget semivariance / total semivariance) X 100

***S = Strong spatial dependency (C/C+Co % > 75); M = Moderate spatial dependency (C/C+Co % between 75 and 25) Chien et al., (1997).

3.4.4. Pearson correlation coefficient for Veris SOC with other variables

Pearson correlation coefficient was used to determine the strength of possible relationships between Veris SOC, and other soil properties. Table 3.4 displays the linear correlation coefficient among the four variables. Veris SOC was significantly positively correlated with TN (0.807**), TC (0.811**), and Lab-analyzed SOC (0.805**).

Table 3.4. Pearson Correlation coefficient for Veris SOC with other variables

Variables	Total nitrogen	Total carbon	Lab-analyzed SOC	Veris Predicted SOC
Total nitrogen	-	0.992**	0.992**	0.807**
Total carbon	0.992**	-	0.989**	0.811**
Lab-analyzed SOC	0.992**	0.989**	-	0.805**
Veris predicted SOC	0.807**	0.811**	0.805**	-

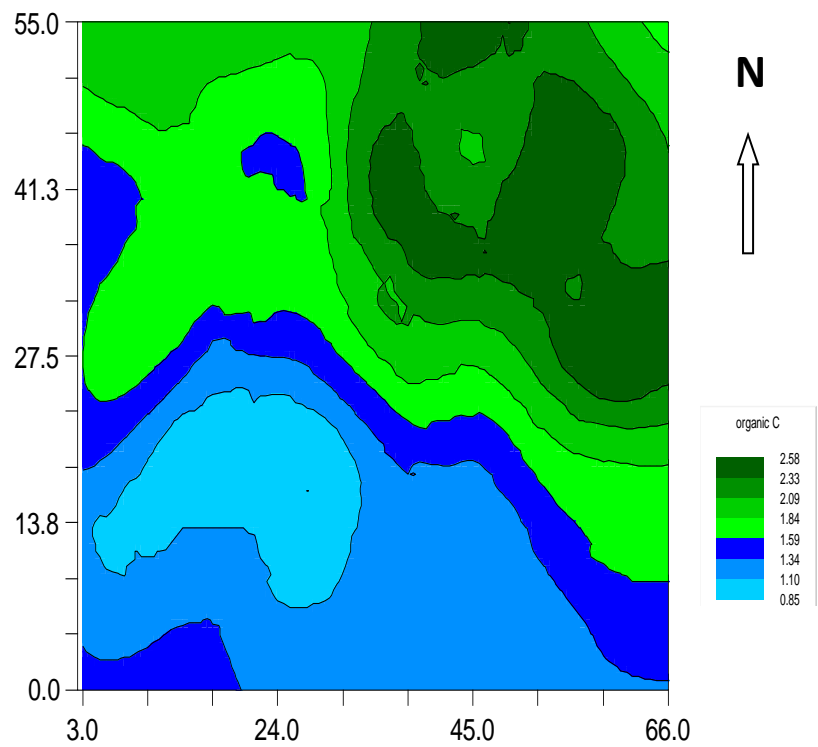
SOC=soil organic carbon

** significant at <0.05

3.4.5. Soil mapping

Kriged maps of the spatial distribution of SOC, TC, and TN were prepared based on Semivariogram models (Figure 3.4 to 3.6). Figure 3.4 to 3.6 show the spatial variability of soil properties of the experimental field. The spatial pattern of the laboratory analyzed soil organic carbon, total carbon, and total nitrogen are similar to those estimated using the Veris OpticalMapper. The North-East region of the field had higher values of the 3 properties while the South-West region had lower values.

a. Laboratory organic carbon



b. Veris predicted organic carbon

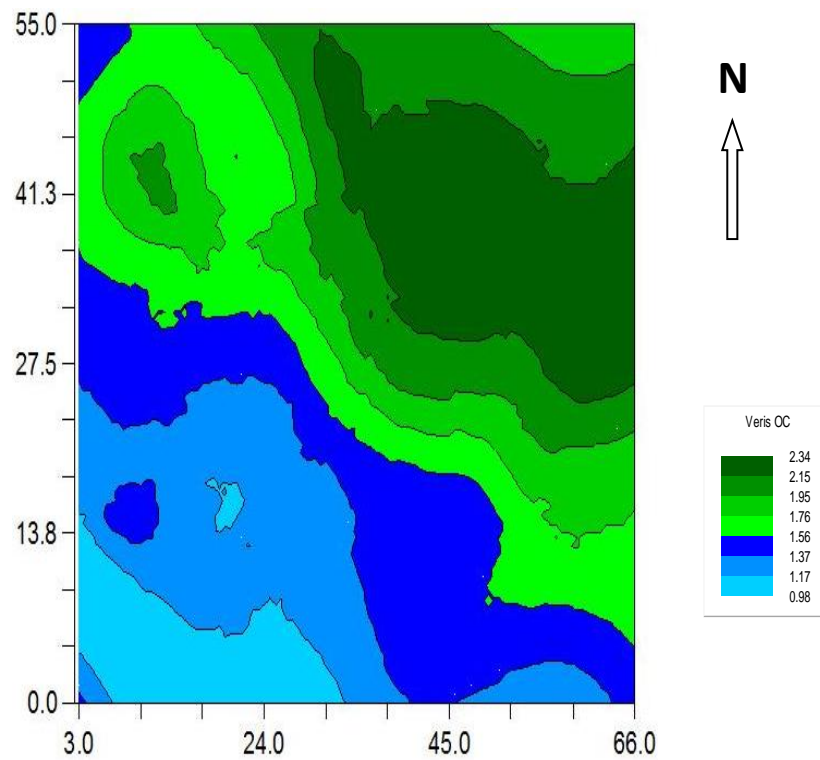
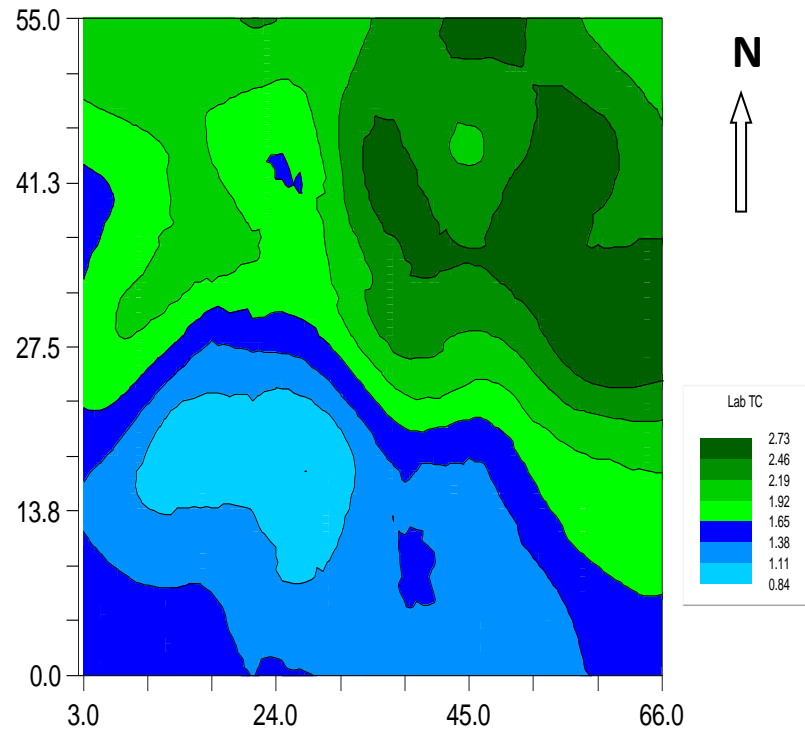


Figure 3.2: Kriged maps of soil organic carbon content as measured (a) conventionally and (b) as estimated using the Veris OpticalMapper.

a. Laboratory total carbon



b. Veris predicted total carbon

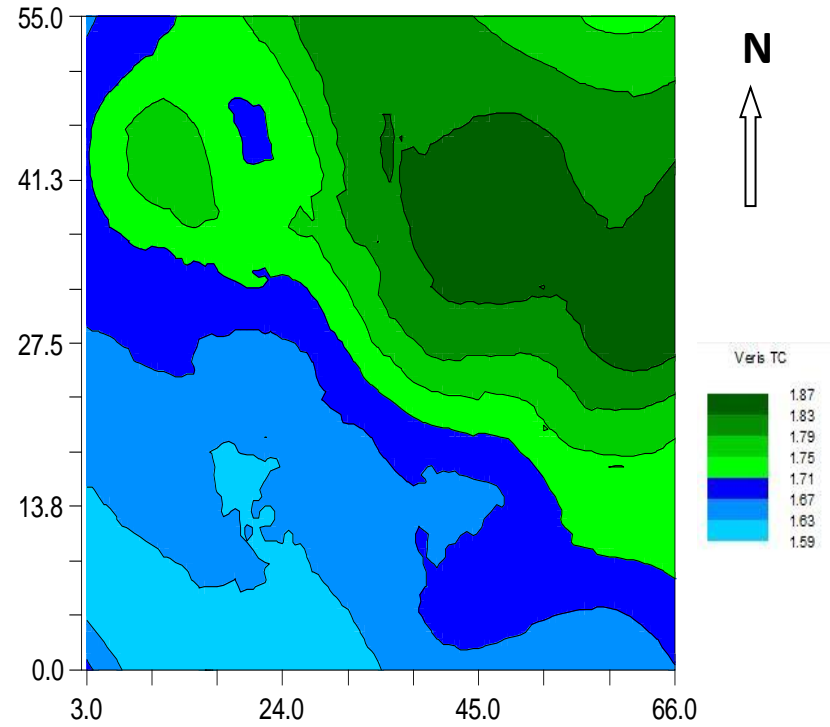
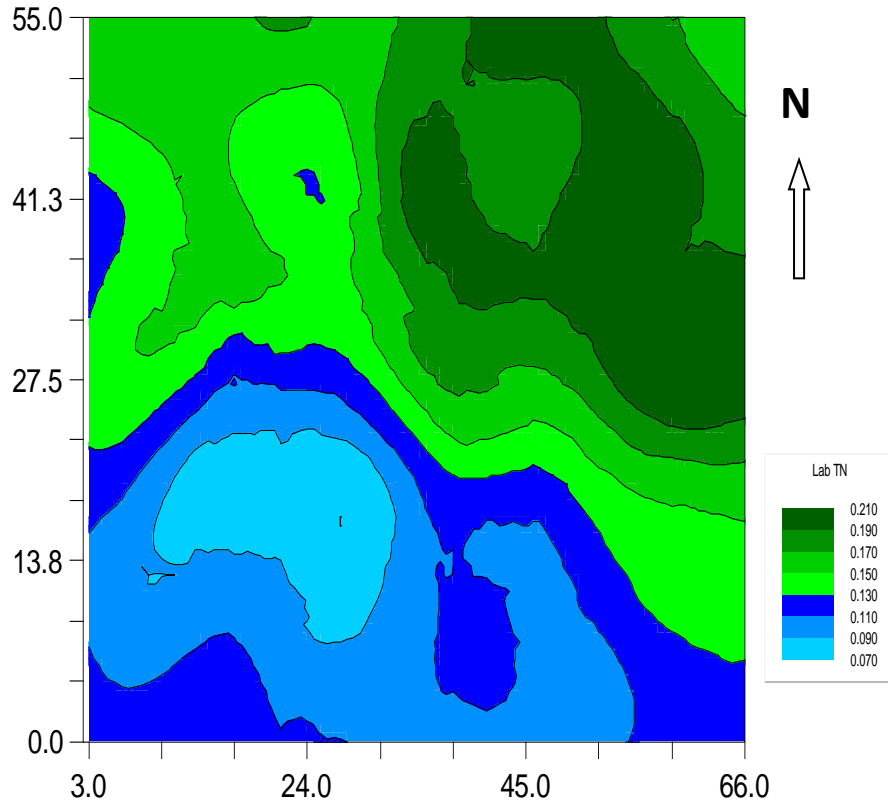


Figure 3.3: Kriged maps of soil total carbon content as measured (a) conventionally and (b) as estimated using the Veris OpticalMapper.

a. Laboratory total nitrogen



b. Veris predicted total nitrogen

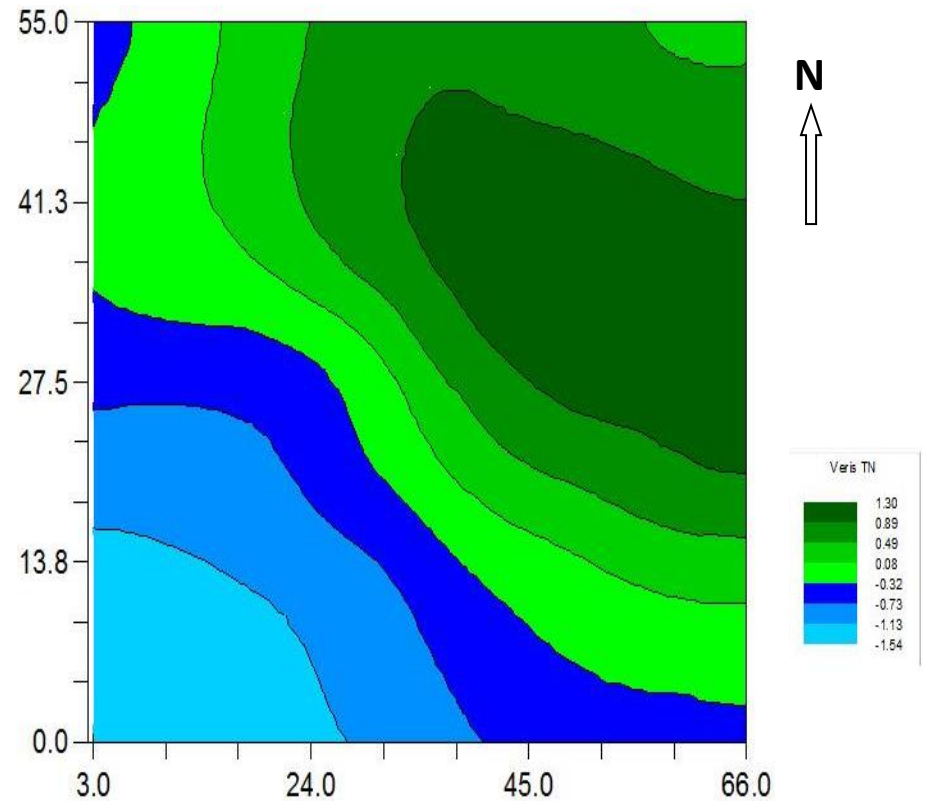


Figure 3.4: Kriged maps of soil total nitrogen content as measured (a) conventionally and (b) as predicted using the Veris OpticalMapper.

3.5. Discussion

3.5.1. Performance of the calibration model

The strong relationship between laboratory measured soil organic carbon and spectral reflectance from the Veris OpticalMapper indicates that SOC can be modelled using soil reflectance (Liu et al., 2018; Minu and Shetty, 2018). Different spectra have been examined to determine the most suitable wavelength for organic carbon (Bellon-Maurel and McBratney, 2011; Rodionov et al., 2015). Using the accuracy classification by Peng et al. (2014), the calibration set proved to be excellent for SOC and TC with the RPD above 2 similar to what was reported by (Kweon et al. 2013; Aliah Baharom et al., 2015; Minu and Shetty, 2018). For TN, the RPD was between 1.4 and was regarded as moderate in agreement with (Malley et al., 2009) who obtained a moderate calibration when analyzing total nitrogen on the Canadian Prairie (Table 3.2 and Figure 3.1). St.Luce et al. (2014) reported an RPD > 2 for SOC and TN using the visible near infrared spectroscopy. The coefficient of determination R^2 , showed that 70 % of the variability in SOC was explained by the Veris predicted SOC and 68 % of the variability of field measured total nitrogen was explained by the Veris TN, while 67 % of the variability in measured TC was explained by the Veris TC. Christy (2008) reported an R^2 of 0.75 for organic matter using on-the-go near infrared reflectance spectroscopy. Sun et al. (2018) reported R^2 of 0.70 for soil organic carbon estimated in a coal mining area using Vis-NIR spectroscopy. The value obtained by Grinand et al. (2017) was R^2 of 0.72 while estimating temporal changes in soil carbon stock with remote sensing.

The performance of the Veris OpticalMapper in this study could have been influenced by the small range of SOC and to some extent low clay content as the dominant soil texture at this site is loamy sand (Ladoni et al., 2010; Brickleyer and Brown, 2010; Deiss et al., 2017; Vivekanahan et al., 2018). Soil organic carbon, TC, and TN were low in areas with high sand content, and high in areas with high clay content. Clay content was positively correlated with SOC (Figure 2.10) (Vanek et al., 2008; Xiao-Wei et al., 2012). It has also been reported that variations in soil moisture affects the performance of NIR in the field by changing the refractive index and diffusion of light (Kweon et al. 2013; Rodionov et al., 2015; Deiss et al., 2017). Rienzi et al. (2013) observed a decline in reflectance with increasing soil moisture content when predicting soil organic carbon under varying moisture levels. Also, because of the small nature of the plot and heavy traffic, wheel tract compaction can cause sensor anomalies like streaks or shifts (Deiss et al., 2017). These effects are more significant to the optical sensor as it only investigates a few inches of the topsoil (Brickleyer and Brown, 2010).

3.5.2. Geostatistics and Pearson analysis

These maps show that the experimental field is spatially heterogeneous (Figure 3.4 to 3.6). The residual sum of squares for all measured values were roughly equals to zero, which indicated that the model efficiently reflected the experimental variogram (Liu et al., 2011; Wang et al., 2017). The value of $C_0 / (C + C_0)$ ranged from 89.7 % to 93.0 % which showed that the soil properties exhibited strong spatial dependency. Other studies have previously reported strong spatial dependency for SOC, TC, TN, and Veris OC (Wang et al., 2009; Liu et al., 2014; Wang et al., 2017). The highest R^2 , which shows how well the model fit was 0.98 for all soil properties in this study (PingguoYang et al., 2016; Wang et al., 2017; Wang et al., 2009). The landscape texture has caused many of the soil parameter to vary, a phenomenon which was also observed by (Piotrowska, 2011; Hu et al., 2104; Naveed at al., 2016; Mingjun et al., 2017; Vivekanahan et al., 2018). The variability of these parameters may be due to the influence of other soil properties, such as soil bulk density, which has a negative correlation with SOC, TC, and TN (Figure 2.2) (Beleke et al., 2013; Bameri et al., 2015; Zhang et al., 2015; Wang at al., 2017). Kweon et al. (2013) reported variations in soil organic matter due to soil texture. Soil moisture content had a positive correlation with SOC, TC, and TN, where regions with high moisture content also had high SOC, TC, and TN. This is because soils with high organic matter can hold more water.

3.6. Conclusion

Laboratory analysis of soil carbon is time consuming and expensive especially for a large field size. In an attempt to address this problem, different types of sensors have been developed to map these soil properties that are useful for precision agriculture. This study evaluated the potential of Veris OpticalMapper to estimate SOC, TC, and TN. Pearson correlation coefficient between the soil properties indicated positive linear relationship. The results showed that capability of measuring SOC, TC, and TN of Canadian prairie soil with Veris OpticalMapper. Mapping of chemical properties with the Veris OpticalMapper will be useful in monitoring large-scale variability, help to improve site-specific management, and field experiments e.g. in application of fertilizers, herbicides, monitoring carbon sequestration, and nitrogen leaching.

3.7. References

- Baharom, S.N., Shibusawa, S., Kodaira, M., Kanda, R. 2015.** Multile-depth mapping of soil properties using a visible and near infrared real-time soil sensor for a paddy field. *Engineering in Agriculture, Environment and food*. 8: 13-17.
- Bameri, A., Khormali, F., Kiani, F., Dehghani, A.A. 2015.** Spatial variability of soil organic carbon in different hill-slope positions in Toshan area, Golestan Province, Iran: Geostastical approaches. *Journal of mountain science*. 12: 1422-1433.
- Bellon-Maurel, V. and McBratney, A. 2011.** Near-infrared (NIR) and mid-infrared (MIR) spectroscopic techniques for assessing the amount of carbon stock in soils – critical review and research perspectives. *Soil biology & biochemistry*. 43: 1398-1410.
- Brickleymer, R.S. and Brown, D.J. 2010.** On-the-go VisNIR: Potential and limitations for mapping soil clay and organic carbon. *Computers and electronics in Agriculture*. 70: 209-216.
- Christy, C.D. 2008.** Real-time measurement of soil attributes using on-the-go near infrared reflectance spectroscopy. *Computers and electronics in Agriculture*. 61: 10-19.
- De Gryze, S., Six, J., Bossuyt, H., Van Oost, K. and Merckx, R. 2008.** The relationship between landform and the distribution of soil C, N and P under conventional and minimum tillage. *Geoderma*. 144: 180-188.
- Deiss, L., Franzluebbers, A., Moraes, A. 2017.** Soil texture and organic carbon fractions predicted from Near-infrared spectroscopy and Geostatistics. *Journal of nutrient management and soil plant analysis*. 81: 1222-1234.

- Fulton, A., Schwankl, L., Lynn, K., Lampinen, B., Edstrom, J. and Prichard, T. 2011.** Using EM and Veris technology to assess land suitability for orchard and vineyard development. *Journal of irrigation science*. 29: 497-512.
- Gebbers, R. and Adamchuk, V.I. 2010.** Precision Agriculture and Food security. *Science*. 327: 828-831.
- Gomez, C., Coulouma, G. 2018.** Importance of the spatial extent for using soil properties estimated by laboratory VNIR/SWIR spectroscopy: Examples of the clay and calcium carbonate content. *Geoderma*. 330: 244-253.
- Grinand, C., Le Maire, G., Vieilledent, G., Razakamanarivo, H., Razafimbelo, T. 2017.** Estimating temporal changes in soil carbon stocks at ecological scale in Madagascar using remote-sensing. *International journal of applied earth observation and geoinformation*. 54: 1-14.
- Hbirkou, C., Patzold, S., Mahlein, A.K. and Welp, G. 2012.** Airborne hyperspectral imaging of soil organic carbon heterogeneity at the field-scale. *Geoderma*. 175-176: 21-28.
- Hezarjaribi, A. and Sourell, H. 2007.** Feasibility study of monitoring the total available water content using non-invasive electromagnetic induction-based and electrode-based soil electrical conductivity measurements. *Irrigation and drainage*. 56: 53-65.
- Hill, J., Udelhoven, T., Vohland, M. and Stevens, A. 2010.** The use of Laboratory spectroscopy and optical remote sensing for estimating soil properties. *Precision crop protection. The challenge and use of heterogeneity*. 67-85.

- Hu, K., Wang, S., Li, H., Huang, F., Li, B. 2014.** Spatial scaling effects on variability of soil organic matter and total nitrogen in suburban Beijing. *Geoderma*. 226-227: 54-63.
- Ji, W.J., Shi, Z., Huang, J.Y., Li, S., 2014.** In situ measurement of some soil properties in paddy soil using visible and near-infrared spectroscopy. *PLoS One* 9: 11.
- Ji, W., Adamchuk, V. I., Chen, S., Mat Su, A. S., Ismail, A., Gan, Q., Shi, Z. and Biswas, A. 2019.** Simultaneous measurement of multiple soil properties through proximal sensor data fusion: A case study. *Geoderma* 341:111-128.
- Jiang, Q., Chen, Y., Guo, L., Qi, K. 2016.** Estimating soil organic carbon of cropland soil at different levels of soil moisture using VIR-NIR spectroscopy. *Remote sensing*. 8: 755.
- Katuwal, S., Knadel, M., Mouldrup, P., Norgaard, T., Greve, M.H., Jonge, L.W. 2018.** Visible-Near infrared spectroscopy can predict mass transport of dissolved chemicals through intact soil. *Scientific reports*. 8: 11188.
- Kweon, G. and Maxton, C. 2013.** Soil organic matter sensing with an on-the-go optical sensor. *Biosystems engineering*. 115: 66-81.
- Li, H.Y., Shi, Z., Webster, R., Triantafilis, J., 2013.** Mapping the three-dimensional variation of soil salinity in a rice-paddy soil. *Geoderma* 195–196, 31–41.
- Liu, J., Han, J., Zhang, Y., Wang, H., Kong, H., Shi, L. 2018.** Prediction of soil organic carbon with different parent materials development using visible-near infrared spectroscopy. *Spectrochimica Acta Part A: Molecular and Biomolecular Spectroscopy*. 204: 33-39.

- Liu, W., Su, Y., Yang, R., Yang, Q., Fan, G. 2011.** Temporal and spatial variability of soil organic matter and total nitrogen in a typical oasis cropland ecosystem in arid region of Northwest China. *Environmental earth science*. 64: 2247-2257.
- Lui, L., Wang, H., Dai, W., Lei, X., Yang, X., Li, X. 2014.** Spatial variability of soil organic carbon in the forestlands of northeast China. *Journal of forestry research*. 25: 867-876.
- Malley, D.F. and Williams, P. 2014.** Analysis of sediments and suspended material in lake ecosystems using near-infrared spectroscopy: A review. *Aquatic Ecosystems health and management*. 17: 447-453.
- Malley, D.F., Martin, P.D., McClintock, L.M., Yesmin, L., Eilers, R.G., Haluschak, P. 2009.** Feasibility of analysing archived Canadian prairie agricultural soils by near infrared reflectance spectroscopy. In: Davies, A.M.C., et al. (Eds.) *Near Infrared Spectroscopy: Proceedings of the 9th International Conference*. NIR Publications, Chichester, UK. pp. 579- 585.
- Malley, D.F., McClure, C., Martin, P.D., Buckley, K. and McCaughey, W.P. 2005.** Compositional analysis of cattle manure during compositing using a field-portable Near-Infrared spectrometer. *Communications in Soil science and Plant analysis*. 36: 455-475.
- Martin, P.D., Malley, D.F., Manning, G. and Fuller, L. 2002.** Determination of soil organic carbon and nitrogen at the field level using near-infrared spectroscopy. *Canadian journal of soil science*. 82: 413-422.

- Mingjun, T., Lixiong, Z., Wenfa, X., Zhiling, H., Zhixiang, Zhaogui, Y., Pengcheng, W. 2017.** Spatial variability of soil organic carbon in three Gorges reservoir area, China. *Science of total environment*. 599-600:1308-1316.
- Minu, S. and Shetty, A. 2018.** Prediction accuracy of soil organic carbon from ground based visible near-infrared reflectance spectroscopy. *Journal of the Indian society of remote sensing*. 46: 697-703.
- Mouazen, A.M., Maleki, M.R., De Baerdemaeker, J. and Ramon, H. 2007.** On-line measurement of some selected soil properties using a VIS-NIR sensor. *Soil and tillage research*. 93: 13-27.
- Naveed, M., Herath, L., Moldrup, P., Arthur, E., Nicolaisen, M., Norgaard, T., Ferre, T.P.A., Jonge, L.I. 2016.** Spatial variability of microbial richness and diversity and relationships with soil organic carbon, texture and structure across an agricultural field. *Applied soil ecology*. 103: 44-55.
- Nawar, S and Mouazen, A.M. 2018.** Optimal sample selection for measurement of soil organic carbon using on-line Vis-NIR spectroscopy. *Computers and electronics in Agriculture*. 151: 469-477.
- Nyamadzawo, G., Shukla, M.K., Lal, R. 2008.** Spatial variability of total carbon and nitrogen stocks for some reclaimed mine soils of Southeastern Ohio. *Land degradation and development*. 19: 275-288.
- Peng, X., Shi, T., Song, A., Chen, Y., Gao, W. 2014.** Estimating soil organic carbon using Vis-NIR spectroscopy with SVMR and SPA methods. *Remote sensor*. 6: 2699-2717.

- Pingguo, Y., Byrne, J.M., Yang, M. 2016.** Spatial variability of soil magnetic susceptibility, organic carbon and total nitrogen from farmland in northern China. *Catena*. 145: 92-98.
- Piotrowska, A. 2011.** Spatial variability of total and mineral nitrogen content and activities of the N-Cycle Enzymes in a Luvisol topsoil. *Pol. Journal of environmental studies*. 20: 1565-1573.
- Rienzi, E.A., Mijatovic, B., Mueller, T.G., Matocha, C.J., Sikora, F.J., Castrignano, A. 2014.** Prediction of soil organic carbon under varying moisture levels using reflectance spectroscopy. *Soil science society of America journal*. 78: 958-967.
- Rodionov, A., Welp, G., Damerow, L., Berg, T., Amelung, W. and Patzold, S. 2015.** Towards on-the-go field assessment of soil organic carbon using Vis-NIR diffuse reflectance spectroscopy: Developing and testing a novel tractor-driven measuring chamber. *Soil & Tillage research*. 145: 93-102.
- SAS Institute Inc. 2014. SAS® 9.4 Statements: Reference. Cary, NC: SAS Institute Inc.
- Serrano, J., Shahidian, S. and Marques da Silva, J. 2014.** Spatial and temporal patterns of Apparent Electrical conductivity: DUALEM vs. Veris Sensors for monitoring soil properties. *Sensors*. 14: 10024-10041.
- Shi, Z., Ji, W., Viscarra Rossel, R.A., Chen, S., Zhou, Y., 2015.** Prediction of soil organic matter using a spatially constrained local partial least squares regression and the Chinese vis-NIR spectral library. *Eur. J. Soil Sci*. 66: 679-687.

- St. Luce, M., Ziadi, N., Zebarth, B., Grant, C.A., Tremblay, G.F. and Gregorich, G. 2014.** Rapid determination of soil organic matter quality indicators using visible near infrared reflectance spectroscopy. *Geoderma*. 232: 449-45.
- Stevens, A., Nocita, M., Toth, G., Montanarella, L., Wesemael, B.V. 2013.** Predicting of soil organic carbon at the European scale by visible and near infrared reflectance spectroscopy. *PLoS ONE*. 8: e66409.
- Sudduth, K.A., Kitchen, N.R., Bollero, G.A., Bullock, D.G. and Wiebold, W.J. 2003.** Comparison of Electromagnetic Induction and direct sensing of soil Electrical Conductivity. *Journal of Agronomy*. 95: 472-482.
- Sudduth, K.A., Kitchen, N.R., Wiebold, W.J., Batchelor, W.D., Bollero, G.A., Bullock, D.G., Clay, D.E., Palm, H.L., Pierce, F.J., Schuler, R.T. and Thelen, K.D. 2005.** Relating apparent electrical conductivity to soil properties across the north central USA. *Computers and Electronics in Agriculture*. 46: 263-283.
- Sun, W., Li, X., Niu, B. 2108.** Predicting of soil organic carbon in a coal mining area by Vis-NIR spectroscopy. *PLoS ONE*. 13: e0196198.
- Vanek, J., Balik, J., Shlha, J., Cerny, J. 2008.** Spatial variability of total soil nitrogen and Sulphur content at two conventionally managed fields. *Plant soil environment*. 54: 413-419.
- Vasques, G.M., Grunwald, S. and Harris, W.G. 2010.** Spectroscopic models of soil organic carbon in Florida, USA. *Journal of environmental quality*. 39: 923-934.

Veris technology 2009. Measuring soil carbon under cap-and-trade: Accurate, Affordable field verification using Veris spectroscopic sensors. www.veris.com .

Wang, H., Piazza, S.C., Sharp, L.A., Stagg, C.L., Couvillion, B.R., Steyer, G.D., McGinnis, T.E. 2017. Determining the spatial variability of wetland soil bulk density, organic matter, and the conversion factor between organic matter and organic carbon across Coastal Louisiana, U.S.A. *Journal of coastal research*. 33: 507-517.

Wang, J., Lu, X., Feng, Y. and Yang, R. 2018. Integrating multi-fractal theory and Geostatistics methods to characterize spatial variability of particle size distribution of minesoils. *Geoderma*. 317: 39-46.

Wang, T., Kang, F., Cheng, X., Han, H., Bai, Y., Ma, J. 2017. Spatial variability of organic carbon and total nitrogen in the soils of a subalpine forested catchment at Mt. Taiyue, China. *Catena*. 155: 41-52.

Wang, Y., Zhang, Xingchang, Z., Huang, C. 2009. Spatial variability of soil total nitrogen and soil total phosphorus under different land uses in a small watershed on the Loess Plateau, China. *Geoderma*. 150: 141-149.

Xiao-Wei, C., Xian-Jin, H., Wan-Jing, W., Mei, Z., Li, L., Qi-Lin, L. 2012. Spatial variability of soil organic carbon and related factors in Jiangsu Province, China. *Pedosphere*. 23: 404-414.

XLSTAT 2017 (Data Analysis and Statistical Solution for Microsoft Excel. Addinsoft, Paris, France.

- Xu, S., Zhao, Y., Wang, M., Shi, X. 2018.** Comparison of multivariate methods for estimating selected soil properties from intact soil cores of paddy fields by Vis-NIR spectroscopy. *Geoderma*. 310; 29-43.
- Zhang, H., Zhuang, S., Qian, H., Wang, F., Ji, H. 2015.** Spatial variability of the topsoil organic carbon in the Moso Bamboo forests of southern China in association with soil properties. *PLoS ONE* 10: e0119175.
- Zornoza, R., Guerrero, C., Mataix-Solera, J., Scow, K.M., Arcenegui, V. and Mataix-Beneyto, J. 2008.** Near infrared spectroscopy for determination of various physical, chemical and biochemical properties in Mediterranean soils. *Soil biology & biochemistry*. 40: 1923-1930.

4. SOIL MOISTURE CONTENT ESTIMATION USING GROUND PENETRATING RADAR

4.1. Abstract

Soil moisture content is an important index that influences irrigation scheduling and crop yield. However, conventional sampling method for site-specific evaluations cannot be used to acquire the large dataset required for soil water content. Therefore, geophysical investigation performed using the Ground Penetrating Radar technique with a wide-angle reflection and refraction survey method was used to estimate soil moisture content in the Northwest of Carberry in Southwestern Manitoba, Canada. This study was carried out to evaluate the potential of the Ground Penetrating to measure soil moisture content. In this study, a Pulse EKKO PRO GPR system with a central frequency of 500 MHz antenna was used at a loamy sand soil site. Soil moisture content was measured using the thermogravimetric method. The travel time and depth of reflector were used to calculate the dielectric permittivity, and volumetric water content was estimated using Topp's equation. The linear regression between the moisture content estimated using Topp's equation and lab-analyzed soil moisture content gave an R^2 of 0.83, and RMSE of $0.014 \text{ m}^3 \text{ m}^{-3}$. Dielectric permittivity was linearly related to soil moisture content with an R^2 of 0.95, and RMSE of 0.44. The obtained calibration curve shows that the dielectric permittivity measured by GPR is a good proxy for soil moisture content. These results indicate that Ground Penetrating Radar has the potential as an indirect technique for reliable measurement of soil moisture content at the field scale.

4.2. INTRODUCTION

The monitoring of soil moisture content is important for irrigation scheduling and optimizing crop yield (Grote et al., 2010). Other areas where the soil moisture content is important includes the; hydrologic cycle and fluxes (Steelman and Endres, 2012), remediation of contaminated lands and soil erosion (Ercoli et al., 2018), ground water recharge (Klotzsche et al., 2018), and meteorological and climatological researches (Reza and Ardekani, 2013). Conventional methods of measuring soil moisture content such as the thermogravimetric method, neutron scattering, and capacitance sensors provides point measurements (Weihermuller et al., 2007; Qin et al., 2013), and are not suited for taking measurement of an entire field (Cosenza, 2016). This is a major limitation in the management of irrigation (Galagedara et al., 2005).

To address this limitation, non-invasive methods of monitoring soil moisture content such as Ground Penetrating Radar (GPR), Time Domain Reflectometry (TDR), electromagnetic induction, ground-based radiometers, and Frequency Domain Reflectometry (FDR) are currently being used (Qin et al., 2013; Sharma et al., 2017; Ercoli et al., 2018). Ground penetrating radar has been the most extensively used non-invasive technique for estimating soil water content in the field or laboratory (Shamir et al., 2016). These non-invasive techniques are promising in advancing the current knowledge of soil moisture content and its variability by producing a more accurate sub-surface view than the one provided by conventional methods. Parsekian et al. (2012) recorded dielectric permittivity using a 1.6 MHz ground penetrating radar antenna at multiple water contents on four peats monoliths and confirmed that GPR is an effective tool for investigating soil moisture content in peat soil.

Gacitua et al. (2012) investigated soil moisture content with the GPR (400 MHz antenna) and concluded that GPR can provide continuous information in large areas without soil disturbance. El-Behiry and Hanafy (2013) used GPR tomography and reflection method to image relative soil moisture. Bakken and Stolt (2018) investigated subaqueous soils in created and natural lakes in Southern New England with GPR. Three common methods of survey are employed by the GPR. The Fixed offset (FO) method, Common mid-point (CMP) method, and the Wide-angle reflection and refraction (WARR) method. During the fixed offset survey, the distance between the transmitting and receiving antenna are fixed throughout the survey (Paz et al., 2017). In the CMP survey, both the transmitting and receiving antenna are moved apart during survey (Steelman and Endres, 2012). This is different for the WAAR method where the transmitting antenna is kept at a fixed position and the receiving antenna moved at increasing distances away from the transmitting antenna (Huisman et al., 2003).

The ground penetrating radar is a geophysical indirect technique for estimating soil moisture content. This is made possible because the electromagnetic wave velocity of the Ground Penetrating Radar is determined primarily by the dielectric constant of the medium (Galagedara et al., 2005; Mangel et al., 2017), a parameter that is strongly influenced by soil moisture content. In a GPR survey, the electromagnetic energy with a frequency ranging from 1 – 1000 MHz is transmitted to into the ground. Changes in dielectric properties of various soil component in the subsurface causes reflections, refraction or scattering of energy to occur which is then detected by the receiving antenna on the surface (Benedetto and Tosti, 2013; Raffelli et al., 2017). Aside the velocity analysis from the two-way travel time, which is the most common approach, other GPR methods employed in soil studies for water content include; Ground wave velocity, guided wave velocity and scattering, reflection coefficient, early-time signal analysis and full-time wave

inversion, which is mostly used in GPR signal numerical modelling (Zajicova and Chuman, 2019). Several studies have been carried out using these GPR survey methods. Lu et al. (2017) used both the common mid-point and fixed offset methods to measure soil moisture in steep slopes and observed a high accuracy with RMSE of $0.0101 \text{ m}^3 / \text{m}^3$ and $0.0068 \text{ m}^3 / \text{m}^3$ respectively. A study carried out in Guelph, Ontario, Canada used the wide-angle reflection and refraction and fixed offset methods to estimate soil water content during irrigation and drainage and obtained similar results between the two methods (Galagedara et al., 2005).

There are no fixed rules for determining the antenna frequency that should be used for a survey. The antenna frequency of the GPR used is based on the objectives of the study. The choice of antenna frequency is always dependent on the depth of penetration needed. Higher frequencies have higher resolutions and lower penetration depths, and lower frequencies have lower resolutions and higher penetration depths (Ludwig et al., 2009; Raffeli et al., 2017). Steelman and Endres (2012) used three sets of frequency, 225 MHz, 450 MHz, and 900 MHz, and reported their preference for the 450 MHz and 900 MHz frequencies for better resolution. Galagedara et al. (2005) investigated four different depths corresponding to higher and lower frequencies. A 900 MHz at a depth of 0.05 m, 450 and 200 MHz at a depth of 0.10 m, 100 MHz at a depth of 0.20 m.

Possible drawbacks in the estimation of soil moisture content using the GPR are bound to occur due to the heterogeneity of the soil. Clustering, considered to be noise, reduces the quality of the signal, and the amount of cluster depends on the degree of soil heterogeneities (Gacitua et al., 2012; Takahasi et al., 2015; Beauchamp et al., 2018). The degree of soil heterogeneity can be linked to soil stratigraphy, where contrasting soil horizons differ in the property that controls soil water content (Zajicova and Chuman, 2019).

Surface roughness can affect reflection resulting in distortion of incident and refracted rays (Agliata et al., 2018). Algeo et al. (2016) reported that soils with high clay content due to its high conductivity can impair the radar energy of the GPR by obscuring the reflection (Zajicova and Chuman, 2019).

The time interval of the electromagnetic wave between the transmitting antenna and the receiving antenna is termed the travel time, measured in nanoseconds (Parsekian et al., 2012; Huang et al., 2014; Lui et al., 2017). The velocity of electromagnetic wave in the air 3×10^8 m/s (0.3 m/ns) is a constant, hence the travel time for electromagnetic wave in the air is the same as the velocity of electromagnetic wave in the air (Lunt et al., 2005).

The dielectric permittivity measures the polarizability of a material, causing displacement current to flow, thereby affecting the propagation of electromagnetic waves (Mansi et al., 2017). The dielectric permittivity is directly related to the velocity of the electromagnetic waves, which is an essential property for processing and analyzing Ground Penetrating Radar data (Qin et al., 2013; Paz et al., 2017).

In relating the dielectric permittivity measured by the Ground Penetration Radar to soil moisture content, petrophysical relationships (Steelman and Endres, 2011) such as the Topp's equation or dielectric mixing model can be used to estimate soil water content (Lui et al., 2016; Klotzsche et al., 2018). The most commonly used relationship between apparent permittivity, ϵ_r , and volumetric soil water content, Θ_v ($\text{cm}^3 \text{cm}^{-3}$), was proposed by (Topp et al., 1980). The quality of the data in terms of accuracy and reliability can be checked. This is done by calibrating the indirect measurement of soil bulk density and moisture content from ground penetrating radar with direct sampling from laboratory measures (Ercoli et al., 2018).

Although innovative data analysis has been initiated for ground penetrating radar sensing of soil moisture content in civil engineering and geosciences, it has not been widely explored in agricultural research. There is an increasing relevance of soil moisture determination for understanding global weather dynamics, flooding and drought severity, crop yield estimation, movement of fertilizers and pesticides as well as many other applications. This increase in the demand for soil moisture data has led to the development of various techniques to quantify soil moisture (Ojo et al., 2015).

Therefore, the objective of this study was to

(a) to evaluate the potential of the GPR to measure soil moisture content.

Hypothesis: GPR travel time data, and a petro-physical relationship between dielectric constant and soil moisture content can be used to estimate soil moisture content on a Canadian Prairies field.

4.3. Materials and methods

4.3.1. Study area and description

The study was carried out on a farmer's cooperator field that is located about 10 km, northwest of Carberry in Southwestern Manitoba, Canada (SW-19-11-15W). The region is characterized by an average annual precipitation of 456 mm, with approximately 70 % falling as rain from April-October and 30 % as snow during the winter months and mean annual temperature of 2.1 °C. The site is located over the Assiniboine Delta Aquifer, an unconfined aquifer this is the source of drinking water. The site consists of Orthic Black Chernozem soils, which developed on lacustrine deposits. These are medium textured, well drained soils, where the upper (0 - 90 cm) depth increment is classified as loamy sand, and the underlying layer (> 90 cm) is sandy loam to loam. Sand content decreases with depth, from about 78% in the upper layer (0-10 cm) (Vivekanahan et al., 2018), while pH increases with depth from 6.37 at the surface layer to 8.33 at the 120 cm depth, and bulk density also gradually increases from 1.31 Mg m⁻³ at the top soil to 1.50 Mg m⁻³ at the 120 cm depth (Enns, 2004). The experimental field was 65 × 55 m (0.36 ha) in size. The cropping system followed a Barley-wheat rotation with conventional agronomic management starting in 2002.

4.3.2. Sampling scheme and soil sampling

Vivekanahan et al. (2018) used a method developed by Zar (2010) to determine the number of sampling points (178) for analysis using the variability of sand percentage at 0 - 10 cm and 60 - 90 cm depth of the field. We selected fifty (50) of the 178 sampling points as the number of samples required to identify significant difference in bulk density at the site. This was calculated using the bulk density data obtained in 2001 (Enns, 2004) and the preliminary bulk density data for this study acquired in August 2017. Based on these two datasets fifty samples were required to detect the variability at 1 % difference with the power of test of 0.8. The site was surveyed, field boundaries were marked and spatial coordinates for each sample points were recorded. In each of the 50 sampling points, Universal Transverse Mercator (UTM) coordinates were measured using a GPS. Undisturbed soil samples were taken from 0 - 90 cm depth in 3" plastic sleeves with a Giddings hydraulic soil punch. After the soil samples were collected, they were stored in totes containing ice during transport to the laboratory and immediately stored in the refrigerator (4 °C) on arrival to prevent moisture loss.

4.3.3. Ground Penetrating Radar data collection

This study used the pulse EKKO PRO GPR at a central frequency of 500 MHz shielded antenna (Sensors and Software Inc., Mississauga, Ontario, Canada). The instrument is fitted with an odometer wheel for triggering antennas, and a Panasonic Toughbook for data collection, to conduct a wide-angle reflection and refraction survey along a fixed survey line at each of the 50 sampling points (0 - 0.1 m), and a Global Positioning System (GPS) antenna to provide positional information.

Repeated measurements were taken at the same location with increasing antenna spacing using the wide-angle reflection and refraction method. This method allowed the same feature to provide the echoes, but at different antenna spacing, making the wide-angle reflection and refraction method excellent at obtaining good velocity estimates. The transmitting antenna was held stationary at the sampling location, and the receiving antenna (Rx) was moved out from the transmitting antenna (Tx) in increment of 2.5 cm up to 0.1 m and readings taken at each increment.

4.3.4. Ground Penetrating Radar processing

The Ground Penetrating Radar data was processed using the EKKO project software (Sensors & software 2019). The processing was applied only to the data collected at the 50 sampling (test holes) for laboratory analysis, using the positional information provided by the GPS. Prior to processing, a typical wide-angle reflection and refraction section showed multiple half parabolas (Figure 4.1). This radargram needs hyperbola fitting to calculate the electromagnetic wave velocity from the reflection. This velocity can be used to estimate the soil moisture content.

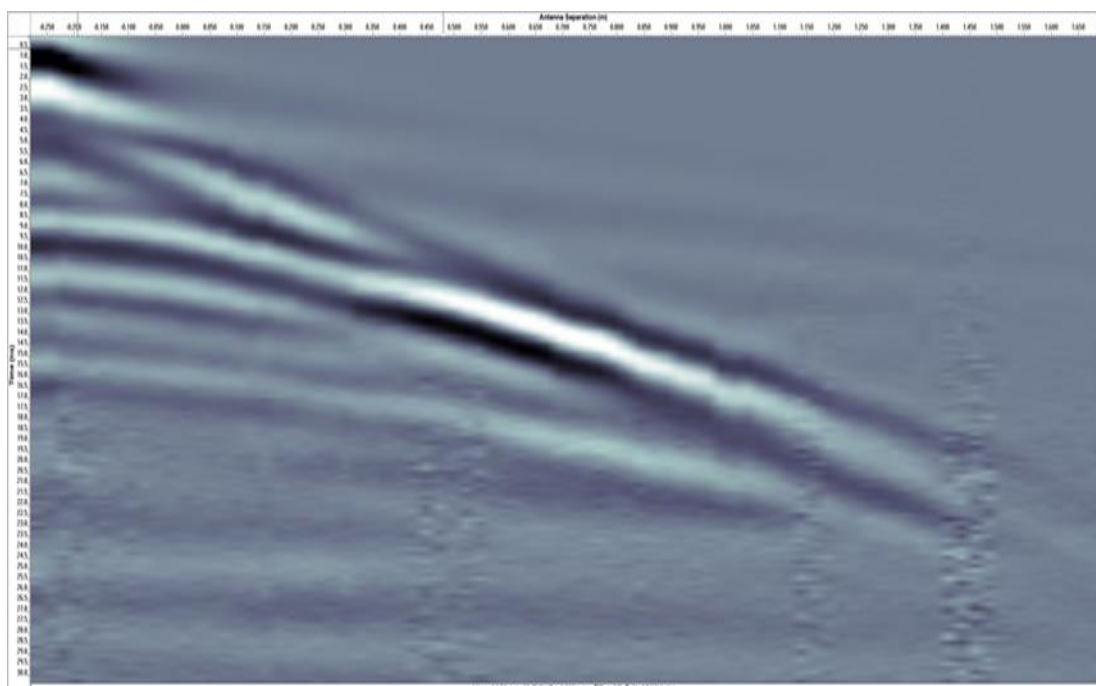


Figure 4.1. Raw GPR data (radargram) showing hyperbolic reflections.

To ensure accurate depths, the first break at time zero was examined, adjusted and repicked on each trace on an amplitude deviation corresponding to 5 % of the maximum amplitude (Hans et al., 2015; Jazayeri et al., 2018; Nyquist et al., 2018). Background subtraction was then applied to the sections (raw data). The background subtraction was completed with a filter width that is equal to the survey line length (Akpan et al., 2018). With this filter length, multiple echoes due to noise such as antenna ringing were removed while retaining signals from any flat laying reflectors. Background subtraction essentially removes the average trace amplitude of all traces from each trace (Paz et al., 2017; Godio et al., 2018). The next step was enveloping (Figure 4.2), this operation converts the traces from a wavelet with both positive and negative amplitudes to a monopulse wavelet with all positive amplitude (Castrignano et al., 2018). Enveloped data gives a better representation of reflection strength, removes oscillatory nature, and leaves true resolution. The acquired GPR signal represents the original portion of the signal.

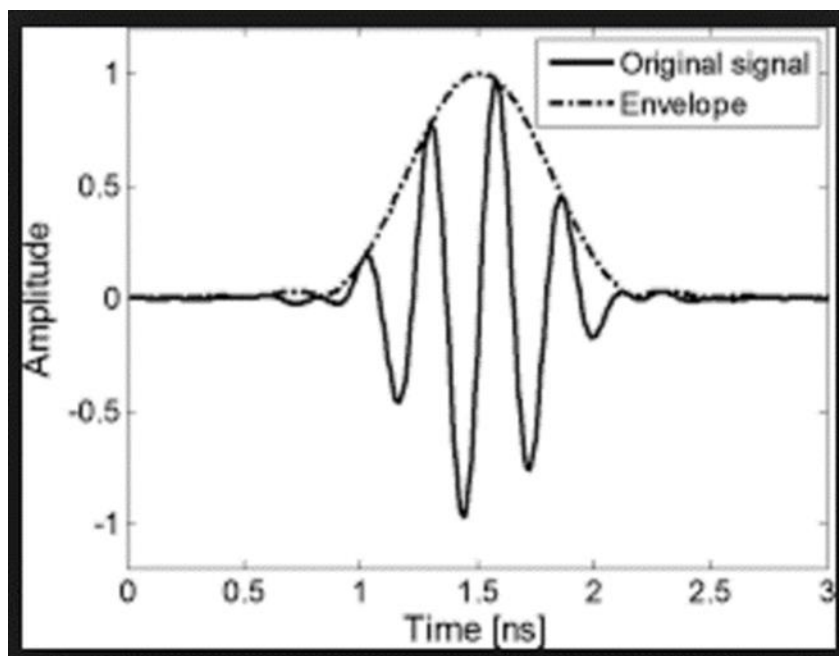


Figure 4.2. Typical ground penetrating radar trace (thick black line) and corresponding envelope (broken line) from a sampling point in the field.

A spreading exponential calibrated compensation (SEC) gain was applied to the data to boost returns from weak reflectors. The SEC gain is the closest to physical reality. It starts at the Start Gain and becomes constant at the Max Gain (Figure 4.3). The spreading exponential calibrated compensation gain was used because it has an exponential component, a constant component, and most accurately compensates for signal loss due to energy / wave front size factors and amplify the strength of the signal (Castrignano et al., 2018; Nyquist et al., 2018). The exponential component was used to compensate for the dissipation of energy that occurred as the wave propagates and the physical dilution of the signal that occurred due to increased wave front area.

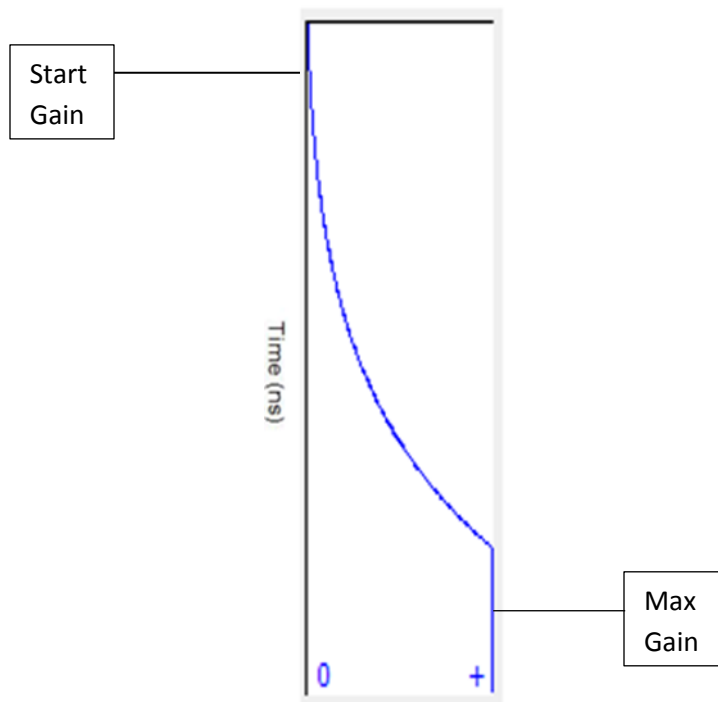


Figure 4.3. Shape of the SEC gain function.

Data stacking was done using semblance analyses. This analysis essentially stacks the data traces at multiple velocities in very small velocity increments. For this study, data was stacked at 0.01 m/ns. Data stacking reduces noise and reveals the true velocities as traces stacked at their true velocity tend to be additive and shows stronger signal, whereas traces stacked at improper velocities tend to stack destructively (Campbell et al., 2018; Lu et al., 2018). Figure 4.4. shows a stacked WAAR traces, and from semblance plots velocity and return time, the travel depth and electromagnetic wave velocity were obtained.

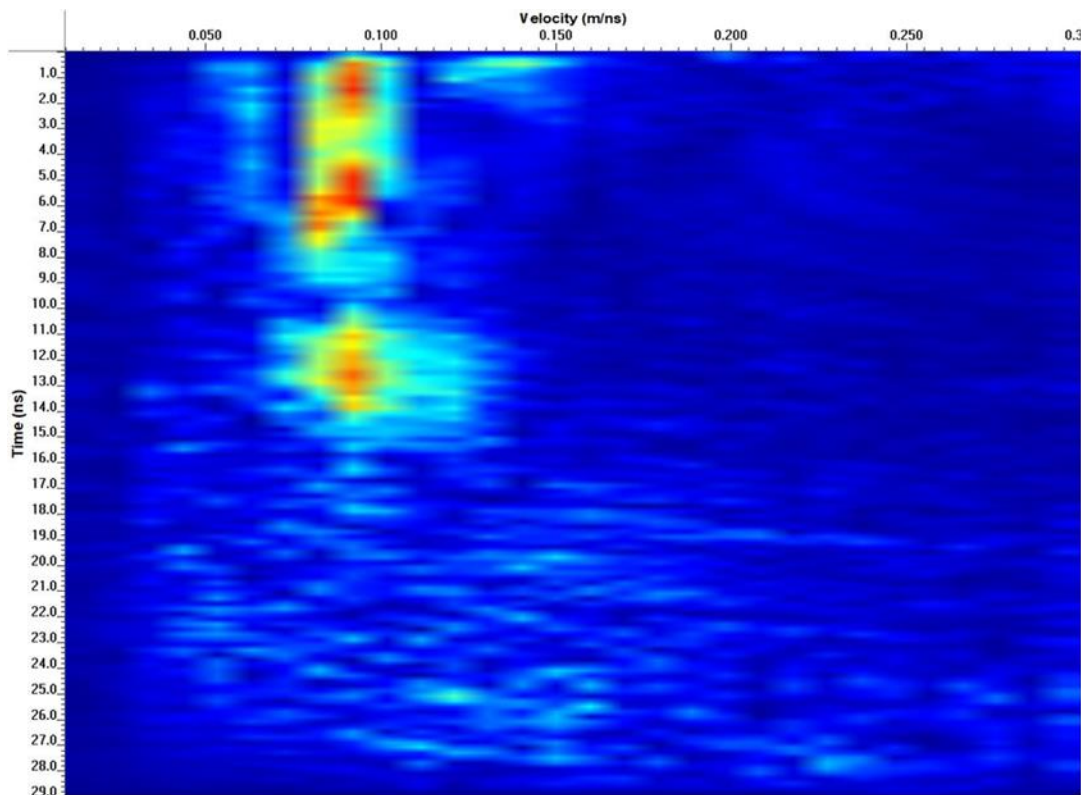


Figure 4.4. Semblance plot of the wide-angle reflection and refraction measurement to illustrate how electromagnetic wave velocity vs time are obtained. The red colours indicate high semblance.

4.3.5. Laboratory analysis and calculations used for calibration

The Ground Penetrating Data mapping requires calibration equations for soil moisture content. The soil in the sleeve was divided into six depths at 15 cm interval (0-15 cm, 15-30 cm, 30-45 cm, 45-60 cm, 60-75 cm, 75-90 cm), and the top soil (0-15 cm) was used for analysis. The total wet weight of each sample was measured and a subsample (50 g) was taken for moisture content determination by drying in an oven (105 °c) for 48 hours (Gardner, 1986). Volumetric water content was calculated as follows.

$$\theta_g = \frac{M_w}{M_s} \quad (1)$$

where M_s is the mass of dry soil, M_w is the mass of water, and θ_g is the gravimetric water content.

$$\rho_b = \frac{M_s}{V_t} \quad (2)$$

Bulk density (ρ_b) was calculated as the ratio of the total mass of the dry soil (M_s) to the total volume of the soil (V_t). The total volume of soil was calculated using the formula for volume of a cylinder, $\pi r^2 h$.

$$\theta_v = \frac{\theta_g \times \rho_b}{\rho_w} \quad (3)$$

Where θ_v = Volumetric water content, and ρ_w = density of water

4.3.6. Soil moisture content - Permittivity relationship

Topp's equation was used to relate the Ground Penetration Radar measurement of dielectric permittivity to soil moisture content in this study.

The velocity of propagation V is given by:

$$V = \frac{C}{\sqrt{\epsilon_r}} \quad (4)$$

C = propagation velocity of an electromagnetic wave in free space (3×10^8 m/s)

ϵ_r = relative permittivity.

V = velocity of propagation

using the expression

$$\epsilon_r = \left[\frac{ct}{2d} \right]^2 \quad (5)$$

The ϵ_r was determined from the electromagnetic wave travel time (signal time) (t) that a voltage pulse takes to travel forward and backward along a wave-guide (transmission line) of length L / depth D (Fantello et al., 2018). ϵ_r as a function of θ_v is only weakly dependent on soil type, bulk density, temperature, and EC of the soil. Topp's equation to determine θ_v was used as thus (Hillel, D. 1998);

$$\theta_v = - 5.3 \times 10^{-2} + 2.9 \times 10^{-2} \epsilon_r - 5.5 \times 10^{-4} \epsilon_r^2 + 4.3 \times 10^{-6} \epsilon_r^3 \quad (6)$$

4.3.7. Statistical analysis

Descriptive statistical parameters such as the mean, standard deviation, and test for normality were calculated with SAS 9.4 (SAS Institute Inc, 2014) software. Standard statistical analysis such as

coefficient of determination, and root-mean-square error (RMSE) were measured. For validation, the 50-soil moisture content values (0-15 cm) were used to obtain a simple linear regression between the dielectric permittivity and soil moisture content obtained from volumetric method, and between the Ground Penetrating data reflection travel times and wave velocity (relative permittivity), and lab-analyzed soil moisture content. The statistical software XLSTAT 2017 (least squares method) (Data Analysis and Statistical Solution for Microsoft Excel. Addinsoft, Paris, France) was used to assess these relationships.

4.4. Results and discussion

4.4.1. Soil moisture content and Ground Penetrating Radar.

The soil moisture content at this site ranged from 0.06 cm³ cm⁻³ to 0.30 cm³ cm⁻³. The estimated soil moisture content from the ground penetrating radar ranged from 0.15 cm³ cm⁻³ to 0.26 cm³ cm⁻³, and dielectric permittivity ranged from 6.24 to 14.04 (Table 4.1). The coefficient of variation due to experimental error was highest in lab-analyzed soil moisture content and lowest in estimated soil moisture content.

Table 4.1. Descriptive summary statistics for measured soil moisture content, GPR estimated soil moisture content and dielectric permittivity (0- 15 cm).

Soil property (0-15 cm)	Mean	Coefficient of variation (%)	Standard deviation	Minimum	Maximum
Soil Moisture content (Lab) (cm ³ cm ⁻³)	0.17	43	0.07	0.06	0.30
GPR* (cm ³ cm ⁻³)	0.19	17	0.03	0.15	0.26
Dielectric permittivity (GPR)	10.26	19	2.0	6.24	14.04

* GPR = Ground Penetrating radar estimated soil water content.

4.4.2. Dielectric permittivity and soil moisture content

Dielectric permittivity depends on factors such as temperature, salt content, soil texture and soil moisture content, but strongly on soil moisture content. Figure 4.1. shows the relationship obtained between dielectric permittivity and soil moisture content with a coefficient of determination of 0.95 and root means square error of 0.44. The success of this relationship is attributed to the large contrast in permittivity of water within the frequency bandwidth (10 MHz to 1 GHz) of the ground penetrating radar (Huisman et al., 2003; Hans et al., 2015; Cosenza, 2016). The high correlation indicates that the dielectric permittivity is a good proxy for soil moisture content. Both Kaplanvural et al. (2018) and Agliata et al. (2018) reported that the permittivity determined from the electromagnetic wave velocity also agreed well with the gravimetric method. This result was in line with the Mahmoudzadeh Ardekani (2013) who reported a coefficient of determination of 0.96 during a field-scale mapping of soil moisture using the GPR technique. Hans et al. (2015) also reported an R^2 of 0.97 for thawed wood and $R^2 = 0.99$ for frozen wood when GPR was used to measure the water content of the log.

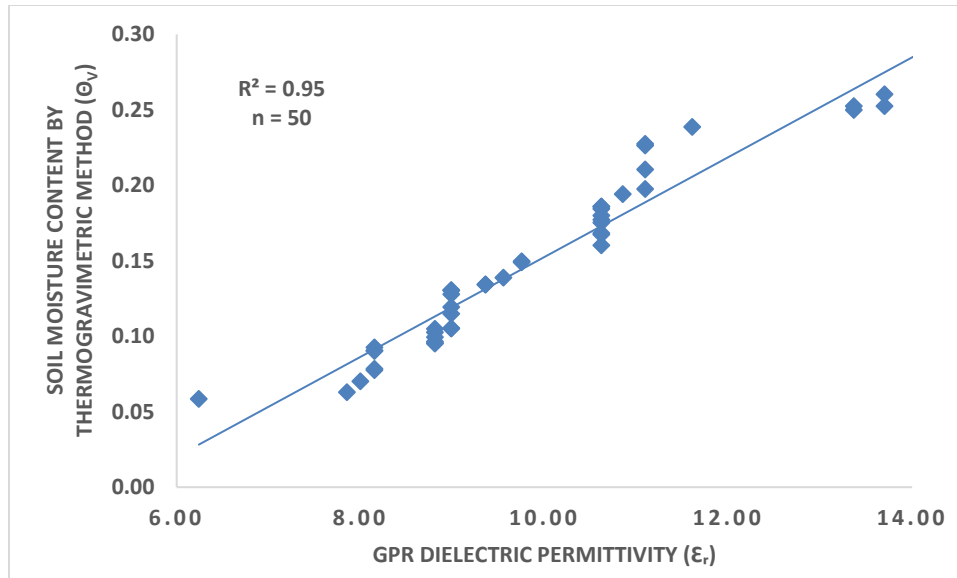


Figure 4.5. Relationship between dielectric permittivity estimated from the GPR and soil moisture content from thermogravimetric method.

4.4.3. Soil moisture content.

Soil moisture content by thermogravimetric method was used as standards to validate the GPR derived soil moisture content that was estimated from Topp's equation. A simple linear regression was used for the validation. Based on the coefficient of determination (R^2) and RMSE, the accuracy of the method was determined. Relating the volumetric water content derived from Topp's equation to the soil moisture content by volumetric method gave a RMSE of $0.014 \text{ cm}^3 \text{ cm}^{-3}$ and a coefficient of determination of 0.83, which implies that the ground penetrating radar measurement results are reliable on a Canadian Prairies (Figure 4.2).

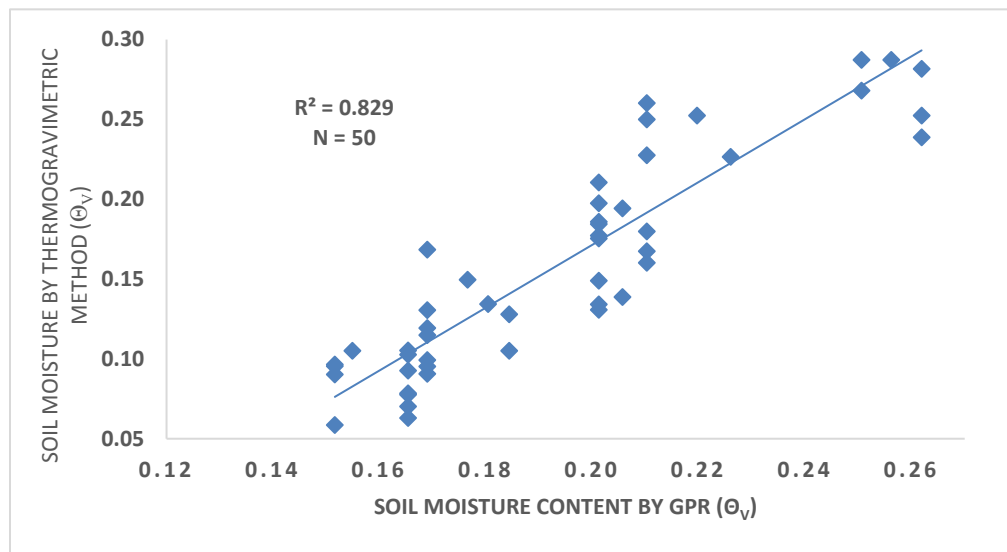


Figure 4.6. Graph of conventionally measured and GPR estimated soil moisture content derived from Topp's equation.

The good relationship between measure soil moisture and GPR estimated soil moisture (Figure 4.6b) was in line with the results reported by (Lunt et al., 2005; Huang et al., 2014; Cui et al., 2015; Ercoli et al., 2018). The sources of errors could be due to the site condition. The performance of the Ground Penetrating Radar is affected by soil texture (Grote et al., 2010). Sandy soils reduce the reflected wave. A study carried out by Cui et al. (2015) investigated the relationship between radar wave energy and the level of compaction of a sandy loam. They reported an increase in radar wave energy in areas with low sandy loam and compaction.

4.5. Conclusion

High frequency electromagnetic soil water sensors are promising techniques to fulfil the goal of Precision Agriculture. We have specifically demonstrated the potential of estimating moisture content on a Canadian Prairies field using a non-destructive Ground Penetrating Radar. Wide-angle reflection and refraction survey method was used in measuring soil moisture content. Ground Penetrating Radar has shown to be an excellent tool for subsurface mapping of soil moisture content due to its ability to provide continuous information. The soil moisture content measurement by ground penetrating radar was consistent with the thermogravimetric method result, with a RMSE of $0.014 \text{ cm}^3 \text{ cm}^{-3}$. Compared with conventional method, ground penetrating radar can rapidly measure soil moisture content without wrecking the soil layers. The correlation between the Ground Penetrating Radar and thermogravimetric method was remarkably good (R^2 0.83) for soil moisture content. Further studies should be carried out on the application of different ground penetrating radar method of survey in the Canadian Prairies, with the combination of other GPR and soil water model. The results showed satisfactory applicability of the Ground Penetrating Radar in estimating soil moisture content, by verifying this accuracy using the thermogravimetric method. These are important in modelling ground water recharge, transport of pollutant to ground water, preferential flow, managing the vadose zone and irrigation.

4.6. References

- Agliata, R., Bogaard, T.A., Greco, R., Mollo, L., Slob, E.C., Steele-Dunne, S.C. 2018.** Non-invasive estimation of moisture content in tuff bricks by GPR. *Construction and Building Materials*. 160: 698-706.
- Akpan, A.E., Ekwok, S.E., Ebong, E.D., George, A.M., Okwueze, E.E. 2018.** Coupled geophysical characterization of shallow fluvio-clastic sediments in Agwagune, Southeastern Nigeria. *Journal of African Earth Sciences*. 143: 67-78.
- Algeo, J., Van Dam, R.L., Slater, L. 2016.** Early-Time GPR: A method to monitor spatial variations in soil water content during irrigation in clay soils. Open access. *Soil Science Society of America*.
- Allred, B., Freeland, R., Grote, K., McCoy, E., Martinez, L., Gamble, D. 2016.** Ground penetrating radar water content mapping of Golf Course Green sand layers. *Journal of Environmental and Engineering Geophysics*. 21: 215-229.
- Bakken, J. and Stolt, M. H. 2018.** Mapping freshwater subaqueous soil resources: Examples from Southern New England. *Soil Science Society of America Journal*. 82: 403-412.
- Beauchamp, R. M., Arumugam, D.D., Burgin, M.S., Bush, J.D., Khazendar, A., Gim, Y., Almorqi, S., Almalki, M., Almutairi, Y.A., Alsama, A.A., Alanezi, A.G. 2018.** Can airborne ground penetrating radars explore groundwater in Hyper-Arid Regions? *Open Access Journal*. 10: 1109.

- Benedetto, F. and Tosti, F. 2013.** GPR spectral analysis for clay content evaluation by the frequency shift method. *Journal of Applied Geophysics*. 97: 89-96.
- Campbell, S., Affleck, R. T. and Sinclair, S. 2018.** Ground-penetrating radar studies of permafrost, periglacial, and near-surface geology at McMurdo Station, Antarctica. *Cold Regions Science and Technology* 148:38-49.
- Castrignano, A., Buttafuoco, G., Quarto, R., Parisi, D., Viscarra Rossel, R.A., Terribile, F., Langella, G., Venezia, A. 2018.** A geostatistical sensor data fusion approach for delineating homogenous management zones in Precision Agriculture. *Catena*. 167: 293-304.
- Cosenza, P. 2016.** Indirect determination of soil water content. *E3S Web of Conferences*. 9: 04004.
- Cui, F., Wu, Z., Wang, L., Wu, Y. 2015.** Application of the Ground Penetrating Radar ARMA power spectrum estimation method to detect moisture content and compactness values in sandy loam. *Journal of Applied Geophysics*. 120: 26-35.
- El-Behiry, M.G. and Hanafy, S.M. 2013.** Imaging soil moisture using GPR tomography and reflection field experiments. *Arab Journal of Geoscience*. 6: 3493-3503.
- Enns, J. M. 2004.** The effect of liquid hog manure and commercial fertilizer on nutrient movement in a sandy soil, M. Sc thesis, University of Manitoba.
- Ercoli, M., Di Matteo, Pauselli, C., Mancinelli, P., Frapiccini, S., Talegali, L., Cannata, A. 2018.** Integrated GPR and laboratory water content measures of sandy soils: from laboratory to field scale. *Construction and Building Materials*. 159: 734-744.

- Fantello, N., Parsekian, A.D., Anthony, M.W. 2018.** Estimating winter ebullition bubble volume in lake ice using ground penetrating radar. *Geophysics*. 83: H13-H25.
- Gacitua, G., Tamstorf, M.P., Kristiansen, S.M., Uribe, J.A. 2012.** Estimations of moisture content in the active layer in an Arctic ecosystem by using ground-penetrating radar profiling. *Journal of Applied Geophysics*. 79: 100-106.
- Galagedara, L.W., Parkin, G.W., Redman, J.D., Von Bertoldi, P., Endres, A.L. 2005.** Field studies of the GPR ground wave method for estimating soil water content during irrigation and drainage. *Journal of Hydrology*. 301: 182-197.
- Gardner, W.H. 1986.** Water content. In: Klute, A., ed., *Methods of Soil Analysis: Part I--Physical and mineralogical methods: Soil Science Society of America Book Series No. 5*, Soil Science Society of America, Madison, Wisconsin, p. 493-544.
- Godio, A., Frigo, B., Chiaia, B., Maggioni, P., Freppaz, M., Ceaglio, E., Dellavedova, P. 2018.** Integration of upward GPR and water content reflectometry to monitor snow properties. *Journal of Near Surface Geophysics*. 16: 154-163.
- Grote, K., Anger, C., Kelly, B., Hubbard, S., Rubin, Y. 2010.** Characterization of soil water content variability and soil texture using GPR groundwave techniques. *Journal of Environment and Engineering Geophysics*. 15: 93-110.
- Hans, G., Redman, D., Leblon, B., Nader, J., La Rocque, A. 2015.** Determination of log moisture content using early-time ground penetrating radar signal. *Wood Material Science and Engineering*. 1: 112-129.
- Hillel, D. 1998.** *Environmental soil physics*. Academic Press.

- Huang, W., Lu, F., Lee, Y. 2014.** GPR system for monitoring paddy moisture content in a drying process. *Journal of drying technology*. 32: 679-685.
- Huisman, J.A., Hubbard, S.S., Redman, D.J., Annan, A.P. 2003.** Measuring soil water content with Ground Penetrating Radar: A review. *Vadose Zone Journal*. Soil Science Society of America. 2: 476-491.
- Jazayeri, S., Klotzsche, A., Kruse, S. 2018.** Improving estimates of buried pipes and infilling material from ground-penetrating radar profiles with full-waveform inversion. *Journal of Geophysics*. 83: 27-41.
- Jonard, F., Mahmoudzadeh, M., Roisin, C., Weihermuller, L., Andre, F., Minet, J., Vereecken, H., Lambot, S. 2013.** Characterization of tillage effects on the spatial variation of soil properties using ground-penetrating radar and electromagnetic induction. *Geoderma*. 207-208: 310-322.
- Kaplanvural, I., Peksen, E., Ozkap, K. 2018.** Volumetric water content estimation of C-30 concrete using GPR. *Construction and Building Materials*. 166: 141-146.
- Kazunori, T., Igel, J., Preetz, H., Sato, M. 2015.** Sensitivity analysis of soil heterogeneity for ground penetrating radar measurements by means of a simple modelling. *Radio Science*. 50: 79-86.
- Klotzsche, A., Jonard, F., Looms, M.C., Van der Kruk, J., Huisman, J.A. 2018.** Measuring soil water content with Ground Penetrating Radar: A decade of progress. *Vadose Zone Journal*. 17: 180052.

- Lebron, I., Robinson, D.A., Goldberg, S., Lesch, S.M. 2004.** The dielectric permittivity of calcite and arid zone soils with carbonate minerals. *Soil Science Society of America Journal*. 68: 1549-1559.
- Liu, X., Dong, X., Daniel, I.L., 2016.** Ground penetrating radar for underground sensing in agriculture: a review. *Journal of international agrophysics*. 30: 533-543.
- Liu, X., Dong, X., Xue, Q., Leskovar, D.I., Jifon, J., Butnor, J.R., Marek, T. 2018.** Ground penetrating radar (GPR) detects fine roots of Agricultural crops in the field. *Journal of plant science*. 423: 517:531.
- Lu, Y., Song, W., Lu, J., Wang, X., Tan, Y. 2017.** An examination of soil moisture estimate using Ground Penetrating Radar in Desert Steppe. *Journal of Water*. 9: 521.
- Ludwig, r., Gerhards, H., Klenk, P., Wollschlager, U., Buchner, J. 2009.** Electromagnetic methods in applied geophysics. Institute of Environmental Physics, Heidelberg University, Heidelberg, Germany. pp 59.
- Lunt, I.A., Hubbard, S.S., Rubin, Y. 2005.** Soil moisture content estimation using ground-penetrating radar reflection data. *Journal of Hydrology*. 307: 254-269.
- Mahmoudzadeh Ardekani, M.R. 2013.** Off-and-on ground GPR techniques for field-scale soil moisture mapping. *Geoderma*. 200-201: 55-66.
- Mangel, A.R., Moysey, M.J, Van der Kruk, J. 2017.** Resolving infiltration-induced water content profiles by inversion of dispersive Ground Penetrating Radar data. *Vadose Zone Journal*. 16: 10.

- Mansi, A.H., Castillo, M.P., Bernasconi, G. 2017.** Controlled laboratory test for the investigation of LNAPL contamination using a 2.0 GHz ground penetrating radar. *Bollettino di Geofisica Teorica ed Applicata*. 58: 169-180.
- Nikiema, P., Buckley, K. E., Enns, J. M., Qiang, H., and Akinremi, O. O. 2013.** Effects of liquid hog manure on soil available nitrogen status, nitrogen leaching losses and wheat yield on a sandy loam soil of western Canada. *Can. J. Soil Sci.* 93: 573–584.
- Ojo, E.R., Bullock, P.R., L’Heurex, J., Powers, J., Mc Nairn, H., Pacheco, A., 2015.** Calibration & evaluation of a Frequency Domain Reflectometry sensor for real time soil moisture monitoring. *Vadose zone journal*.
- Parsekian, A., Slater, L., Gimenez, D. 2012.** Application of Ground Penetrating radar to measure near-saturation soil water content in peat soils. *Water resources research*. 48: W02533.
- Paz, C., Alcalá, F.J., Carvalho, J.M., Ribeiro, L. 2017.** Current uses of ground penetrating radar in groundwater-dependent ecosystems research. *Science of Total Environment*. 595: 868-885.
- Qin, Y., Chen, X., Zhou, K., Klenk, P., Roth, K., Sun, L. 2013.** Ground penetrating radar for monitoring the distribution of near surface soil water content in the Gurbantunggut Desert. *Environmental Earth Science*. 70: 2883-2893.
- Raffelli, G., Previati, M., Canone, D., Gisolo, D., Bevilacqua, I., Capello, G., Biddoccu, M., Cavallo, E., Deiana, R., Cassiani, G., Ferraris, S. 2017.** Local-and plot-scale measurements of soil moisture: Time and spatially resolved field techniques in Plain, Hill, and Mountain Sites. *Water*. 9: 706.

SAS Institute Inc. 2014. SAS® 9.4 Statements: Reference. Cary, NC: SAS Institute Inc.

Sensors and Software Inc., Mississauga, Ontario, Canada.

Sensors & Software 2019. EKKO_Project Software. Mississauga, ON, Canada

<https://www.sensoft.ca/products/ekko-project/overview/>

Sharma, P., Kumar, B., Singh, D., Gaba, S.P. 2017. Critical Analysis of background subtraction techniques on real GPR data. Defence Science Journal. 67: 559-571.

Steelman, C.M. and Endres, A.L. 2012. Assessing vertical soil moisture dynamics using multi-frequency GPR common-midpoint soundings. Journal of Hydrology. 436-437: 51-66.

Steelman, C.M., and Endres, A.L. 2011. Comparison of petrophysical relations for soil moisture estimation using GPR ground waves. Vadose Zone Journal. 10: 270-285.

Topp, G.C., Davis, J.L., Annan, A.P., 1980. Electromagnetic determination of soil water content: measurements in coaxial transmission lines. Water resources research, 16, 574-582.

Tosti, F., Patriarca, C., Slob, E., Benedetto, A., Lambot, S. 2013. Clay content evaluation in soils through GPR signal processing. Journal of Applied Geophysics. 97: 69-80.

Vivekanahan. K, Akinremi, O., Moulin, A.P. and Kumaragamage, D. 2018. Importance of terrain attributes in relation to the spatial distribution of soil properties at the micro scale: a case study. Canadian journal of soil science. 98: 292-305.

Weihermuller, L., Huisman, J.A., Lambot, S., Herbst, M., Vereecken, H. 2007. Mapping the spatial variation of soil water content at the field scale with different ground penetrating radar techniques. *Journal of Hydrology*. 340: 205-216.

Zajicova, K. and Chuman, T. 2019. Application of ground penetrating radar methods in soil studies: A review. *Geoderma*. 343: 116-129.

Zar, J. H. 2010. Bio statistical analysis, Prentice Hall, Upper Saddle River, NJ. pp 211-213.

5. General Synthesis

Spatial variability of soil properties that exists in the field, and within the soil profile has received increased attention in recent times. However, conventional sampling of these variable soil properties has not been able to meet the goal of Precision Agriculture, which is to utilize soil, water resources, and chemical input based on the variability in soil properties. Hence, the introduction of proximal sensors which provides more detailed information about the field and allows for repeated measurements. Several studies have emphasized the susceptibility of the Assiniboine Delta Aquifer to leaching (Vivekanahan et al., 2018).

The leachate produced was influenced by the variability of soil texture. To further understand the influence of texture, a detailed analysis on the spatial distribution of soil bulk density and moisture content with depth was conducted in this study. Investigation on the spatial variability of bulk density with depth has not been undertaken on prairie soils. There is also a growing demand for proximal sensors in areas where conventional methods are limited. This study was conducted to investigate the spatial distribution of bulk density with depth, and soil moisture in two seasons. We also evaluated the potential of using proximal sensors to estimate soil physical and chemical properties, and to produce maps showing variability of soil properties within the field and in the soil profile on a Canadian Prairies field. Thus, a geospatial sampling scheme was used for sampling to capture such variabilities in the field. Undisturbed soil samples were taken from 0 - 90 cm depth in 3" plastic sleeves with a Giddings hydraulic soil punch. They were analyzed for soil bulk density and moisture content. Soil samples from the top 15 cm were analyzed for soil organic carbon, total carbon, and total nitrogen.

The Veris OpticalMapper equipped with a GPS was pulled with a truck through the field to measure spectral reflectance at approximately 7 cm below the soil surface, which can be related to soil organic carbon, total carbon, and total nitrogen. Ground Penetrating Radar with a frequency of 500 MHz was used to measure electromagnetic wave velocity and travel time, which can be used to estimate the dielectric permittivity of the soil.

Soil bulk density and moisture content were spatially autocorrelated and varied significantly within the field. Soil bulk density showed strong spatial autocorrelation from 0 cm to 75 cm depth where more than 80 % of the total variation was accounted for by spatial variability. However, the spatial dependence increased with depth as the residual sum of square values decreased. The interpolated maps clearly showed the spatial variability of bulk density at the study site. However, the variability of bulk density increased with depth (Gilsonley et al., 2016). We found that the top soil was less spatially coherent compared to other depth which we attributed to directional tillage over the years (Barik et al., 2014). The increase in bulk density with depth suggests the effect of compaction which occurs at the soil surface but increases with depth. We also observed that soil texture had a major influence on the variability of bulk density at this site.

Soil moisture content in both seasons were strongly autocorrelated from the top soil to the 75 cm depth, where more than 75 % of the total variation was accounted for by spatial variability. The weak correlation observed at the 90 cm depth in the Fall of 2017 suggests that variability at this depth was due to random effect. Interpolated maps clearly showed a mirror image of bulk density. This suggests a negative correlation between moisture content and bulk density.

Geospatial pattern of soil moisture in both seasons was almost invariant as they both had the same regions with high and low soil moisture content, which suggests that the spatial pattern of soil texture controls soil moisture at this site. Our results showed the dominant effect of soil texture and bulk density on soil water content.

Spectral reflectance measured by the Veris OpticalMapper was strongly related with laboratory values of organic carbon. This suggest that organic carbon can be modelled with spectral reflectance because of the relationship between the wavelengths, overtones and combination bands of molecular vibrations of C-H, O-H, and N-H. This result was validated by the ratio of predictive deviation (RPD), which was accurate (> 2.0) for both organic carbon and total carbon, and moderate (between 1.4 – 2.0) for total nitrogen. We found out that variability in soil texture, moisture, and bulk density influenced the performance of the Veris OpticalMapper, with the dominant soil texture being loamy sand at this site. The regions having high bulk density and sand content were low in soil organic carbon, total carbon, and total nitrogen, and the regions with high clay content and soil moisture were high in the soil properties investigated. This suggest the retaining ability of organic matter to soil water, and the ability of clay soils to retain organic matter.

Our results showed that the distribution of soil texture, bulk density, and soil moisture influenced the variability of soil organic carbon, total carbon and total nitrogen. Also, bulk density and sand content were negatively correlated with SOC, TC, and TN, and positively correlated with moisture content and clay content. Soil organic carbon, total carbon, and total nitrogen showed strong autocorrelation (0 – 15 cm), where more than 80 % of total variation was accounted for by spatial variability.

Our results thereby suggest that continuous tillage, fertilizer application, and mineralogy could also lead to variability in soil organic carbon, total carbon, and total nitrogen. We found the Veris soil organic carbon from the Pearson analysis to be significantly (> 0.05) and positively correlated with Lab-analyzed soil organic carbon, total carbon, and total nitrogen. The coefficient of determination (R^2) between the dielectric permittivity obtained by the Ground Penetrating Radar and soil moisture content by volumetric method was 0.95. This high correlation suggests that the dielectric permittivity of the medium is strongly influenced by soil moisture content and essential in analyzing Ground Penetrating Radar data, hence a good proxy to determine soil moisture content. The validation method to determine the accuracy of the estimated soil moisture content obtained from Topp's equation gave an R^2 of 0.83 for soil moisture content. This result suggests the reliability of the ground penetrating radar measurement of soil moisture content on a Canadian Prairies.

This study provides an insight into the significance of microspatial variability on a Canadian Prairies and demonstrated the potential of proximal sensors to accurately measure and provide detailed information on soil physical and chemical properties. We recommend that the spatial distribution of soil texture, moisture, and bulk density should be considered in delineating management zones for irrigation, and application of fertilizers. We also recommend the evaluation of spatial variability of bulk density over time. Further studies should also be done on other GPR and soil moisture models in using the GPR to estimate soil moisture on a Canadian Prairies field.

References

- Barik, K., Aksakal, E.L., Islam, K.R., Sari, S. and Angin, I. 2014.** Spatial variability in soil compaction properties associated with field traffic operations. *Catena*. 120: 122-133.
- Gilsonley Lopes dos Santos, L.S., Pereira, M.G., Marcos, S.S., Ceddia, B., Mendonca, V.M., Delgado, R.C. 2016.** Landform Curvature and Its Effect on The Spatial Variability of Soil Attributes, Pinheiral-Rj/Br. *Cerne*. 22: 431-438.
- Vivekanahan, K., Akinremi, O., Moulin, A.P. and Kumaragamage, D. 2018.** Importance of terrain attributes in relation to the spatial distribution of soil properties at the micro scale: a case study. *Canadian journal of soil science*. 98: 292-305.